November/December 2019 | Volume 67 | Issues 5/6
BioTechniques.com

BioTechniques®

The International Journal of Life Science Methods

Tech News: Spotting 'unproven' stem cell therapies in the wild

Single-cell analysis for drug development using convex lens-induced confinement imaging

Improvement of multiplex semi-nested PCR system for screening of rare mutations by high-throughput sequencing

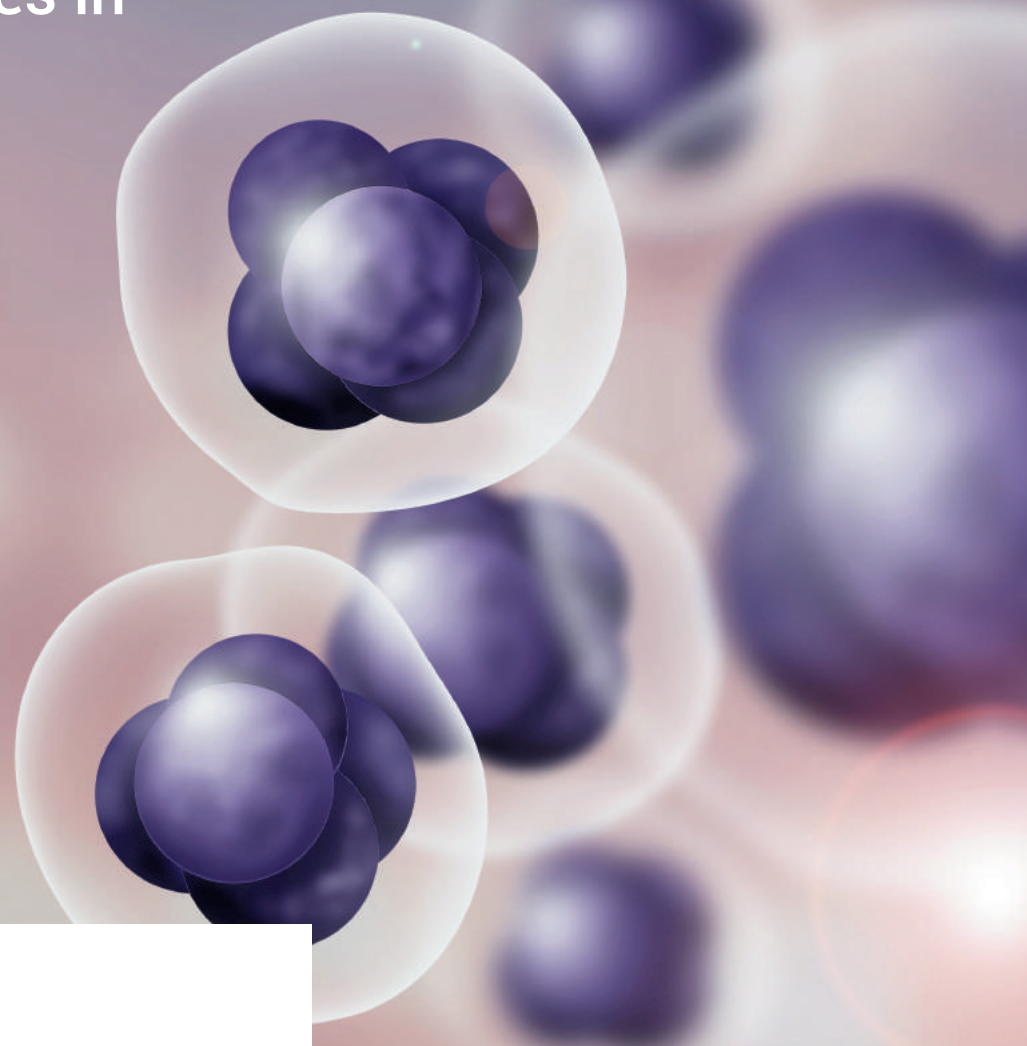

REDESIGNED WITH ALL OF US IN MIND

Introducing the Stericup® E and Steritop® E sterile filtration devices—**evolved with an eco-conscience**.

This progressive rethinking of filter design reduces your lab's environmental impact by eliminating the need for a receiver funnel, significantly decreasing packaging and biohazardous waste.

Expect the same faultless filtration you trust from Stericup® devices—and leave a smaller footprint.

Up to 48% Reduced Plastics

Up to 69% Reduced Packaging

Stericup® E family of sterile filters thread directly onto virtually any media bottle

SigmaAldrich.com/Stericup-E

*Up to 48% plastic reduction and 69% packaging reduction (depending on receiver volume), derived from comparison to traditional Stericup® sterile filters.

2019 - 24573 08/2019

The life science business of Merck operates as MilliporeSigma in the U.S. and Canada.

Millipore®

Preparation, Separation, Filtration & Monitoring Products

Contents

BioTechniques

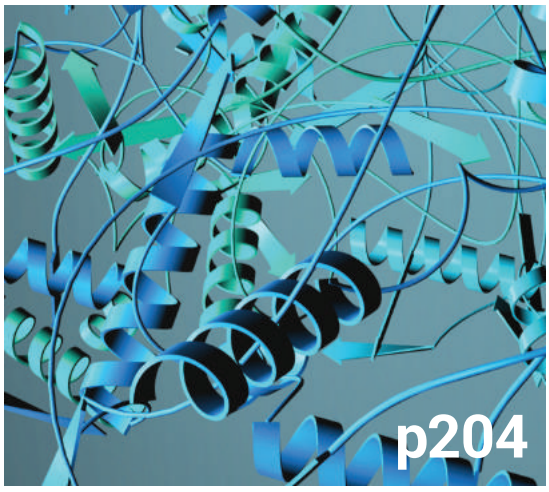

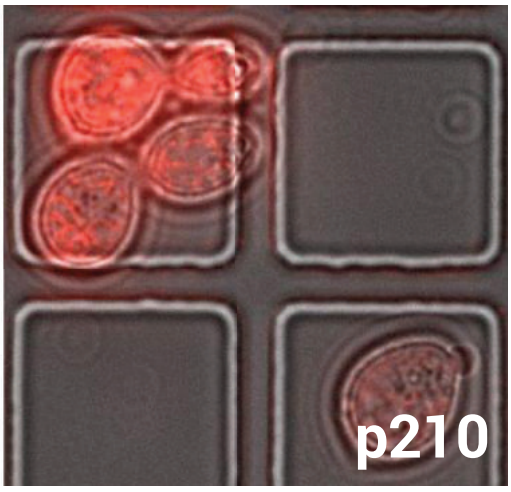

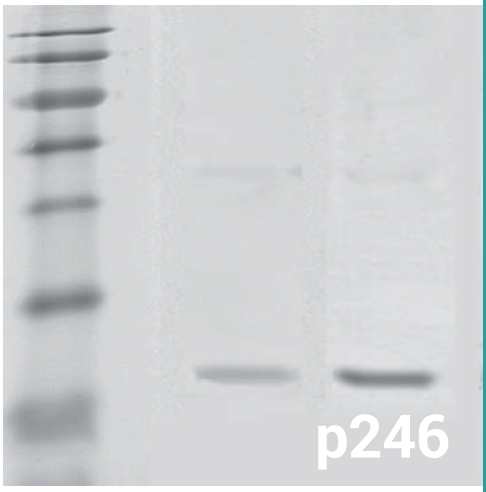

Vol. 67, Issues 5 & 6 – A compilation of the content highlights from issues 1 and 2 of *BioTechniques*

Features

Reports

Benchmarks

This issue of *BioTechniques* was brought to you by the following sponsors:

BIOSPEC
NEW LOGO TO COME
PRODUCTS

BMG LABTECH
The Microplate Reader Company

CoolLED
Simply Better Control

MERCK

MP

OLYMPUS

BlotCycler™
by PRECISION BIOSYSTEMS

VistaLab™ TECHNOLOGIES
Think Differently. Feel Better.

From the editor

Saving the trees, revitalizing your coffee table and shoring up the future

Many of our readers know *BioTechniques* from the print edition that finds its way onto the coffee table every month. Lately, many of our readers will also have become aware of how our website has evolved, becoming a place to discover expert commentary and discussion, with thought-provoking Interviews, Opinion pieces, Podcasts and panel discussions examining the latest tools and techniques available to the lab researcher, in addition to our educational webinars and News section.

Both our online and print articles are free to read, and it is our intention to keep it that way. However, the publishing landscape is changing, and *BioTechniques* must, like our labs, continually evolve to keep up. That's why we have some changes coming in 2020.

First up, we are revitalizing our print edition. We care about the planet, and thus as of 2020 we will be consolidating our articles into quarterly print editions, helping us reduce our impact on the environment and save trees. This won't mean you lose out – we will be publishing the same (if not more!) content, but it will arrive on your coffee table with a refreshed feel – Reports and Benchmarks will remain alongside exciting editorial content such as our traditional Tech News, Interviews, Top Tips and other fascinating articles.

> ***"...publishing is changing, and BioTechniques must, like our labs, continually evolve to keep up."***

Second up, the way you use the website is changing. Going forward, readers will be able to access three articles a month before they are required to log-in with their (free) subscription – and I emphasize that that subscription will be free. Our peer-reviewed articles will remain open access, as they always have been.

In the rapidly changing landscape of scientific research and publishing, these changes will shore up the future for *BioTechniques*, allowing us to maintain our editorial excellence and continue to provide you, our reader, with free-to-access content. By continuing your subscription, you will help us continue to provide the latest in methods, tools and technical advances freely to researchers across the globe, regardless of where they are.

So please, continue to read and enjoy *BioTechniques* for free, for years to come, and email me if you have any queries regarding the above at flake@biotechniques.com.

Francesca Lake
Editor in Chief, Future Science Group, Unitec House, 2 Albert Place, London, UK.
flake@biotechniques.com

BioTechniques **is a peer-reviewed journal dedicated to the publication of original laboratory methods, related technical tools and methods-oriented review articles that are of broad interest to scientists engaged in basic applied life science research. Complete Instructions for Authors are available at: https://mc04.manuscriptcentral.com/fs-btn, *BioTechniques'* website for online manuscript submission. All manuscripts should be submitted at this site.**

Introducing the new CLARIOstar® *Plus*

Unbox your potential

Do not be restricted by your reader! The new CLARIOstar® *Plus* multi-mode microplate reader with LVF Monochromators™ comes with new features that will expand your capabilities in the lab.

- Enhanced Dynamic Range technology allows easy and reliable detection of samples at the largest range of concentrations in a single read - no manual intervention
- Rapid, full-plate autofocus automatically provides the best sensitivity for any assay in top or bottom read
- Dedicated detectors improve performance in red-shifted fluorescence and expand assay flexibility

The most sensitive monochromator-based microplate reader got even better!

BMG LABTECH

The Microplate Reader Company

www.bmglabtech.com

BioTechniques

NATIVE MASS SPECTROMETRY: A POWERFUL TOOL FOR STRUCTURAL BIOLOGY?

Mass spectrometry has been used for decades and continues to be an integral part of analytical research. This feature explores its latest applications.

Just over 100 years since the development of the first mass spectrometer by Francis Aston (University of Cambridge, UK), the technique of mass spectrometry (MS) remains, to this day, a vital tool in the arsenal of researchers throughout the multifaceted field of life science [1]. The modern-day spectrometer exists in a form that Aston would unlikely recognize and can now perform tasks that must surpass the wildest aspirations of the technology's pioneer.

Developments to the ionization, flight path and analysis protocols in MS have helped keep the spectrometer a relevant and valuable piece of equipment. Key examples of these developments include electrospray ionization, which has enabled the conversion of analytes from solution into the gas phase without too much disruption to the natural conformation of the molecule. This has led to an increase in the importance of the mass spectrometer in the field of structural biology, where it can now provide valuable information on the structure of proteins and other biological molecules in their native state – a technique known as native MS (nMS).

TECHNOLOGICAL DEVELOPMENTS IN NMS FOR STRUCTURAL BIOLOGY

One such recent development in the process of nMS is the combination of the technique with surface-induced dissociation (SID) – a high-energy method of fracturing native molecules in the gas phase [2].

A team of researchers from Ohio State University (OH, USA), led by Vicki Wysocki and Steffen Lindert, identified that SID could be used to study the complex structure and binding behaviors of protein complexes in a mass spectrometer [3].

Typically, structural biologists aim to glean structural and binding information on protein complexes while they are intact. Wysocki and Lindert, however, identified that by using SID they could flip this entrenched system of thought on its head, instead observing the complexes as they are split apart and examining how they divide to establish information regarding their structure, binding and subunit interaction.

When ionizing samples to the gas phase, the team subjected the native structures of the molecules to SID, which involves colliding the ionized molecules with a surface, as opposed to using traditional collisional activation techniques that rely on the ions colliding with buffer gas molecules. SID provides more rapid, higher energy impacts that lead to complex shattering into intact subunits, as opposed to slowly unfolding subunits into their secondary structures until they are released [2].

Using this method to separate the complexes, the team was able to generate mass spectra data from the fully folded subunits, which they used to identify a quality that they termed SID appearance energy (AE). AE is defined as 10% fragmentation of the complex (Figure 1). Combining this experimental approach with the Rosetta modelling environment to create a 'SID Score' enabled the researchers to infer key pieces of information regarding the nature of the protein–protein interactions and poses at which the fragmentation takes place; for instance, subunit rigidity and the number of unsatisfied H-bonds (Figure 1) [3].

This is but one key example of the ways nMS is developing in order to uncover new and vital information within structural biology. While technological developments continue to improve the mass spectrometer, the applications of the technique widen.

USING NMS TO EXPLORE GLYCOSYLATION

Post-translational modification (PTM) of proteins is a well-established and staggeringly abundant phenomenon. Of all the PTMs to occur in the domain of *Eukaryota*, glycosylation is the most prevalent, modifying almost half of the human proteome. Due to this abundance, the impact of its dysfunction is catastrophic, while the need to clearly understand this process is clear [4].

As a result of the flexibility and heterogeneity of oligosaccharides, more established methods of structural examination, such as cryo-electron microscopy and x-ray crystallography, are ineffective. nMS, meanwhile, is fully capable of examining the extent and type of glycosylation present in such molecules as IgG, as mass shifts can be detected with a high enough resolution to correlate them to individual hexose rings [5]. ▶

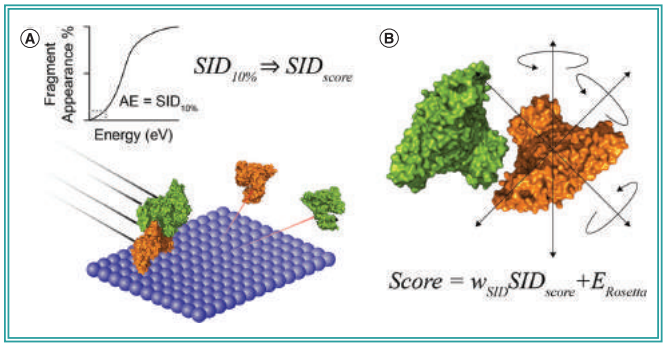

Figure 1. Combining surface-induced dissociation appearance energy and Rosetta to create a surface-induced dissociation score. (A) A depiction of surface-induced dissociation (SID) and a graphical representation of the generation of SID appearance energy. (B) A molecule model generated in Rosetta and the Scoring function equation.

This ability recently enabled researchers from the University of Oxford (UK), led by the world-renowned practitioner of nMS, Carol Robinson, to establish the effects of glycosylation on the drug–protein interactions between warfarin and the serum protein alpha-1-acid glycoprotein [6].

By conducting analyses of native mass spectra of the alpha-1-acid glycoprotein (Figure 2), Robinson and her team found that elevated N-glycan branching of the glycoprotein, alongside terminal fucosylation, led to a decreased binding affinity of the glycoprotein to warfarin. This information provides an indication of how glycosylation can affect drug–protein interactions and, in turn, reveals useful insights about drug transport in the blood [6].

This example of nMS's high resolving power not only demonstrates the versatility of the technique, but also highlights its potential application in the study of disease and drug discovery.

NMS IN MICROBIOLOGY

The refinement of MS has not only allowed for the analysis of viral and bacterial proteins in the native state, but advances that have reduced the limitations imposed on the technique by the size of the analyte have now enabled the ionization of full-size virions and capsids into the spectrometer for analysis [7].

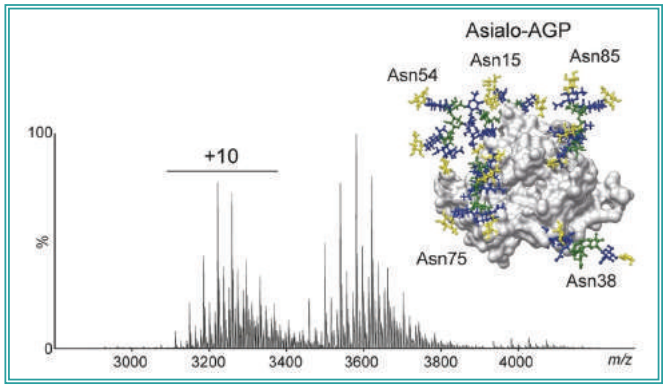

Figure 2. A native mass spectrum of asialo-AGP with highly branched N-glycans, color coded in line with the Consortium for Functional Glycomics guidance and marked with the Asparagine residue they are bound to. Blue: GlcNAc; Green: Man; Yellow: Gal.

This advancement in technology has provided microbiologists with a whole new tool to analyze and explore aspects of virology. One such example of this is the recent study by Nyiri *et al.*, which explored the UTPase family of proteins encoded by the genome of phage (Figure 3) that target *Staphylococcus aureus*. These UTPases can be dimeric or trimeric, and have previously been shown to engage with the *S. aureus* repressor protein StI, impacting the bacterium's pathogenicity island *SaPIbov1* in the *S. aureus* genome [8].

The team decided to explore the interactions between the UTPases, identifying their properties while also documenting the nature of the binding mechanism between the StI protein and the dimeric φNM1 phage dUTPase. To accomplish this, a combination of nMS, cross-linking and hydrogen deuterium exchange-MS experiments were employed [8].

The team were able to identify that the StI protein is capable of displaying disparate stoichiometry and regions of peptide sequences depending on which phage UTPase it was interacting with, indicating the functional plasticity of StI. The nMS data were particularly vital in demonstrating that the mechanism by which StI interacted with and inhibited the dimeric UTPases was due to the architecture of the active site of the protein, which resides at the dimer binding site of the protein [8].

Just as nMS has evolved to accommodate the analysis of larger molecules, as exemplified by its increasing use in virology, the increased acuity and resolution of the technique allow for the study of more delicate molecules than proteins, such as nucleic acids.

NMS IN THE STUDY OF NUCLEIC ACIDS

The application of MS in the field of genomics has previously included the detection of single-nucleotide polymorphisms and short tandem repeats; an application enabled by the development of matrix-assisted laser desorption/ionisation and electrospray ionization techniques [9].

However, a recent paper published in *Analyst* describes the application of nMS to study the structure of telomeric G-quadruplexes [10].

G-quadruplexes are structures formed at the end of strands of DNA and RNA in the telomeres that help protect telomeres from degradation, a process vital to the safeguarding of chromosome integrity and, consequently, cell proliferation. The polymorphic nature of these structures leads to difficulty studying their conformation using typical structural biology techniques [10].

Speaking to study co-author Valérie Gabelica at the inaugural Celebration of Native Mass Spectrometry (Oxford, UK, 24–26 March 2019) while this research was being conducted, Gabelica noted that, "*There are some aspects of the folding that we can reveal quite readily with MS, and which are difficult to get a hint of with traditional biophysical techniques*" [11].

With this in mind, Gabelica and co-author Valentina D'Atri set out to employ native ion mobility MS (IM-MS) to characterize the structure of different G-quadruplex topologies and to reveal aspects of their interactions such as cation binding and multimer formation in both four and eight repeat sequences of DNA and RNA.

The researchers found that in 8-repeat sequences of DNA, subunit folding of different topologies are linked – the formation of one subunit inhibits the folding of a second – while in RNA the subunits fold collaboratively via cation mediated stacking [10].

This structural knowledge could prove valuable when trying to understand conditions of aging or chromosomal damage and clearly extolls the power of nMS in structural biology.

EXPLORING EVOLUTION

The direct application of nMS to pathogenic and human molecules and complexes in order to discover new avenues for research into our health and to identify targets for drug discovery could result in benefits for our future. Looking deep into the evolution of specific complexes, however, could also prove of significant value.

With this in mind, a recent study led by Michal Sharon of the Weizmann Institute of Science (Rehovot, Israel) used nMS techniques to study the evolutionary history of the 20S proteasome. This proteolytic complex is ubiquitous throughout all three kingdoms of life, making it an ideal candidate to study throughout evolution.

20S proteasomes were isolated from yeast, rat liver and human cells, all of which were reported in a paper published in *Biomolecular Engineering*, although in a presentation at the Celebration of Native Mass Spectrometry Sharon revealed that the proteasomes of archaea and a rabbit were also analyzed [12].

"*Specifically, we applied ion mobility, SID, collision induced dissociation, collision induced unfolding profiles and top-down pseudo-MS3 experiments in order to study the structural properties of the ortholog proteasomes,*" noted Sharon, speaking to *BioTechniques* at the conference [13].

The results of this analysis were surprising, as the structural properties of each species' 20S proteasome did not align with the linear increase in size and stability that was expected to follow the evolutionary development of the proteasome by the research team.

"*We saw that yeast was the most stable and biggest proteasome, more than mammalian complexes, and it could be that stability is not a feature that is advantageous, maybe the more flexible structures are those that facilitate functionality. Indeed, the number of intrinsically unstructured proteins that are identified is growing, so maybe flexibility in structure is a feature that assists function,*" Sharon theorized.

CHALLENGES IN NMS

The power of nMS as a tool for structural biology is clear to see, but it is important to remain critical of the process and to regard all results through a slightly reserved lens. Many researchers working with nMS will note the frequent skepticism that they meet when attempting to convince researchers from other fields that the analytes that fly through the spectrometer are indeed in their 'native' state.

This skepticism is by no means unfounded. The structures analyzed are commonly found in solutions or are taken from the membrane of the cell. To convince a molecular biologist that these structures to remain intact when in the gas phase takes a great deal of evidence to accomplish.

Gabelica, for instance, noted that in "*…fields like structural chemistry and biophysics, there is always this suspicion about nMS, because we are analyzing things in the gas phase and we want to infer information on what existed in the solution. In every community, you have to convince and prove that what you are claiming to deduce from MS is valid. In different communities, it's a different challenge. For example, among organic chemists and supramolecular chemists, a few are really convinced, but most will want to crystallize the structure and analyze it by NMR, because that is more conventional and thus better accepted by their peers.*"

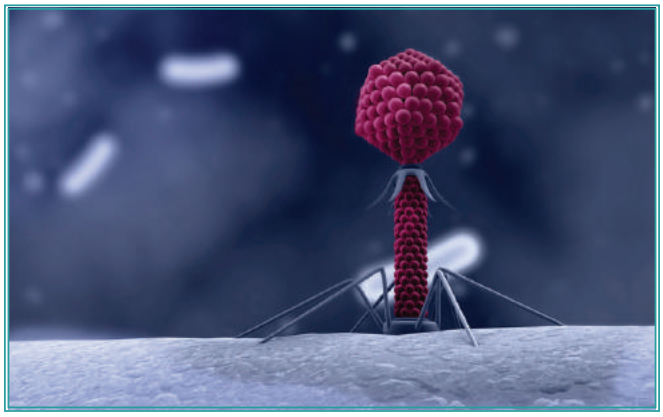

Figure 3. A bacteriophage.

In her own study into G-quadruplex structure, Gabelica noted herself that there is an element of structural difference in the solution structure compared with the gas phase structure of G-quadruplexes, as identified by ion mobility spectroscopy [10].

These differences do not spell the doom of nMS as a technique, nor provide cause to deride and dismiss the results obtained by the procedure. They are identified and considered aspects of using these methods that any conscientious researcher should certainly consider when drawing conclusions and constructing experiments.

What these limitations truly highlight is that, while the instrumentation and technique is continually improving, the development of nMS is not yet complete. Further understanding of the alterations acquired in the transition from solution to gas phase are required alongside an established method accounting for or minimizing them. nMS is currently a powerful tool for structural biology, but there is plenty of work to do yet.

Written by Tristan Free

REFERENCES

1. Aston F. A positive ray spectrograph. *Lond. Edinb. Phil. Mag.* 38(228), 707–714 (1919).
2. Gault J, Robinson C. Cracking complexes to build models of protein assemblies. *ACS Cent. Sci.* 5(8), 1310–1311 (2019).
3. Seffernick J, Harvey S, Wysocki V, Lindert S. Predicting protein complex structure from surface-induced dissociation mass spectrometry data. *ACS Cent. Sci.* 5(8), 1330–1341 (2019).
4. Struwe W, Robinson C. Relating glycoprotein structural heterogeneity to function – insights from native mass spectrometry. *Curr. Opin. Struct. Biol.* (2019).
5. Rose R, Damoc E, Denisov E, Makarov A, Heck A. High-sensitivity Orbitrap mass analysis of intact macromolecular assemblies. *Nat. Methods* 9(11), 1084–1086 (2012).
6. Wu D, Struwe W, Harvey D, Ferguson M, Robinson C. N-glycan microheterogeneity regulates interactions of plasma proteins. *Proc. Natl Acad. Sci. USA* 115(35), 8763–8768 (2018).
7. Dulfer J, Kadek A, Kopicki JD, Krichel B, Uetrecht C. Structural mass spectrometry goes viral. *Adv. Virus Res.* 105, 189–238 (2019).
8. Nyíri K, Harris M, Matejka J *et al.* HDX and native mass spectrometry reveals the different structural basis for interaction of the staphylococcal pathogenicity island repressor StI with dimeric and trimeric phage dUTPases. *Biomolecules* 9(9), 488 (2019).
9. Meng Z, Simmons-Willis TA, Limbach P. The use of mass spectrometry in genomics. *Biomol. Eng.* 21(1), 1–13 (2004).
10. D'Atri V, Gabelica V. DNA and RNA telomeric G-quadruplexes: what topology features can be inferred from ion mobility mass spectrometry? *Analyst* 144(20), 6074–6088 (2019).
11. *BioTechniques*. Valérie Gabelica on native mass spectrometry for nucleic acids. www.biotechniques.com/interview/valerie-gabelica-on-native-mass-spectrometry-for-nucleic-acid/
12. Ben-Nissan G, Vimer S, Tarnavsky M, Sharon M. Structural mass spectrometry approaches to study the 20S proteasome. *Methods Enzymol.* 619, 179–223 (2019).
13. *BioTechniques*. Probing the proteasome. www.biotechniques.com/chemical-biology-bio-and-analytical-chemistry/probing-the-proteasome/

OLYMPUS®

Discover the Possibilities

Expand your multiplex capabilities with near-infrared solutions for the FLUOVIEW™ FV3000 microscope

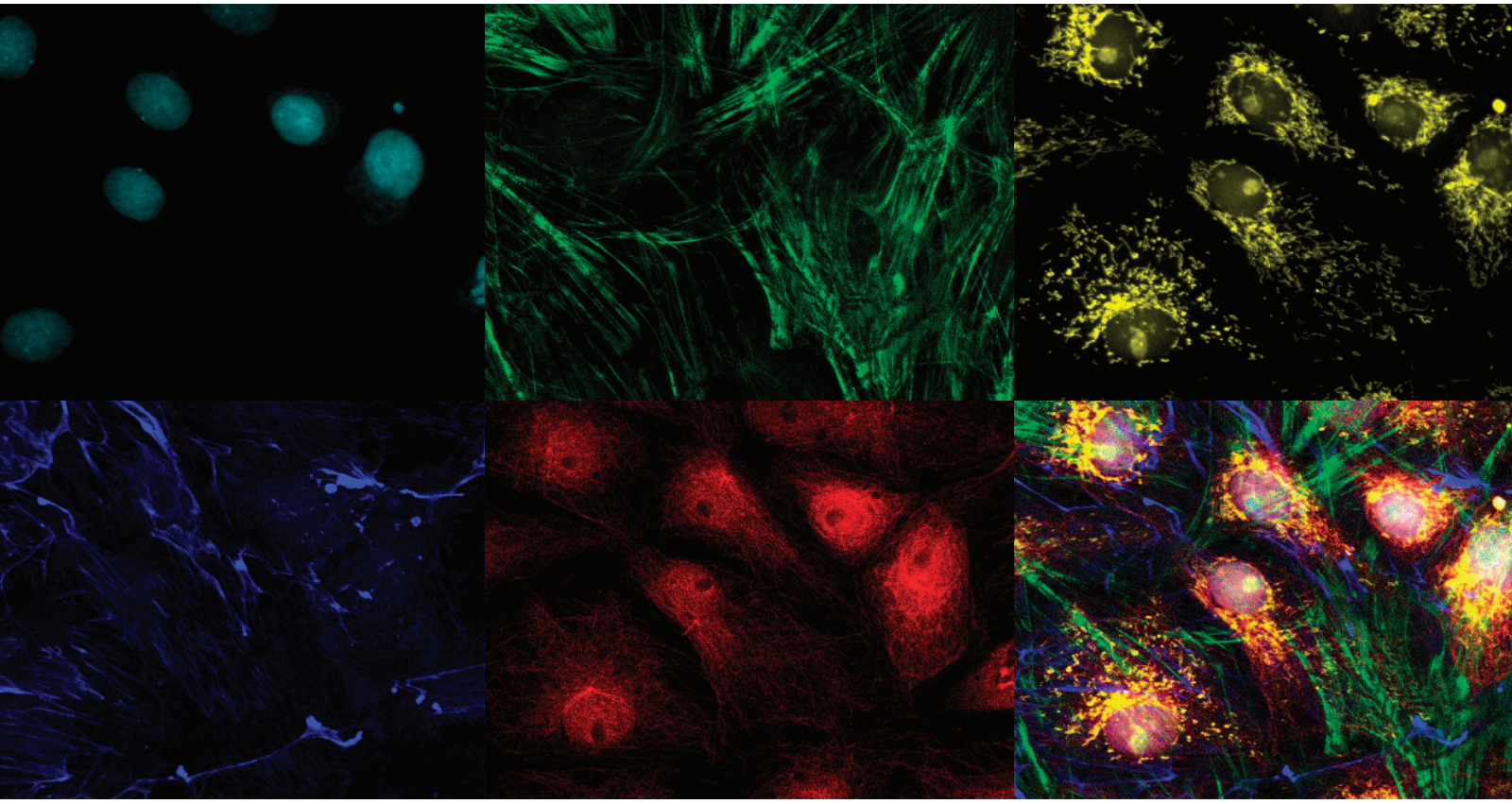

PtK2 cells captured with the FV3000RS microscope, showing nuclei (405 nm/cyan), actin (488 nm/green), mitochondria (561 nm/yellow), cell membrane (640 nm/blue), and microtubules (730 nm/red).

Interested in imaging with far-red fluorescent probes? Expand your multiplex capabilities with near-infrared (IR) upgrades for your FLUOVIEW® FV3000 confocal laser scanning microscope. Olympus offers a suite of near-IR equipment custom-made for the FV3000 system, including a 730 nm diode laser and red-shifted PMTs for high-sensitivity detection up to 900 nm. Upgrade to a 730 nm laser today and enjoy the following benefits of near-IR imaging:

- Greater multiplexing capabilities
- Decreased autofluorescence
- Gentler live-cell imaging
- Deeper imaging with less absorption and scattering

Your Science Matters™

To learn more, contact your local Olympus confocal sales representative or visit:

www.olympus-lifescience.com

BioTechniques

SPOTTING 'UNPROVEN' STEM CELL THERAPIES IN THE WILD

Freya Leask explores how to spot an 'unproven' stem cell-based therapy and why producing an effective stem cell-based therapy is so challenging.

When Masayo Takahashi (Figure 1) shared the results of the first clinical trial testing induced pluripotent stem cells (iPSCs) in humans in the *New England Journal of Medicine*, she was surprised to see, next to her article, another article reporting on the same autologous stem cell-derived treatment.

Takahashi, formerly based at RIKEN (Japan) but who recently spun out a standalone company called Vision Care, made headlines in 2014 when she implanted a sheet of retinal pigment epithelium (RPE) cells, produced by first reprogramming the patient's own cells into iPSCs then differentiating them into the RPE cells, into the patient's eye to treat age-related macular degeneration. The process, which Takahashi described as "*a momentous first step*" towards applying iPSCs to regenerative medicine, was noteworthy for the its complexity and difficulty, as well as the speed at which it was carried out after the Japanese health ministry gave approval for a potential clinical trial.

By 2017, having followed the patient for a year to determine there were no ill effects, she was ready to publish her report. However, the other article, published by a coalition of physicians, had different news to share.

In the paper, the team describe three Florida patients who also received 'stem cell' treatments. However, unlike Takahashi's patient, they were left blinded after their treatment caused vision loss, detached retinas and hemorrhage. They had received an unproven treatment, seemingly without the careful planning and preparation that usually accompanies a procedure like this.

The term 'unproven treatment' is hugely emotive to scientists aiming to develop 'proven' treatments, commercial providers arguing against it, and patients looking for answers and, ultimately, hope. In 2015, the International Society for Cell Therapy (ISCT), now the International Society for Cell and Gene Therapy, set out to define exactly what makes a therapy 'unproven'.

HOW IT WORKS... OR DOESN'T

The first criterion to denote an 'unproven therapy' is the lack of scientific rational to suggest potential efficacy. There's "*little evidence that adipose, bone marrow and amniotic stem cells can be used safely and effectively for the diverse array of conditions marketed by for-profit clinics*," according to Paul Knoepfler, speaking to RegMedNet in 2018 [1]. Paul is a professor at University of California, Davis (CA, USA) and runs the noted stem cell blog *The Niche* [2]. He has been monitoring the rise of unproven stem cell treatments on *The Niche* as well as in peer-reviewed literature.

Although some studies have demonstrated that stem cell-based treatments can be safe, there is little clinical evidence of a high enough quality that indicates they are effective in humans [3].

There should also be an understanding of the mechanism of action to support clinical use of the therapy. In 2019, research conducted at Arizona State University (AZ, USA) into the clinics offering stem cell-based therapies found that although 60% of staff listed on the clinics' websites had medical degrees, over a quarter had other medical qualifications such as Doctor of Osteopathy, and Doctor of Chiropractic and Doctor of Naturopathic Medicine [4], a range of qualifications and specialties unlikely to have the expert knowledge into how and why stem cell treatments work the way they do, if at all.

A WOBBLY EVIDENCE BASE

Another reason to be wary of 'unproven' treatments is they may possess insufficient data from *in vitro* assays, animal models and clinical studies regarding the safety profile to support the use in patients. They may also misrepresent early-stage data showing safety as conclusive proof of efficacy.

Many businesses marketing unproven treatments make "*positive but imprecise, unquantified claims about the therapeutic promise* ▶

Figure 1. Masayo Takahashi (right) was the lead scientist in the first human trial involving iPSCs. Kyodo News via Getty Images.

of the stem cell interventions they promote," explained Leigh Turner, Associate Professor at University of Minnesota Center for Bioethics, School of Public Health and College of Pharmacy (MN, USA), speaking to RegMedNet following his 2018 research into the Canadian landscape of unproven treatments. In the paper, he detailed the ways in which some clinics get around the lack of published evidence in the field.

"*I'm very concerned about the risks associated with businesses making dramatic claims about stem cell treatments … without doing the careful, costly and time-consuming work needed to develop a compelling evidence base for such representations*," continued Turner.

Such clinics are using "*tokens of scientific legitimacy*", he explained, such as personal testimonials, eminent scientific advisory boards, professional affiliations and technical language to make their proffered treatment more acceptable [5]. Without links to "*peer-reviewed publications, unpublished data or other sources of evidence*", it's "*impossible to know whether meaningful data support such assertions.*"

> *"The unproven clinic part always muddies the waters and risks damaging the public's perceptions of stem cell research and regenerative medicine."*

The one thing patients need to remember, says Kieran Breen, Head of Research and Development, St Andrew's Healthcare (UK): "*If it sounds too good to be true, it probably is.*"

QUALITY NOT QUANTITY

Living medicinal products, such as stem cell-based treatments, are complex by nature and generally involve multiple steps to produce a quality product. 'Unproven' products, according to the ISCT, lack a standardized approach to confirm product quality and ensure consistency in cell manufacturing, or are used within nonstandardized or nonvalidated administration methods.

With the many stem cell-based therapies currently under investigation, a sample of patient or donor cells is collected and is then expanded. Cell lines can also be obtained from validated cell banks. In her first trial, Takahashi used autologous cells, or cells obtained from the patient receiving the therapy. In the second, she obtained cell lines from the CiRA iPSC bank (Japan) [6].

The cells are then differentiated, with multiple quality controls at every step. These measures range from assessing the cells' morphology, viability and density to potential tumorigenicity and presence of viral or mycoplasma contamination, as well as looking for specific cell surface markers to ensure the desired final cell type has been produced [7].

With Takahashi's first trial, after this stage an RPE cell sheet was surgically implanted into the subretinal space of the patient's eye. The process took 10 months, from initial skin biopsy to collection of patient fibroblasts to production of an RPE cell sheet that was ready to be implanted. Since then, other cell-based treatments have reported manufacture times of around 3–4 weeks [8].

By contrast, the Florida patients received a therapy much closer in nature to their original cell sample. A sample of adipose tissue was obtained via liposuction and stromal vascular cells were separated out using enzyme treatment and centrifugation. This cell fraction was then resuspended in a small amout of platelet-rich plasma, separately obtained from a sample of the patient's whole blood, before being used immediately for intravitreal injection [9].

There are usually many more steps in producing a cell or gene therapy, explains Karen Magers, Head of Regulatory for Cell & Gene Technologies, Lonza Pharma & Biotech (Switzerland), because "*the manufacturing process is designed with the objective of consistently manufacturing products derived from cell-based starting material that meet target quality attributes linked to the desired patient safety and clinical outcome.*" Ultimately, a standard, effective product is vital before it can be administered to human subjects.

Why is there such a difference between the treatments? The answer lies in a definition that has been rigorously debated since its inclusion in a publication of 2005.

MINIMAL MANIPULATION… OR NOT

The FDA is responsible for regulating an exhaustive list of products to ensure the safety of the US public, including therapeutic products such as cell therapies. Most of the products require a new drug application or biologics license application before they can be marketed. The process of securing a new drug application or biologics license application can be lengthy, as rigorous preclinical and clinical study data are required. Could there be a way of bringing the benefits of stem cell-based therapies to patients without have to submit so much paperwork?

Many clinics currently marketing 'stem cell-based' treatments, of which there may be over 700 in the US alone [10], cite an exemption over 'minimal manipulation' and 'homologous use'. Where a human tissue or cell-based product has been minimally manipulated – for example, nothing more than centrifugation or cryopreservation – and will produce the same function in the recipient as they did in the donor, it doesn't need the formal approval of the FDA.

However, Magers explains, "*As manufacturing steps completed to produce cell-based products have the potential, and in many cases the intended outcome, of altering the relevant characteristics of the cells, the processing that occurs during the manufacturing process is more than minimal manipulation.*" As an example, "*if cells are isolated from structural tissues such as adipose tissue, the process of isolating the cells is more than minimal manipulation … manufacturing steps that alter biological characteristics such as metabolic activity, differentiation state or proliferation potential [are] more than minimal manipulation.*"

The FDA agrees, and since 2017 has taken a tougher line on 'unproven' clinics, sending out warning letters and even taking some to court [11].

WHERE THERE'S A WILL, THERE'S A WAY

The problem with the 'unproven clinics', explains Takahashi, is that the patient desire is there. "*Patients come from all over Japan*" to her clinic in Kobe; "*we're not treating anything*", she says, "*but still they come*". For some patients, the risk of the unknown is worth the risk.

"*My vision was very poor … I was unable to read, see faces, or drive*," says Doug Oliver, who received a stem cell transplant to treat his macular degeneration and now advocates for patients in the regenerative medicine field through founding the Regenerative Outcomes Foundation. "*I was suicidal just 2 years prior*" to his treatment, he explained. Five months later, he got his driving licence back.

However, the information he received was "*simple and general*". In the case of the Florida patients, at least two out of the three believed they were taking part in clinical trials, and inability to provide proper informed consent due to inadequate information is yet another ISCT hallmark of an 'unproven' treatment.

Before his 2018 work into the Canadian stem cell landscape, in 2017, Turner investigated businesses using ClinicalTrials.gov, a registry of clinical trials run by the United States National Library of Medicine and currently holding registrations from over 318,000 trials from 209 countries in the world. He was alarmed to see companies using this registry as an exercise in 'direct-to-consumer' marketing.

"*If you take a careful look at many of these pay-to-participate studies you find what in numerous cases appear to be studies with serious scientific and ethical shortcomings … in some instances, there is no record of peer-reviewed preclinical studies being done before stem cells are administered – for thousands or tens of thousands of dollars – to humans*," Turner explained. Without businesses being transparent about the evidence that exists for these treatments, "*patients are exposed to an unnecessary and avoidable level of risk when they pay to participate in such studies.*" [12].

PUBLIC PERCEPTION & FUTURE DEVELOPMENT

"*The unproven clinic part always muddies the waters and risks damaging the public's perceptions of stem cell research and regenerative medicine*," explains Knoepfler, who often deals with emails from desperate patients looking for information [1].

Oliver believes that more patient education is needed: "*as regulatory expectations become clearer and take more form in the US, it is clear the real 'bad actors' are getting worse.*" The process of manufacturing and receiving a stem cell-based treatment needs to be made more transparent, to "*standardize informed consent, provide opportunity for patient input, and train practitioners to gather robust data that can actually be used in clinical trials.*"

If the real bad actors aren't dealt with soon, he says, more "*patients will start getting hurt*".

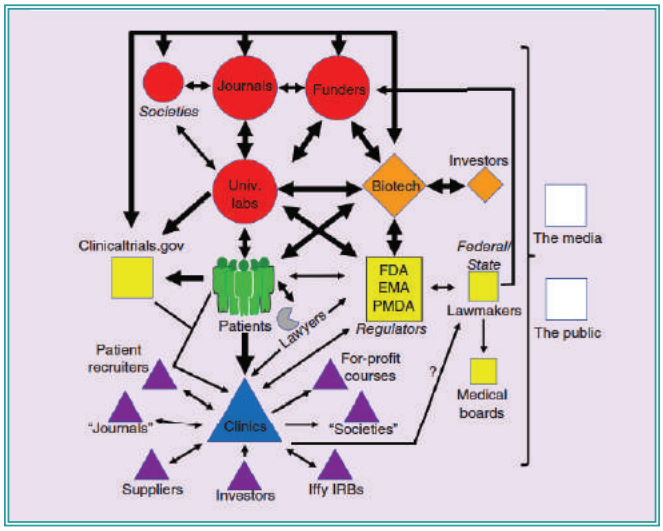

Figure 2. In his original *Regenerative Medicine* article, Knoepfler mapped the complex and interwoven stem cell ecosystem. The degree of separation, or lack thereof, means that unravelling the relationships between stakeholders is time-consuming, and identifying where education and authority would be of most benefit is difficult [13].

Written by Freya Leask

REFERENCES

1. Leask F. Mapping the stem cell ecosystem: an interview with Paul Knoepfler. *RegMedNet*. https://www.regmednet.com/users/3641-regmednet/posts/41639-mapping-the-stem-cell-ecosystem-an-interview-with-paul-knoepfler (Accessed 21 October 2019).
2. Knoepfler lab stem cell blog: The Niche. https://ipscell.com/ (Accessed 11 October 2019).
3. Iijima H, Isho T, Kuroki H, Takahashi M, Aoyama T. Effectiveness of mesenchymal stem cells for treating patients with knee osteoarthritis: a meta-analysis toward the establishment of effective regenerative rehabilitation. *NPJ Regen. Med.* 3, 15 (2018).
4. Frow EK, Brafman DA, Muldoon A *et al.* Characterizing direct-to-consumer stem cell businesses in the southwest United States. *Stem Cell Rep.* 13, 2 (2019).
5. Turner L. Direct-to-consumer marketing of stem cell interventions by Canadian businesses. *Regen. Med.* 13, 6 (2018).
6. Leask F. Speaking with Masayo Takahashi: targeting age-related macular degeneration in the first iPSC clinical trial. *RegMedNet*. https://www.regmednet.com/users/24427-freya-leask/posts/14546-targeting-age-related-macular-degeneration-in-the-first-ipsc-clinical-trial-an-interview-with-masayo-takahashi (Accessed 22 October 2019).
7. https://www.nejm.org/doi/suppl/10.1056/NEJMoa1608368/suppl_file/nejmoa1608368_protocol.pdf
8. Novartis Pharmaceuticals Corporation. Starting Kymriah. A guide for patients and caregivers. https://www.us.kymriah.com/globalassets/products49.com/kymriah---day-0/acute-lymphoblastic-leukemia-all/startingkymriah.pdf (Accessed 22 October 2019).
9. Kuriyan AE, Albini TA, Townsend JH *et al.* Vision loss after intravitreal injection of autologous "stem cells" for AMD. *N. Engl. J. Med.* 376, 1047–1053 (2017).
10. Knoepfler PS. Rapid change of a cohort of 570 unproven stem cell clinics in the USA over 3 years. *Regen. Med.* 14, 8 (2019).
11. Mordock J. DOJ moves to shut down two stem cell clinics. *The Washington Times*. https://www.washingtontimes.com/news/2018/may/9/doj-moves-shut-down-two-stem-cell-clinics/ (Accessed 11 October 2019).
12. Leask F. "Pay-to-participate" stem cells studies: an interview with Leigh Turner. *RegMedNet*. https://www.regmednet.com/users/1122-regenerative-medicine/posts/18659-pay-to-participate-stem-cells-studies-an-interview-with-leigh-turner (Accessed 22 October 2019).
13. Knoepfler PS. Mapping and driving the stem cell ecosystem. *Regen. Med.* 13, 7 (2018).

NEW

All Synthetic FBS Replacement

FastGro™

Fully Chemically Defined FBS Replacement for Cell Culture

- Chemically defined nature without lot-to-lot variations
- No animal or human derived materials or compounds
- No interference with hormones or growth factors
- Elimination of the risk of contaminants – viruses, mycoplasma, prions, etc.
- Wide range of cell culture practices
- No thawing necessary – Store in the refrigerator
- Eliminates biorisk and increases cell culture consistency

HaCaT cells in medium enriched with 10% FastGro

HaCaT cells in medium enriched with 10% FBS

Outgrow your wildest cell growth
No bull inside, all you need is FastGro

LEARN MORE
www.mpbio.com/fastgro

MP Bio North America
1-800-854-0530

MP Bio Europe
00800-7777-9999

MP

Letter to the Editor

BioTechniques

Higher percentage of horse serum in culture media blocks attachment of PC12 cells

Jennifer L Meth[1] & Alan R Schoenfeld*,[1]

The rat pheochromocytoma cell line, PC12, has become a major model system to study many aspects of neuronal activity since its development and characterization in the 1970s [1]. One of its most useful properties is that, following stimulation by nerve growth factor (NGF), these cells extend processes or neurites in a differentiation program that is reversible upon NGF removal. The NGF-mediated differentiation includes the formation of functional synapses as well as electrical excitability [2,3]. Because of these remarkable properties, PC12 cells have been an important tool to uncover the mechanisms of neuronal differentiation as well as the NGF signaling pathway. PC12 cells have also been used extensively to study exocytosis, especially of catecholamines (reviewed in [4]).

According to their initial characterization [1], PC12 cells are round or polygonal, loosely adherent, and tend to grow in clumps. We report here that their cellular morphology and adherence is affected greatly by the percentage of horse serum contained in their culture medium. While the original growth conditions in Greene and Tischler specify the addition of 10% horse serum and 5% fetal calf serum (FCS) in the growth medium, which is reinforced by recommendations of the culture repository, ATCC, not all researchers use the same amount of horse serum in their PC12 cultures. Although 10% horse serum is most common, amounts ranging between as low as 5% [5] and as high as 15% [6] have been used. Moreover, reasons for utilizing a specific concentration of horse serum are routinely not provided and the literature also lacks sufficient explanation as to its effects. We initially observed, after changing our source of horse serum, that a larger percentage of cells were more rounded and seemingly loosely attached several days after plating, which led us to further analyze the effects of horse serum on the growth of PC12 in culture.

PC12 cells were grown in DMEM media supplemented with increasing percentages of horse serum (0, 2.5, 5, 10 and 15%). Two different sources of horse serum were used: Donor Equine Serum from either Corning or HyClone (GE Healthcare Life Sciences). However, because the focus here is the percentage of horse serum and not variations between manufacturers (or lots), these two sources are referred to herein simply as horse serum 1 and 2, in no particular order with respect to the manufacturers named above. The percentage of cells that were loosely attached (rounded) was determined for each culture condition, as described in Figure 1. At 24 h post-plating (Figure 1A), as horse serum percent increased, there was a statistically significant, dose-dependent increase in the percentage of cells that were loosely attached ($p < 0.001$ for all comparisons, except 0 vs 2.5% horse serum, for which $p = 0.103$). With 10 and 15% horse serum, the majority of cells were loosely attached at the 24-h time point. At 48 h post-plating (Figure 1B), with horse serum between 0% and 10%, the majority of cells were polygonal and attached, with 10% horse serum showing considerably more cells that were loosely attached than the lower percentages ($p < 0.001$ in comparison with 0, 2.5 and 5% horse serum). At 15% horse serum, the majority of the cells were loosely attached at 48 h post-plating ($p < 0.001$ for all comparisons). These results indicate that higher percentages of horse serum in the culture media prevent attachment and spreading of PC12 cells toward a polygonal morphology and lead to more loosely attached (rounded) cells.

To determine whether the horse serum-mediated differences in cell morphology had a functional effect on the PC12 cells, neurite outgrowth assays were performed, as described in Figure 2. Preincubation with the range of horse serum percentages did not show a statistically significant difference in neurite outgrowth. Although there was substantial neurite outgrowth following preincubation with all percentages of horse serum (including 0%), there was more variability when using lower percentages (i.e., 0, 2.5 and 5%), and while the higher percentages (i.e., 10 and 15%) did seem to foster slightly more neurite outgrowth, there was at best marginal significance, with the comparison of 5 versus 10% horse serum preincubation coming the closest to achieving statistical significance ($p = 0.078$). Thus, while variations in horse serum percentage led to differences in morphology of the PC12 cells prior to NGF-mediated differentiation, they do not seem to overtly change the ability of these cells to differentiate in response to NGF.

> *"According to their initial characterization [1], PC12 cells are round or polygonal, loosely adherent, and tend to grow in clumps."*

Overall, the results contained herein suggest that the choice of horse serum ▶

KEYWORDS

cell attachment • differentiation • horse serum • neurite outgrowth • PC12

[1]*Department of Biology, Adelphi University, Garden City, NY 11530-0701, USA; *Author for correspondence: schoenfeld@adelphi.edu*

BioTechniques 67: 256-258 (December 2019) 10.2144/btn-2019-0073

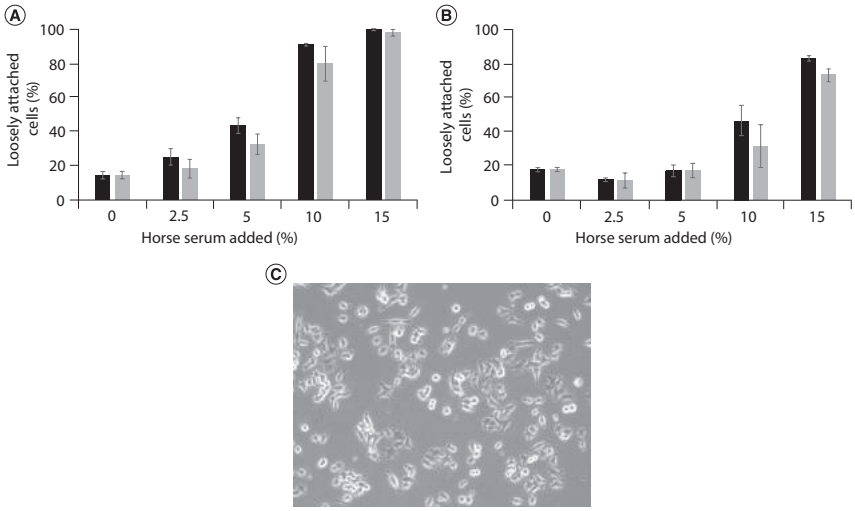

Figure 1. Percent of loosely attached (rounded) PC12 cells. PC12 cells were plated in standard culture dishes in media containing the indicated combination of horse serum and fetal calf serum. Images captured using a Zeiss Primovert inverted microscope (at 40× magnification) equipped with an Excelis high-definition digital camera after (A) 24 h and (B) 48 h were analyzed blindly, counting the percentage of cells loosely attached, as judged by a halo around the cells in the image and a lack of extensions from the cell body. Cell counts from three images for each combination were averaged. For statistical analyses, ANOVA with Tukey HSD *post-hoc* tests were performed. (Note: In both (A) and (B), there was no statistically significant difference between horse serums 1 and 2 at any of the horse serum percentages). (C) A representative image showing loosely attached cells with halos and attached (polygonal) cells.

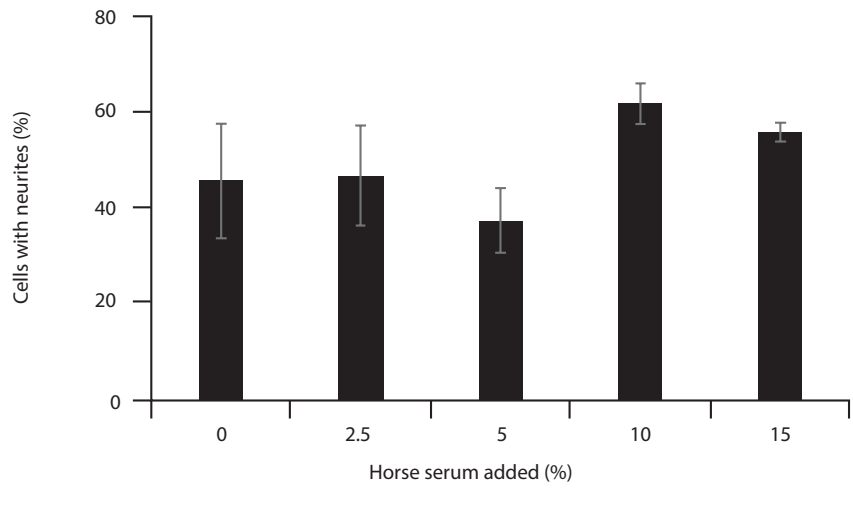

Figure 2. Neurite outgrowth assay. Wells in six-well plates were incubated with 0.5 ml of a 20 μg/ml solution of laminin (Sigma) and allowed to dry. DMEM media containing the indicated percentages of horse serum along with 5% fetal calf serum were added to the wells (3 wells for each horse serum percentage). PC12 cells (1×10^4 cells) were added to each well and allowed to attach for 48 h. Media was replaced with serum-free DMEM, supplemented with 100 ng/ml of NGF (Becton Dickenson), and the cells were allowed to incubate for another 48 h. Five images from each well were captured using a Zeiss Primovert inverted microscope (at 100× magnification). Cells from each image were counted, both total cells and those with neurites, defined as neuron-like extensions of the cell membrane that were equal to or longer than one diameter of the cell. For statistical analyses, ANOVA with Tukey HSD *post-hoc* tests were performed.

▶ percentage used by researchers is mostly a matter of choice, reflecting their culture preferences. As the most common percentages of horse serum used seem to be 10 and 15%, which led to fairly similar performance in neurite outgrowth, the more loosely attached (rounded) cells seen with 15% horse serum may be preferred by researchers that do not use trypsin to subculture PC12 cells, allowing them to grow more as a suspension culture. Of note, our initial observation of changed culture characteristics upon switching horse serum sources, which caused us to consider discarding the horse serum, can be simply remedied by altering horse serum concentration.

One question perhaps worthy of further investigation is the effect of long-term culturing of PC12 cells in medium either devoid of horse serum or containing lower percentages. The more attached polygonal cells observed with low horse serum percentages (short term) in this report may be associated with partial differentiation of these cells toward a non-neuronal cell type that can be reversed by removal of serum and addition of NGF. It is currently unclear what role the horse serum plays in PC12 cell culture, but given that PC12s are progenitor cells and can differentiate along both chromaffin and sympathetic neuronal lineages [1], horse serum may preserve the progenitor status of these cells. Along these lines, horse serum has also been used to maintain hematopoietic progenitor cells in culture, keeping them in a less differentiated state [7,8], and has been seen to block the differentiation of hepatic progenitor cells [9]. Thus, future studies could further clarify the effect of horse serum on the differentiation state of PC12 cells.

The discrepancies in PC12 cell attachment seen with different horse serum sources are likely due to differences in the levels of some factor(s) in these sera. Thus, another potential avenue of future studies is to determine which components in horse serum mediate the effect seen on PC12 attachment and are responsible for the variances observed. Unlike human serum, for which the composition has been characterized [10], sera used in tissue culture are usually minimally defined and the proteins, lipids, and/or growth factors and hormones contained in them may vary among sources

> *"One question perhaps worthy of further investigation is the effect of long-term culturing of PC12 cells in medium either devoid of horse serum or containing lower percentages."*

for many reasons [11,12]. Ditz *et al.* were able to determine that high levels of fatty acid products of phospholipase A2, notably eicosanoids, present in some lots of horse serum inhibited self-renewal of multipotent murine hematopoietic progenitor cells [8]. While it is possible that these compounds may similarly affect PC12 cells, identification of the actual components of horse serum that inhibit attachment (and preserve progenitor status) is needed, which would allow elucidation of the underlying cellular pathways and mechanisms as well.

AUTHOR CONTRIBUTIONS

JLM carried out all of the experiments and the majority of the data analysis. ARS completed the data analysis, performed statistical analysis, and wrote the manuscript.

ACKNOWLEDGMENTS

The authors thank Benjamin Weeks (Adelphi University) for generously supplying the PC12 cells, which were originally obtained from G Guroff (NIH).

FINANCIAL & COMPETING INTERESTS DISCLOSURE

Research reported in this publication was supported by the National Cancer Institute of the National Institutes of Health (award number R15CA121992). The authors have no other relevant affiliations or financial involvement with any organization or entity with a financial interest in or financial conflict with the subject matter or materials discussed in the manuscript apart from those disclosed.

No writing assistance was utilized in the production of this manuscript.

REFERENCES

1. Greene LA, Tischler AS. Establishment of a noradrenergic clonal line of rat adrenal pheochromocytoma cells which respond to nerve growth factor. *Proc. Natl Acad. Sci. USA* 73(7), 2424–2428 (1976).
2. Dichter MA, Tischler AS, Greene LA. Nerve growth factor-induced increase in electrical excitability and acetylcholine sensitivity of a rat pheochromocytoma cell line. *Nature* 268(5620), 501–504 (1977).
3. Schubert D, Heinemann S, Kidokoro Y. Cholinergic metabolism and synapse formation by a rat nerve cell line. *Proc. Natl Acad. Sci. USA* 74(6), 2579–2583 (1977).
4. Westerink RH, Ewing AG. The PC12 cell as model for neurosecretion. *Acta Physiol.* 192(2), 273–285 (2008).
5. Martin TF, Grishanin RN. PC12 cells as a model for studies of regulated secretion in neuronal and endocrine cells. *Methods Cell Bio.* I71, 267–286 (2003).
6. Iuvone T, Esposito G, Esposito R, Santamaria R, Di Rosa M, Izzo AA. Neuroprotective effect of cannabidiol, a non-psychoactive component from Cannabis sativa, on beta-amyloid-induced toxicity in PC12 cells. *J. Neurochem.* 89(1), 134–141 (2004).
7. Spooncer E, Heyworth CM, Dunn A, Dexter TM. Self-renewal and differentiation of interleukin-3-dependent multipotent stem cells are modulated by stromal cells and serum factors. *Differentiation* 31(2), 111–118 (1986).
8. Ditz T, Schnapka-Hille L, Noack N *et al.* Phospholipase A2 products predict the hematopoietic support capacity of horse serum. *Differentiation* 105, 27–32 (2019).
9. Hui H, Ma W, Cui J *et al.* Periodic acid-Schiff staining method for function detection of liver cells is affected by 2% horse serum in induction medium. *Mol. Med. Rep.* 16(6), 8062–8068 (2017).
10. Psychogios N, Hau DD, Peng J *et al.* The human serum metabolome. *PLoS One* 6(2), e16957 (2011).
11. van der Valk J, Brunner D, De Smet K *et al.* Optimization of chemically defined cell culture media – replacing fetal bovine serum in mammalian *in vitro* methods. *Toxicol. Vitr.* 24(4), 1053–1063 (2010).
12. Baker M. Reproducibility: Respect your cells! *Nature* 537(7620), 433–435 (2016).

Single-cell analysis for drug development using convex lens-induced confinement imaging

Ndeye Khady Thiombane[1], Nicolas Coutin[1], Daniel Berard[2], Radin Tahvildari[2], Sabrina Leslie[2] & Corey Nislow*[,1]

ABSTRACT

New technologies have powered rapid advances in cellular imaging, genomics and phenotypic analysis in life sciences. However, most of these methods operate at sample population levels and provide statistical averages of aggregated data that fail to capture single-cell heterogeneity, complicating drug discovery and development. Here we demonstrate a new single-cell approach based on convex lens-induced confinement (CLiC) microscopy. We validated CLiC on yeast cells, demonstrating subcellular localization with an enhanced signal-to-noise and fluorescent signal detection sensitivity compared with traditional imaging. In the live-cell CLiC assay, cellular proliferation times were consistent with flask culture. Using methotrexate, we provide drug response data showing a fivefold cell size increase following drug exposure. Taken together, CLiC enables high-quality imaging of single-cell drug response and proliferation for extended observation periods.

METHOD SUMMARY

In this study, we use convex lens-induced confinement (CLiC) microscopy, which was originally developed for the study of single particles and biomolecules, and apply it to live cell imaging to detect fluorescently labeled cell compartments and compare the system to conventional imaging. We also performed an extended duration live-cell assay in CLiC by confining *Saccharomyces cerevisiae* yeast cells in well-defined pits in a flow cell and observing single-cell proliferation for 8 h. Finally, we assessed the effects of the antifolate drug methotrexate on cell morphology and mitochondria integrity by observing cells during drug exposure.

KEYWORDS

CLiC • dose–response • methotrexate • phenotypic screen • single cell • yeast

*[1]Pharmaceutical Sciences, 2405 Wesbrook Mall, University of British Columbia, Vancouver, BC, V6T1Z3, Canada; [2]Department of Physics, 214 Rutherford Physics Building, McGill University, 3600 rue University, Montreal, QC, H3A 2T8, Canada; *Author for correspondence: corey.nislow@ubc.ca*

BioTechniques 67: 210-217 (November 2019) 10.2144/btn-2019-0067

One of the driving forces in systems biology research is the emergence and development of new data-acquisition tools and technologies to better understand biological and biochemical mechanisms at the single-cell level. At present, most practical molecular and cell biology methods capture the average response of a cell sample population. However, results from these approaches can be misleading due to cellular heterogeneity. Such variation may arise from diverse genetic and nongenetic factors, including noise in gene expression. Factors that substantially define the amplitude of such noise include regulatory dynamics, transcription rates, genetic factors and intracellular copy numbers of molecules involved in the genetic network [1].

Single-cell heterogeneity is indeed a well-known phenomenon in microbial resistance and evolution studies, as well as in cancer research. For instance, most cancer cell lines display genomic alterations, as well as other forms of heterogeneity such as chromosomal instability [1,2]. Stochastic cellular process fluctuations, including the state, location, activity and concentration of polymerases, transcription factors and gene expression regulators, may also lead to diversification in an initially uniform cell population [3]. These variations can have a significant impact on the growth and environmental stress response of cells and cannot be captured using conventional cell biology methods. For instance, conducting a drug response analysis in yeast often requires recording its optical density ($OD_{600\ nm}$) at set time intervals over time. However, the recorded data are a bulk representation of the entire population and, as a consequence, may overlook fluctuations at the individual cell level that could lead to drug resistance [4].

The awareness of cell population heterogeneity and the importance of characterizing it have led to the emergence of a number of single-cell analysis tools such as fluorescence-activated cell sorting, microfluidic lab-on-a-chip and cellular microarrays. Microfluidics are a powerful, relatively recent innovation that are being applied for rapid antibiotic and antifungal susceptibility testing at a single-cell level, which can allow one to determine an isolate's drug susceptibility in less than 30 min [5,6]. A range of antibiotic and antifungal drugs (e.g., penicillins such as mecillinam, amoxicillin-clavulate ampicillin, sulfamethoxazole, and so on) have been investigated using microfluidic lab-on-a-chip, and the results emphasize the utility of this technique to identify individual cells that maintain their fast growth rate against a background of drug susceptible cells [5]. The impact of single-cell analysis techniques on drug discovery and drug resistance studies in recent years underscores the clear need for more techniques that are robust in capturing not only the cell-to-cell variations, but also to chart their real-time proliferation and the evolution of the same individual cells for long periods.

Here we introduce a novel approach for single-cell studies using the convex lens-induced confinement (CLiC) instrument [7] combined with flow cells containing embedded pits. CLiC is an imaging system that was primarily developed for the isolation and visualization of single molecules in a flow cell made of two glass layers (Figure 1A & B). The principle of CLiC is as follows: using a lens-rod perpendicular to the

focal plane, pressure is applied downward directly onto the flow cell. The resulting deformation of the flow cell confines molecules between the smooth glass surfaces and can load them into features such as pits, which are embedded in the surfaces (Figure 1B) [8,9]. This technique had been shown to be able to successfully confine and isolate diffusing [5] and interacting molecules [10–12] for long periods and improve fluorescent signal detection [7]. To date, CLiC has primarily been used to study materials, biomolecules and particles, with only limited information available regarding its suitability for live-cell investigations [13].

In this study, we used the yeast *Saccharomyces cerevisiae*, which is a well-known and extensively studied model organism used in the investigation of diverse eukaryotic cell biology. The insights gained from yeast are simplified but can be extrapolated into mammalian systems. Due to the high degree of conservation existing between yeast and mammalian genes (over 50% for essential genes), yeast is often used to understand the mechanisms of action of small molecules and drugs and to acquire preliminary data for drug discovery efforts [14–16]. Additional advantageous criteria make yeast an ideal model organism to benchmark the CLiC cell assay. These criteria include: its low level of genomic instability compared with cultured cells, its simple and low-cost growth requirements, and its short doubling time, which allows faster drug effects and pathway perturbation assessment. We therefore used yeast to validate the CLiC instrument for single-cell analyses, specifically comparing the CLiC imaging platform to a conventional microscope slide for fluorescent cell imaging, drug response studies and cell-proliferation observations.

MATERIALS & METHODS

Yeast cell propagation & staining

For localization experiments with fluorescent probes, we used BY4743 diploid cells (*MATa/MATα his3Δ1/his3Δ1 leu2Δ0/leu2Δ0 lys2Δ0/+ met15Δ0/+ ura3Δ0/ura3Δ0*) generated from a cross between BY4741 and BY4742 [17].

Vacuolar staining

We inoculated BY4743 cells in 3 ml YPD media and grew them overnight (~16 h) at 30°C. We subsequently adjusted the cell suspension to an $OD_{600\,nm}$ of 10, added 4 μM FM4–64 vacuolar stain in YPD and incubated on an interval mixer for 30 min at 30°C. We then removed the excess probe by centrifuging cells at 500×*g* for 1 min, aspirating the supernatant and washing cells twice in YPD before suspending in 1 ml YPD.

Nuclear DNA live cell staining

We stained BY4743 cells in mid-log phase with an $OD_{600\,nm}$ of 0.5 using 2.5 μg/ml final concentration of 4′,6-diamidino-2-phenylindole (DAPI) on an interval mixer for 30 min at 30°C. We then harvested the cell pellet by centrifugation at 500×*g* for 1 min, washed with 1× phosphate-buffered saline and resuspended in YPD for a final $OD_{600\,nm}$ of approximately 10.

Mitochondrial staining

Upon treatment of BY4743 cells with 2 mM methotrexate or 2% dimethyl sulfoxide

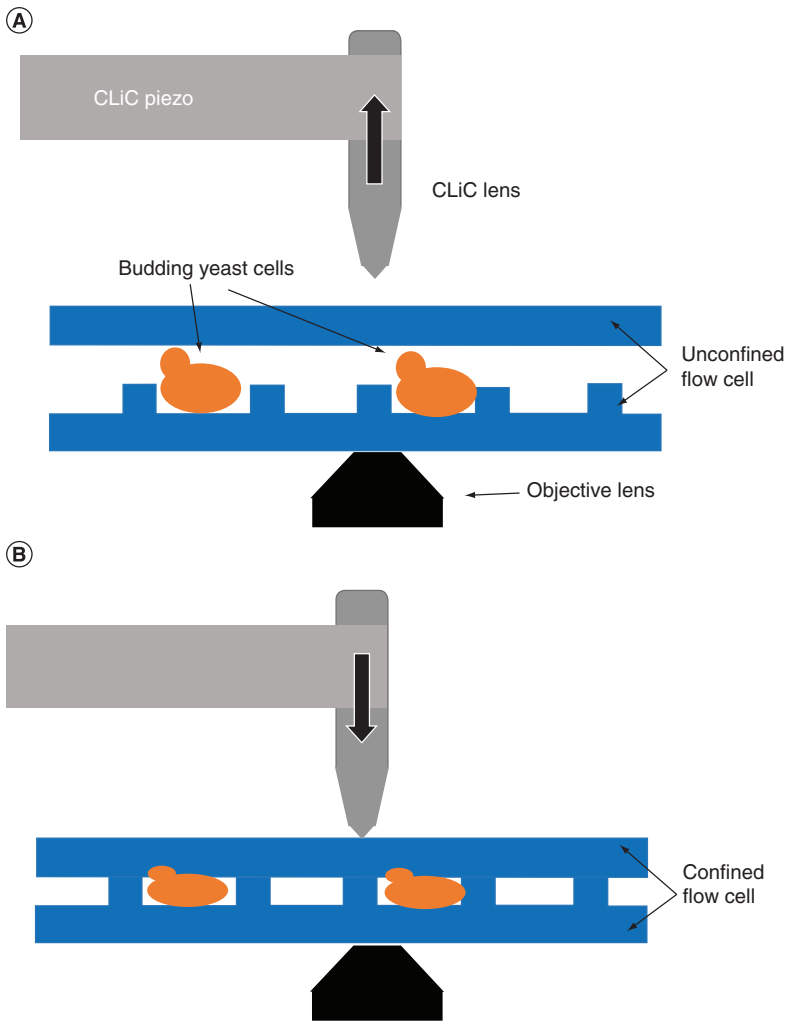

Figure 1. Convex lens-induced confinement instrument. (A) Representative schema of the CLiC instrument with yeast cells loaded into the unconfined flow cell that contains embedded pits. (B) Schematic representation of the CLiC instrument with the lens rod moving downward to confine the yeast cells into the flow cell pits.
CLiC: Convex lens-induced confinement.

▶ (DMSO) as a vehicle control for 20 h, we pelleted and resuspended cells in prewarmed (30°C) staining solution containing YPD media and 200 nM Mitotracker Red CMXRos. We subsequently incubated the cells at 30°C with shaking for 30 min in a thermomixer, pelleted and resuspended them in fresh YPD media prewarmed at 30°C.

CONVEX LENS-INDUCED CONFINEMENT

The CLiC instrument is composed of five major components assembled to allow confinement of single molecules or cells into embedded wells in the CLiC flow cell, which we refer to in this paper as pits. (i) The first component is a mounting stage that perfectly fits into an inverted microscope's main stage. (ii) The second component is a mounting chuck that holds the flow cell, enables fluid exchange and is inserted onto the mounting stage. (iii) The third and main part is the flow cell made of two thin glass coverslips. The bottom coverslip contains embedded wells and is attached to the upper flat coverslip by a 30-μm thick double-sided adhesive [11]. Cell samples can be loaded between the two layers through a fluidic access port. (iv) The fourth component is a piezo, which controls the y-axis of the lens rod. (v) Last is the lens-rod, which consists of a convex lens, mounted curved-side down, on a narrow rod. When lowered, the lens-rod pushes on the top coverslip, deforming it downward, which consequently restrains cells into the embedded wells. This instrument does not tether or stick down cells, but simply confines them. Cells can then be imaged following the microscope's standard protocols.

WIDE-FIELD MICROSCOPY

Image acquisition on microscope slide & processing

We used a 63× 1.4 NA oil-immersion objective mounted on a Zeiss (Oberkochen, Germany) Axiovert 200 m microscope, an Excelitas (MA, USA) X-Cite 120 LED light source and a Zeiss AxioCam HRm Rev.2 camera to capture images of cells in bright-field channel exposed for 10 ms under 4.0-V transmitted light. We used excitation and emission filters appropriate for FM4–64 (Cy3, excitation/emission: 515/640 nm), DAPI (excitation/emission: 359/461 nm) and Mitotracker Red (Cy3, excitation/emission: 579/603 nm) with 830 ms, 125 ms and 150 ms of exposure, respectively. Images were captured using the multi-dimensional acquisition setting on the AxioVision 4.8.2 software (Zeiss).

Image acquisition in flow cell & processing

For cell imaging using the Scopesys (QC, Canada) CLiC instrument, we loaded 5 μl of the stained cell suspension into the flow cell-containing embedded pits and imaged with the 63× oil-immersion objective as described above. We captured images in the brightfield channel using 100 ms exposure under 11.0 V transmitted light and in the DAPI or Cy3 fluorescent channels with acquisition settings identical to those used for imaging cells on a microscope slide.

Microscopy image analysis & fluorescent signal quantification

ImageJ software (with the Fiji plugin) was used to measure the 'area', 'integrated intensity' and 'mean gray value' of fluorescent cells [18,19]. We first selected the regions of interest (ROI) delineating every single cell on channel 1 (brightfield-transmitted channel) and subsequently performed fluorescent signal measurements on channel 2

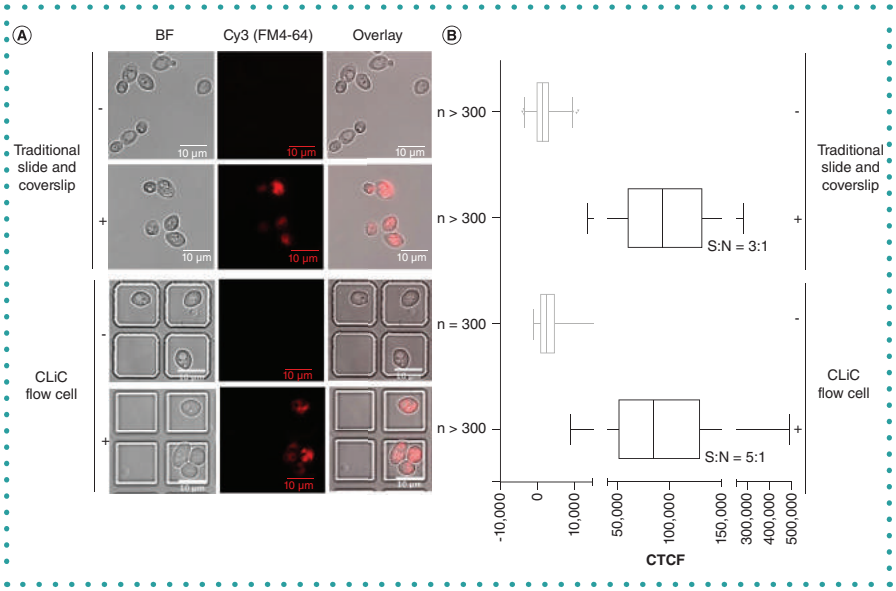

Figure 2. Corrected total cell fluorescence of FM4-64 stained cells under confinement in the convex lens-induced confinement instrument flow cell versus on a traditional microscope slide. (A) Representative images of BY4743 unstained (-) or stained with FM4-64 vacuolar stain (+) and captured under a traditional microscope slide or when confined in the CLiC flow cell. Imaging performed under BF channel and fluorescent channel (Cy3, FM4-64). (B) Box and Whisker plot of corrected total cell fluorescence distribution for n ≥ 300 cells per condition. BF: Brightfield; CLiC: Convex lens-induced confinement; CTCF: Corrected total cell fluorescence; S:N: Signal-to-noise ratio.

(fluorescent channel). For normalization, we measured an empty background area on the field of view and determined the corrected total cell fluorescence (CTCF) using the following formula:

$$\text{CTCF} = \text{Integrated Density} - (\text{Area of selected cell} \times \text{Mean fluorescence of background readings})$$

Cell proliferation under flask versus flow cell platform

For the growth comparison experiment, we used the *dfr1/DFR1* heterozygous deletion strain, derived from BY4743 [20]. This strain is deleted for a single copy of the enzyme dihydrofolate reductase, which is the established target of methotrexate [21].

Yeast growth in flasks

We propagated a cell suspension, characterized by an optical density measured at 600 nm ($OD_{600\ nm}$) of 0.25, in 50 ml YPD in a flask at 30°C for three generations, and performed readings with an Eppendorf (Hamburg, Germany) Biophotometer every 15 min.

Yeast growth in flow cell

We loaded 5 µl of a cell suspension with an $OD_{600\ nm}$ of 5 into a flow cell, and grew the cells at 30°C. To monitor and control the temperature of the flow cell environment, we used a silicon heat tracing cable and temperature sensor wrapped around the 63× oil-immersion objective. The Zeiss Axiovert 200 m microscope captured images of proliferating cells every 15 min for 8 h.

Viability assay

To prepare the samples for the spot assay, we grew BY4743 cells in the presence of 2.0, 1.0, 0.5 or 0.25 mM methotrexate, or 2% DMSO vehicle control for 20 h, normalized them to an $OD_{600\ nm}$ of 1 and transferred them to a 96-well plate. We subsequently performed fivefold serial dilutions on each sample, spotted them onto YPD agar by transferring 5 µl of each suspension, and grew the cells at 30°C for 48 h prior to image acquisition.

RESULTS & DISCUSSION

Fluorescent signal detection comparison in flow cell versus microscope slide

To study the ability to obtain fluorescent signals from live cells on the CLiC instrument and compare the data to that obtained from conventional microscope slides, we captured images of BY4743 cells stained with 4-µM FM4–64 vacuolar rim stain on a microscope slide and a CLiC flow cell under similar fluorescent settings. ▶

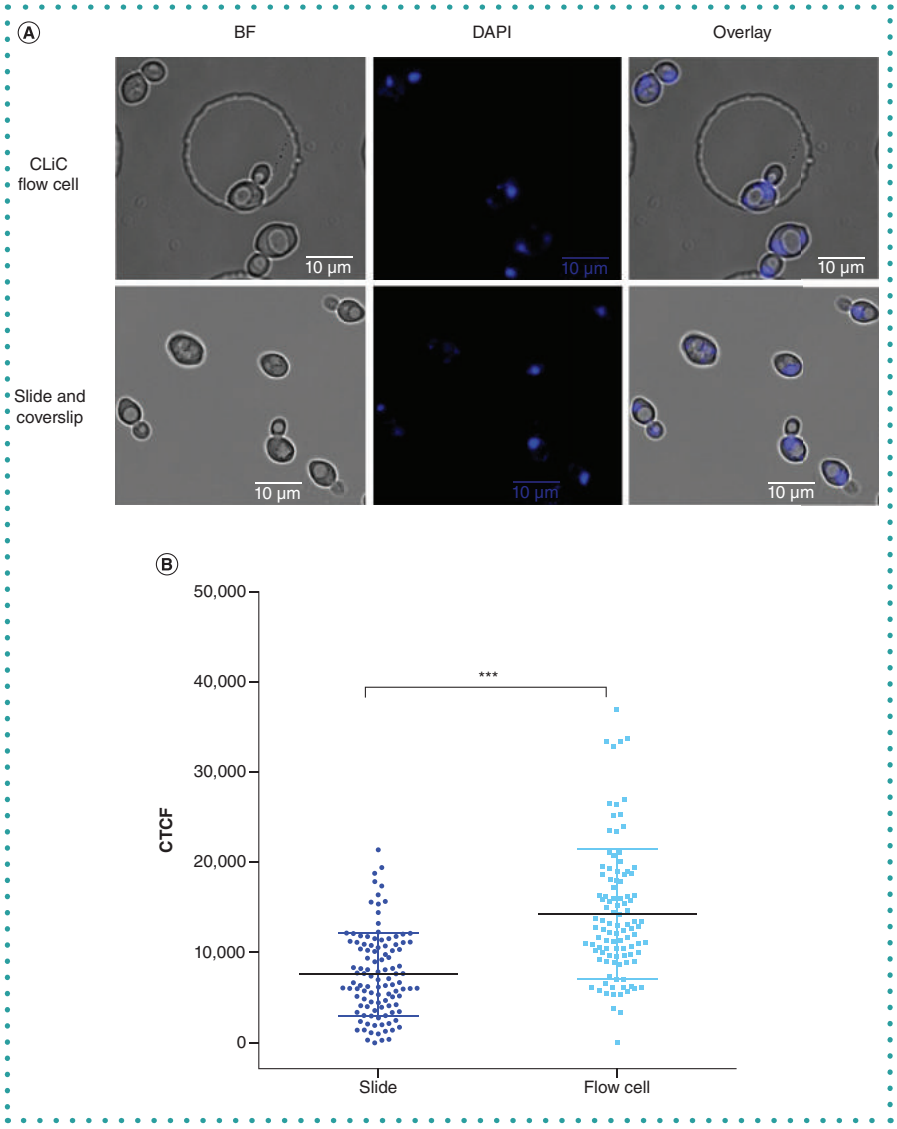

Figure 3. Corrected total cell fluorescence of DAPI-stained cells under confinement in flow cell vs on microscope slide. (A) DAPI-stained BY4743 cells captured under Brightfield (BF) and fluorescent (DAPI) channels. Imaging performed under flow cell confinement (top) and on a microscope slide (bottom). (B) Column scatter plot of CTCF of n ≈ 100 cells per condition. Image displays individual data (blue markers), their average (black horizontal lines) and standard deviation (blue error bars) for each condition. ***p < 0.05 under an unpaired two-tailed t-test.
BF: Brightfield; CLiC: Convex lens-induced confinement; CTCF: Corrected total cell fluorescence; DAPI: 4′,6-diamidino-2-phenylindole.

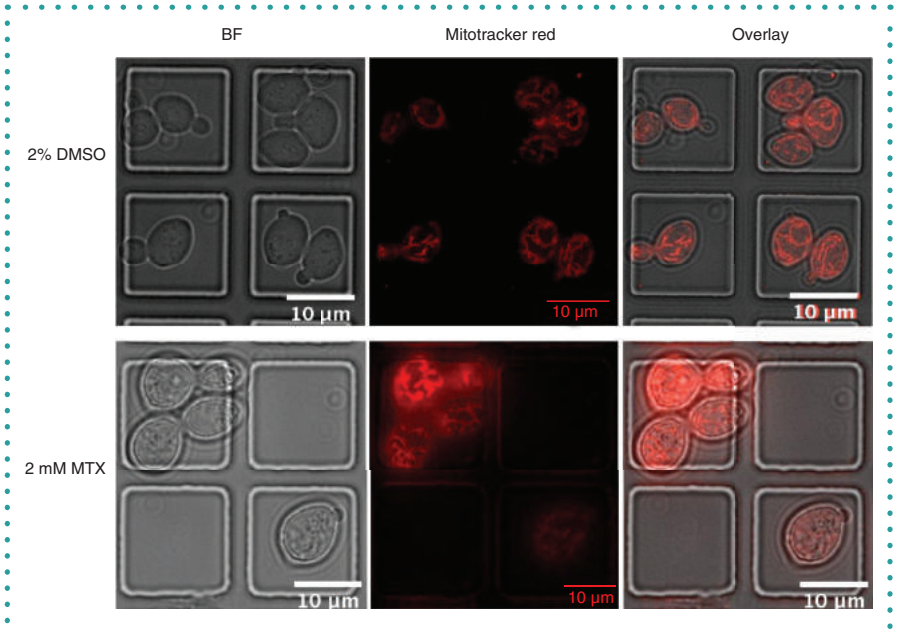

Figure 4. Mitochondria fluorescent imaging of methotrexate versus dimethyl sulfoxide-treated cells. Mitotracker-stained BY4743 cells treated for 20 h with 2% DMSO vehicle control (top) or 2 mM methotrexate (bottom) and captured in flow cells under Brightfield (BF) and Cy3 Fluorescent (Mitotracker Red™) channels.
BF: Brightfield; DMSO: Dimethyl sulfoxide; MTX: Methotrexate.

▶ An unstained BY4743 negative control sample was also analyzed. Both platforms detected fluorescent signals consistent with vacuolar rims in stained cells (Figure 2A). From visual inspection, the CLiC instrument captured the stained vacuolar rims with high contrast. Quantitatively, the average signal-to-noise ratio with CLiC was enhanced compared with the microscope slide, 5:1 versus 3:1, respectively (Figure 2B). The CTCF distribution of the stained samples on the two platforms were not significantly different; however, the distribution obtained with CLiC extended over a larger dynamic range of signals, highlighting the CLiC ability to detect higher signals (Figure 2B).

Signal detection of cells stained with 2.5 μg/ml DAPI for 30 min also demonstrated signal detection sensitivity differences between the CLiC flow cell versus the microscope slide. The average integrated fluorescence per stained cell was 10,517 for n = 110 cells visualized on a microscope slide compared with 17,192 for n = 104 cells imaged under confinement with CLiC. Under a student's two-tailed t-test, assuming equal variances between the samples, the distribution of signals was significantly higher in CLiC flow cells ($p < 0.05$) (Figure 3A & B).

The fluorescence signal detection comparison validated the ability of the CLiC instrument to image cellular compartments with high resolution and precision (Figures 2A & 3A). Additionally, DAPI fluorescent signal detection was greater with increased sensitivity in CLiC flow cells compared with microscope slides. This higher sensitivity could be explained by the decrease in the vertical volume of the cells when squeezed, allowing higher background signal rejection and better fluorophore detection [8].

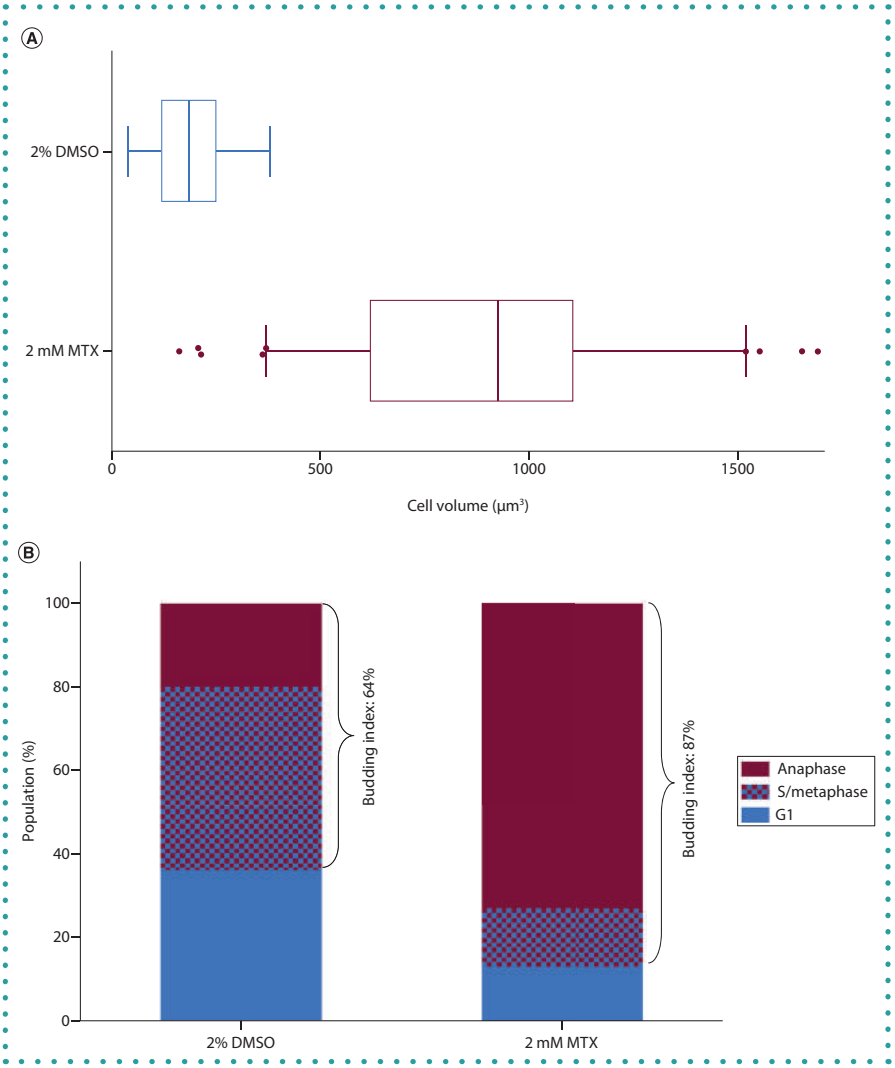

Figure 5. Cell size comparison of methotrexate- versus 2% dimethyl sulfoxide-treated cells. (A) Box and Whisker plot representation of the cell volume distribution of n = 100 BY4743 cells treated for 20 h with 2 mM MTX versus the control treated with 2% DMSO. (B) Population percentage of cells in anaphase, S/metaphase and G1 phase of the cell cycle and the deduced budding indices of MTX- versus DMSO-treated cells.
DMSO: Dimethyl sulfoxide; MTX: Methotrexate.

Methotrexate effect on yeast in flow cells

After validating that the CLiC instrument was suitable for fluorescence imaging, this platform was used to study the effect of the antifolate drug methotrexate, a dihydrofolate reductase inhibitor, on BY4743 cells [21]. In yeast, the dihydrofolate reductase enzyme is encoded by *DFR1* and is required for tetrahydrofolate biosynthesis. This enzyme is functionally conserved between yeast and human cells; that is, the viability and antifolate resistance of a yeast *dfr1* mutant can be rescued by expression of the human enzyme DHFR [20]. Inhibition by methotrexate results in fitness defects of yeast cells, which is likely due to the adverse effects of the drug on nucleic acid and amino acid biosynthesis [21]. *Dfr1* has previously been reported to be necessary for mitochondrial morphology maintenance in the presence of 10 μg/ml doxycycline [22]. We therefore hypothesized that inhibiting *Dfr1* with methotrexate would have an impact on the mitochondrial structure of the cells.

BY4743 cells treated with 2.0 mM methotrexate for 20 h showed no major mitochondrial structural damage based on observations of Mitotracker Red stained cells (Figure 4). Methotrexate treatment did, however, result in a drastic morphology change in BY4743 cells. Treated cells were almost fivefold larger in volume than the 2% DMSO-treated cells, with an average volume ± SEM of 900.8 ± 35.41 μm^3 (n = 100) compared with 185.9 ± 8.168 μm^3 (n = 100), respectively. Most strikingly, methotrexate had a pronounced effect on cell cycle progression. When assayed for budding index [23], we found a 1.36-fold increase in the population budding index of n ≈ 200 treated cells (87%) compared with the DMSO-treated control (64%) (Figure 5A & B). When treated with methotrexate, 73% of the cell population was found in the telophase/ ▶

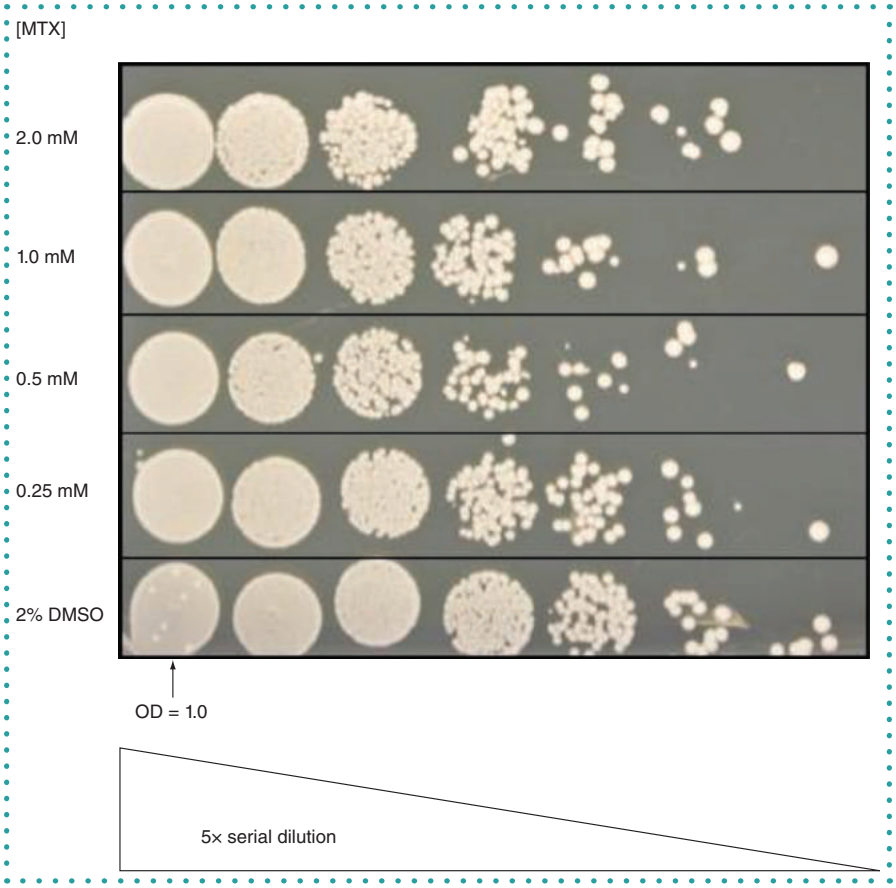

Figure 6. Viability assay on methotrexate-treated BY4743 cells. Cells treated for 20 h with 2.0 mM, 1.0, 0.5 or 0.25 mM MTX, or 2% DMSO, spotted onto YPD agar and incubated for 48 h are displayed on this image. From left to right, spots correspond to 5× serially diluted cells starting with a cell suspension with an $OD_{600\,nm}$ of 1.0.
DMSO: Dimethyl sulfoxide; MTX: Methotrexate.

▶ anaphase stage of the cell cycle compared with 16% for the DMSO-treated control, suggesting that methotrexate either caused mitotic arrest or delayed mitotic exit [24].

To further investigate methotrexate's effect on BY4743 cell viability, cells treated with 2.0 mM methotrexate for 20 h were spotted onto YPD agar for 48 h. To our surprise, despite their dramatic morphology change, budding alterations and growth inhibition (Figures 3, 4A & 4B), methotrexate treatment did not exhibit a major impact on the cell viability following recovery on YPD in the absence of methotrexate (Figure 6). This observation suggests that methotrexate is cytostatic and not cytocidal under the conditions tested.

Yeast cell growth study in flow cell

To investigate whether the CLiC instrument is useful for observing live cell growth, cells in log phase were re-suspended in YPD, adjusted to an $OD_{600\,nm}$ of 5 and loaded into a flow cell confined by CLiC. Observations recorded at 30°C using brightfield illumination (refer to 'Materials & methods' for temperature control). Confined single cells had an initial doubling time that ranged from 1 h 30 min to 2 h 30 min (Figure 7A & B), with an average of 2 h 15 min, which was consistent with the first doubling time recorded when the same strain is grown in flasks (Figure 7C & D, Supplementary Video 1). With the CLiC instrument and a cell suspension with an initial $OD_{600\,nm}$ of 5 prior to loading, we were able to reproducibly observe two cell doublings (Supplementary Videos 1–4). This assay validated the use of the CLiC instrument for single cell proliferation studies and could be used to observe the real-time drug response variabilities among a cell population.

This study validated the use of the CLiC instrument for accurate single-cell investigations. We observed that fluorescently labelled cells had improved background rejection (i.e., lower nonspecific fluorescence), which resulted in a higher signal-to-noise ratio within the flow cell compared with the microscope slides. The platform detected cellular DNA with higher precision and sensitivity, which also applied to other cellular compartments (vacuoles and mitochondria in this study). Most importantly, the CLiC instrument allows robust growth of yeast cells during single-cell confinement and observation in real time. This device could be used in future studies to observe the real-time emergence of resistant drug suppressors as well as yeast and bacterial persistence [4], a phenomenon whereby, upon drug treatment, a small surviving subgroup regrows into a population that has not acquired any resistance and is still as sensitive to the treatment. This device also holds great potential for routine use in fields such as cancer research, where single-cell variabilities and instabilities are especially important for developing effective therapies. While we focused on yeast cells as a model system in this work, previous studies performed on adherent Chinese hamster ovary (CHO-K1) cells demonstrated the feasibility of customizing the CLiC instrument with a cytoindentor, which allows precise indentation and imaging of live mammalian cells without significantly changing their oxidative stress or causing detectable impacts on cell fitness [13]. To manipulate cell adherence, the flow cells could be customized and coated with fibronectin as previously demonstrated [13]. Further optimization and validation studies will, however, be needed for application on drug response and proliferation studies of mammalian cell lines. As with any single-cell technique, we acknowledge that drug response analysis on mammalian cells might be challenging with the CLiC instrument and not completely reflect their response *in vivo*. Nevertheless, single-cell technologies are essential to understand cell-to-cell variations in a heterogeneous population. Additionally, with the open architecture of the flow cell, it is possible to rapidly modify the environment for growth optimization (e.g., a stage-top incubator system enclosing the CLiC instrument can be used to maintain the temperature and humidified CO_2 for mammalian cells). Based on the data collected during this investigation, we suggest that CLiC is a useful new tool for single-cell

Ⓐ

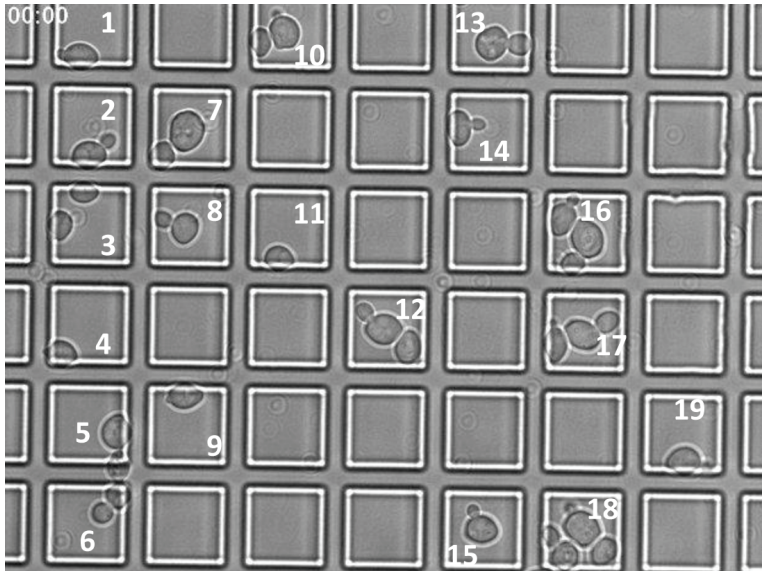

Ⓑ

Cells in flow cell pit #	Average doubling time
1	1 h 30 min
2	2 h 15 min
3	2 h 30 min
4	1 h 45 min
5	1 h 30 min
6	2 h 00 min
7	2 h 15 min
8	2 h 15 min
9	1 h 45 min
10	1 h 45 min
11	1 h 45 min
12	1 h 45 min
13	1 h 30 min
14	1 h 30 min
15	2 h 15 min
16	1 h 45 min
17	1 h 45 min
18	1 h 45 min
19	1 h 30 min
Average	**2 h 15 min**

Ⓒ

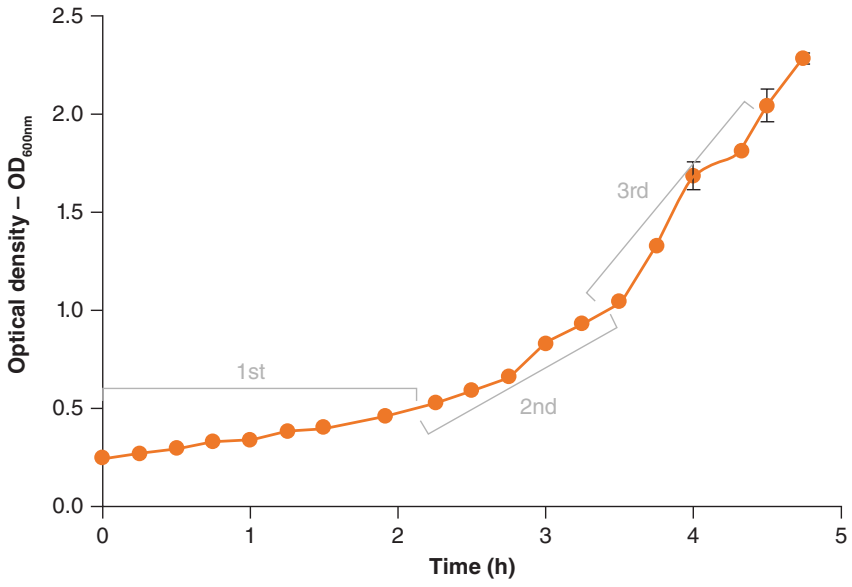

Ⓓ

Cell growth in flask	
Doubling time	**Time (h)**
1st	≃2 h 10 min
2nd	≃1 h 18 min
3rd	≃1 h 05 min

Figure 7. Yeast cell growth comparison in convex lens-induced confinement instrument flow cell versus flask. (A) Timepoint 00:00 image of cells confined in convex lens-induced confinement flow cell and grown at 30°C in YPD for 8 h (refer to Supplementary Video 1 for complete growth cycle) and numeric labeling of pits containing cells. (B) Average doubling time of cells in Figure 7A numerically labelled pits. (C) Growth curve of cells grown in flask at 30°C with shaking in YPD, n = 2. (D) First, second and third doubling time of cells grown in flasks and deduced from Figure 7C.

biology and is well-suited for the study of single-cell heterogeneity in drug response.

FUTURE PERSPECTIVE

While extraordinary progress has been made in developing and implementing high-throughput, high-content screening platforms with powerful analysis software, there are still obstacles to wide adoption of real-time cellular imaging. These challenges can be broadly grouped into: hardware, data collection and analysis, and cost and ease of use. With regards to the hardware issue, the current imaging platforms can be categorized as: i) traditional microscopes that have been automated; ii) automated, dedicated imagers; iii) plate readers with single-cell resolution; and iv) flow cytometers. Each of these platforms is capable of single-cell resolution, but some are unable to re-identify and track individual cells over time (e.g., plate readers and cytometers), and even dedicated imagers struggle to faithfully track large numbers of individual cell trajectories.

The flow cell and CLiC instrument therefore fills several important gaps; ▸

▶ it is a relatively inexpensive accessory that can be added to any inverted microscope and, most importantly, the confinement afforded by CLiC, combined with flow cells containing ordered features, allows one to track individual cell trajectories over an extended period in real-time in physiological conditions. This capability is key to understanding the individual cell's response to drugs or other perturbations. This is especially true when performing high-resolution phenotyping. The improved signal that can be obtained from fluorescently labeled molecules should aid in the subcellular localization of ligands in single cells.

While generating arrays of cells within an imaging field is not a new idea [25], CliC provides a flexible (the only constraints are in the initial flow cell design) means to achieve living cell microarrays that are unique in that no tethers are required to keep cells within the focal plane over extended periods. The next challenges with CLiC as applied to phenotypic screens will be to increase the capacity of the flow cells and to introduce automation, for example, for loading flows cells and liquid exchanges.

SUPPLEMENTARY DATA

To view the supplementary data that accompany this paper please visit the journal website at: www.future-science.com/doi/suppl/10.2144/btn-2019-0067

AUTHOR CONTRIBUTIONS

NKT, NC, DB, SL and CN designed and supported the microscopy experiments; NKT acquired and analyzed the data; RT developed and fabricated the flow cells. NKT, SL and CN wrote the manuscript.

ACKNOWLEDGMENTS

We thank ScopeSys (www.scopesys.ca) for access to the CLiC technology package. The project was supported by a grant from the CFI to CN.

FINANCIAL & COMPETING INTERESTS DISCLOSURE

SL acknowledges the NSERC Discovery, Accelerator, and Idea to Innovation programs as well as McGill University for research funding and support. SL and DB have a financial interest in ScopeSys, the company which is commercializing CLiC imaging. The authors have no other relevant affiliations or financial involvement with any organization or entity with a financial interest in or financial conflict with the subject matter or materials discussed in the manuscript apart from those disclosed.

No writing assistance was utilized in the production of this manuscript.

REFERENCES

1. Abdallah BY, Horne SD, Stevens JB *et al.* Single cell heterogeneity: why unstable genomes are incompatible with average profiles. *Cell Cycle* 12(23), 3640–3649 (2013).
2. Heng HH, Bremer SW, Stevens JB *et al.* Chromosomal instability (CIN): what it is and why it is crucial to cancer evolution. *Cancer Metastasis Rev.* 32(3–4), 325–340 (2013).
3. Elowitz MB, Levine AJ, Siggia ED, Swain PS. Stochastic gene expression in a single cell. *Science* 297(5584), 1183–1186 (2002).
4. Balaban NQ, Merrin J, Chait R, Kowalik L, Leibler S. Bacterial persistence as a phenotypic switch. *Science* 305(5690), 1622–1625 (2004).
5. Baltekin Ö, Boucharin A, Tano E, Andersson DI, Elf J. Antibiotic susceptibility testing in less than 30 min using direct single-cell imaging. *Proc. Natl Acad. Sci. USA* 114(34), 9170–9175 (2017).
6. Dai J, Hamon M, Jambovane S. Microfluidics for antibiotic susceptibility and toxicity testing. *Bioengineering (Basel)* 3(4), E25 (2016).
7. Leslie SR, Fields AP, Cohen AE. Convex lens-induced confinement for imaging single molecules. *Anal. Chem.* 82(14), 6224–6229 (2010).
8. Berard D, McFaul CM, Leith JS, Arsenault AK, Michaud F, Leslie SR. Precision platform for convex lens-induced confinement microscopy. *Rev. Sci. Instrum.* 84(10), 103704 (2013).
9. Berard DJ, Shayegan M, Michaud F, Henkin G, Scott S, Leslie S. Formatting and ligating biopolymers using adjustable nanoconfinement. *Appl. Physics Lett.* 109(3), 033702 (2016).
10. Scott S, Xu ZM, Kouzine F *et al.* Visualizing structure-mediated interactions in supercoiled DNA molecules. *Nucleic Acids Res.* 46(9), 4622–4631 (2018).
11. Scott S, Shaheen C, McGuinness B *et al.* Single-molecule visualization of the effects of ionic strength and crowding on structure-mediated interactions in supercoiled DNA molecules. *Nucleic Acids Res.* 47(12), 6360–6368 (2019).
12. Shayegan M, Tahvildari R, Metera K, Kisley L, Michnick SW, Leslie SR. probing inhomogeneous diffusion in the microenvironments of phase-separated polymers under confinement. *J. Am. Chem. Soc.* 141(19), 7751–7757 (2019).
13. Jia B, Wee TL, Boudreau CG *et al.* Parallelized cytoindentation using convex micropatterned surfaces. *BioTechniques* 61(2), 73–82 (2016).
14. Simon JA, Bedalov A. Yeast as a model system for anticancer drug discovery. *Nat. Rev. Cancer* 4(6), 481–492 (2004).
15. Giaever G, Nislow C. The yeast deletion collection: a decade of functional genomics. *Genetics* 197(2), 451–465 (2014).
16. Lee AY, St Onge RP, Proctor MJ *et al.* Mapping the cellular response to small molecules using chemogenomic fitness signatures. *Science* 344(6180), 208–211 (2014).
17. Brachmann CB, Davies A, Cost GJ *et al.* Designer deletion strains derived from *Saccharomyces cerevisiae* S288C: a useful set of strains and plasmids for PCR-mediated gene disruption and other applications. *Yeast* 14(2), 115–132 (1998).
18. Schneider CA, Rasband WS, Eliceiri KW. NIH Image to ImageJ: 25 years of image analysis. *Nat. Methods* 9(7), 671–675 (2012).
19. Schindelin J, Arganda-Carreras I, Frise E *et al.* Fiji: an open-source platform for biological-image analysis. *Nat. Methods* 9(7), 676–682 (2012).
20. Wong LH, Sinha S, Bergeron JR *et al.* Reverse chemical genetics: comprehensive fitness profiling reveals the spectrum of drug target interactions. *PLoS Genet.* 12(9), e1006275 (2016).
21. Lagosky PA, Taylor GR, Haynes RH. Molecular characterization of the *Saccharomyces cerevisiae* dihydrofolate reductase gene (DFR1). *Nucleic Acids Res.* 15(24), 10355–10371 (1987).
22. Altmann K, Westermann B. Role of essential genes in mitochondrial morphogenesis in *Saccharomyces cerevisiae*. *Mol. Biol. Cell* 16(11), 5410–5417 (2005).
23. Zettel MF, Garza LR, Cass AM *et al.* The budding index of Saccharomyces cerevisiae deletion strains identifies genes important for cell cycle progression. *FEMS Microbiol. Lett.* 223(2), 253–258 (2003).
24. Bi E, Park HO. Cell polarization and cytokinesis in budding yeast. *Genetics* 191(2), 347–387 (2012).
25. Jonczyk R, Kurth T, Lavrentieva A, Walter JG, Scheper T, Stahl F. Living cell microarrays: an overview of concepts. *Microarrays (Basel)* 5(2), (2016).

Sponsored Paper
Application Forum
BioTechniques

New method for measuring fluorescence microscopy illumination

www.CoolLED.com

The intensity of microscope illumination systems has a significant impact on the brightness and contrast of images and therefore data quality. Optimal illumination has been surrounded by complex, confusing and sometimes inaccurate measurements and terminology, but a new method is putting a stop to this.

INTRODUCTION

LED illumination systems for fluorescence microscopy present a modern alternative to mercury and metal halide lamps, affording a range of benefits in terms of cost, functionality and the environment. They are now recognised as a mature technology, but one topic lags behind. The industry has not yet settled on a standardised approach for measuring intensity. Without a quantitative baseline, it is impossible to normalise performance requirements and configure system improvements.

We propose correct terminology alongside an industry standard methodology allowing microscopists to easily quantify the intensity where they need it, at the sample plane. These meaningful data will allow direct comparison of all illumination systems and microscope configurations, enabling scientists to optimise their system to suit their needs.

WHAT ARE WE MEASURING?

When product specifications or discussions surrounding fluorescence microscopy illumination mention illumination intensity, it is not often clear exactly what this refers to. Firstly, let us clarify what is meant by the term intensity:

- **Intensity:** Power per unit area. It can refer to any kind of power (electrical, heat, light etc.) and is measured in W/m^2.
- **Radiant intensity:** Not to be confused with intensity, this measures power per unit steradian (i.e. power per unit cone angle of emission) in W/sr.
- **Power:** Measured in W, this value is largely meaningless since it does not consider how effectively power is focused onto a given surface area.
- **Irradiance:** The radiant power at a surface per unit area, measured in mW/mm^2. This is our preferred term and eliminates any confusion between intensity and radiant intensity.

WHERE TO MEASURE IRRADIANCE?

Some manufacturers quote power from the LED chip, which provides the most impressive sounding statistic. Others might quote light at the end of a liquid light guide. However, these numbers are misleading since they are not representative of the light reaching the sample (Figure 1).

The only significant light is that hitting the sample to excite the fluorophore and the only meaningful place to measure the optical power of an illumination system is therefore at the sample plane. Measuring this irradiance in mW/mm^2 provides accurate values which can form a baseline for the comparison of microscope configurations and illumination systems.

A PROTOCOL FOR MEASURING IRRADIANCE

At CoolLED we quote irradiance values at the sample plane of a typical fluorescence microscope, for example an Olympus BX51 microscope with a 10x (0.3 NA) or 40x (0.85 NA) objective. ▸

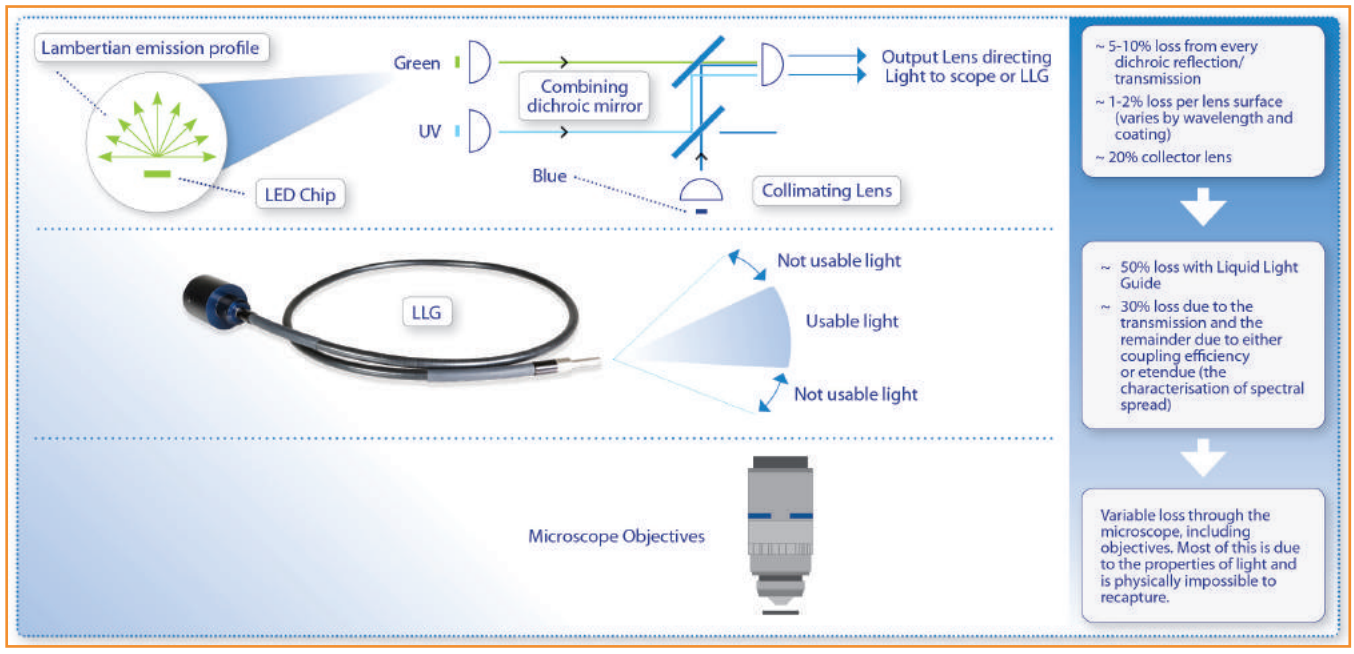

Figure 1: Why measure irradiance at the sample plane. As light travels from the LED to the sample, a portion is lost at each step, for example the Liquid Light Guide (LLG). Measuring light at any point upstream of the sample plane will therefore result in misleading data.

1. Remove the excitation filter from the cube and replace the dichroic mirror with an 100% mirror. This means we are measuring light at the sample plane unaffected by optical filters.

2. When measuring power at the sample plane, use a calibrated optical spectrometer. We also use an integrating sphere or cosine corrector to acquire a power result that is independent of the ray's angle of incidence on the detector.

3. Close the microscope field stop until the field stop image on the sample plane is just outside the field of view. This ensures that light hitting the sample plane will only consist of light rays that are within the field of view for the objective in use, as seen by an eyepiece or camera with a given field number. This removes light that could be escaping from the objective but not making it into the field of view, achieving a more precise measurement by removing any variability caused from the field stop.

4. Calculate irradiance from the power reading using the surface area at the sample plane:
   a. Determine the diameter in mm = Field number (fn) / objective magnification (Mo).
   b. Calculate surface area in mm^2 using the equation πr^2.
   c. Use the surface area and power reading to express irradiance in mW/mm^2.

SUMMARY

As LED illumination technology has evolved, so has the discussion surrounding what is commonly referred to as 'illumination intensity'. The confusion stemming from varying terminology and measurement techniques has created a barrier to identifying which systems truly deliver the most light to the sample plane. We now therefore strongly recommend the use of meaningful irradiance values measured at the sample plane using our standardised protocol, to both compare and boost irradiance when required.

LED irradiance is continuing to improve and we are confident this trend will continue in the coming years. We look forward to enabling the microscopy community to independently monitor these developments with a robust and standardised approach for quantifying irradiance.

For more information, visit www.CoolLED.com

CoolLED
Simply Better Control

BioTechniques

Affimers as anti-idiotypic affinity reagents for pharmacokinetic analysis of biotherapeutics

Hope Adamson[1], Amanda Nicholl[2], Christian Tiede[1], Anna A Tang[1], Alex Davidson[2], Helen Curd[2], Alex Wignall[2], Robert Ford[2], James Nuttall[2], Michael J McPherson[1], Matt Johnson[2] & Darren C Tomlinson*[,1]

ABSTRACT

Therapeutic antibodies are the fastest growing class of drugs in the treatment of cancer, and autoimmune and inflammatory diseases that require the concomitant development of assays to monitor therapeutic antibody levels. Here, we demonstrate that the use of Affimer nonantibody binding proteins provides an advantage over current antibody-based detection systems. For four therapeutic antibodies, we used phage display to isolate highly specific anti-idiotypic Affimer reagents, which selectively bind to the therapeutic antibody idiotype. For each antibody target the calibration curves met US Food and Drug Administration criteria and the dynamic range compared favorably with commercially available reagents. Affimer proteins therefore represent promising anti-idiotypic reagents that are simple to select and manufacture, and that offer the sensitivity, specificity and consistency required for pharmacokinetic assays.

METHOD SUMMARY

Anti-idiotypic Affimer proteins that bind therapeutic antibodies are introduced as alternative affinity reagents to traditional antibodies. A nonbridging ELISA assay for pharmacokinetic analysis of these biotherapeutics in serum is developed.

LAY ABSTRACT

The fastest growing class of drugs are derived from human proteins that are modified to target the processes that cause the disease. Owing to the presence of similarly structured proteins in the blood, it is currently extremely difficult to specifically detect the therapy over the levels of normal human proteins in patients. However, it is vitally important to be able to monitor the levels of these therapies in the blood in order to ensure patients receive appropriate dosages. This paper describes the use of artificially derived proteins, called Affimers, to detect four commonly used therapies. Overall, we demonstrate that Affimer reagents provide a valid approach for monitoring dosing of these types of drugs.

KEYWORDS

Affimer reagents • anti-idiotypic • biotherapeutics • diagnostics • pharmacokinetics

*[1]School of Molecular & Cellular Biology, Astbury Centre for Structural Molecular Biology, University of Leeds, Leeds, LS2 9JT, UK; [2]Avacta Life Sciences, Ash Way, Thorp Arch Estate, Wetherby, LS23 7FA, UK; *Author for correspondence: d.c.tomlinson@leeds.ac.uk*

BioTechniques 67: 261-269 (December 2019) 10.2144/btn-2019-0089

Monoclonal antibody (mAb) drugs have been a resounding clinical and commercial success, applied across a range of therapeutic areas with a particularly significant impact in the treatment of cancer, autoimmune and inflammatory diseases [1–4]. High-interaction surface area binding gives mAbs greater specificity and so lower off-target, toxic effects compared with small-molecule drugs [3]. By the end of 2017, 68 mAbs or biosimilars were in clinical use and the market exceeded US$98 billion in sales, having grown every year since 2013 [5]. This trend looks set to continue; therapeutic antibodies are the fastest growing class of drugs and in 2017 a record number of ten were granted their first marketing approvals in the USA or EU [1,6]. Further acceleration in mAb approvals is expected, with a considerable pipeline of over 550 antibodies in clinical development and over 50 in late-stage clinical trials at the end of 2017 [1,6].

The advance in antibody therapeutics requires a parallel development of pharmacokinetic (PK) assays that can monitor mAb concentration and distribution in patients to guide dosage during clinical trials and practice [7,8]. In PK assays, the natural antigen may not be the optimal mAb capture reagent if it is expensive, hazardous or not reliably available, or when measurements of antigen-bound drug are required [7,9,10]. As therapeutic antibodies are highly humanized and present among up to a million-fold excess of human IgG in serum, it is particularly challenging to generate capture reagents that avoid cross-reactivity [10–12]. Anti-idiotypic reagents that bind to the unique idiotopes of the antibody variable regions are required to specifically target the therapeutic antibody in PK assays [10,13]. Specific anti-idiotypic reagents are also required for immunogenicity assays [7,14–16], affinity purification [17], analytical studies [18] and vaccine development [19–21].

Antibodies are important as successful anti-idiotypic reagents, but their selection and production can be complex and certain limitations exist [7,10–12,18,22,23]. With traditional immunization methods it is hard to select for specific binding to the antibody idiotype, as binding to other regions of the humanized mAb target molecules results in serum cross-reactivity [7,23,24]. Extensive screening may be required and long development times may not match the pace of drug development [7,12,25]. mAb technology can, however, be used to more easily generate anti-idiotypic reagents. Antibody production is also dependent on animals or mammalian cell culture to ensure correct folding, glycosylation and cysteine oxidation [23,26]. This complex manufacture is expensive and some antibodies have lot-to-lot reproducibility issues, meaning extensive validation is required to ensure consistency throughout the drug evaluation process [27–29]. ▶

Table 1. Number of clones in the primary screen.

Target	Clones screened by iQue	Hits sequenced	Unique sequences	Clones selected for ELISA tests
Trastuzumab	360	Top 96	21	21
Rituximab CDR mAb	192	192	102	17
Adalimumab CDR mAb	192	192	15	15
Ipilimumab CDR mAb	192	192	113	16

CDR: Complementary-determining region; mAb: Monoclonal antibody.

▶ mAbs will not have significant lot-to-lot variation but there is still a desire for complementary or alternative reagents to overcome some limitations. Alternatives include anti-idiotypic antibody fragments (antigen-binding fragments [Fabs]) [7], single-chain variable fragments [11,30], camelid nanobodies [31], shark variable new antigen receptors [10] and llama single-domain antibodies [32], and when directed selection and recombinant production is implemented reagents can often have improved consistency and specificity.

Currently, there is a particular interest in developing antibody mimetics based on nonimmunoglobulin scaffold proteins with randomized, selectable binding regions, as they can be engineered to have desirable properties [23,33–35]. Many scaffolds exist [23]; anti-idiotypic DARPins [22] and monobodies [18] have been generated, but not validated as reagents in PK assays. A promising alternative binding protein is the Affimer reagent, which is based on a cystatin scaffold with two variable, nine amino acid loops that allow high-affinity binding to a range of target molecules [36,37]. Affimer reagents have been used in numerous assays from studying protein function to diagnostics [37–47] and exhibit key characteristics that make them potentially suitable as anti-idiotypic reagents [45]. They can be rapidly identified, incorporating the use of negative selection [48] to direct binding towards the idiotype and reduce cross-reactivity. Additionally, the small, stable scaffold can be reproducibly produced at high yield in *E. coli*, to give a reliable, consistent supply [36,37,48]. Here we confirm the suitability of Affimer binders as anti-idiotypic reagents; Affimer reagents against four therapeutic antibodies have been generated, characterized and validated for use in PK assays. Lot-to-lot reproducibility is evaluated and comparisons made with anti-idiotypic Fabs to assess the advantages of Affimer reagents in terms of specificity, detection range and flexibility of assay format.

MATERIALS & METHODS

Target QC

The target antibodies were trastuzumab (anti-HER2; Roche, Switzerland), rituximab CDR (complementary-determining regions) mAb (anti-CD20-hIgG4-mab14; Invivogen, CA, USA), adalimumab CDR mAb (anti-TNFα-hIgG1-mab1; Invivogen) and Ipilimumab CDR mAb (Anti-CTLA4-hIgG1-mab1; Invivogen). Each target antibody concentration was checked by measuring A_{280} and dividing by the extinction coefficient. A 1-μg aliquot of each was analyzed by SDS-PAGE (Bolt 4–12% Bis-Tris; Life Technologies, CA, USA) to determine quality and purity. A 100-μg aliquot of each target mAb was then biotinylated by incubating in a 10× excess of EZ-Link Sulfo-NHS-LC-Biotin (21327, 1 mg no-weigh format; Thermo Fisher Scientific, MA, USA) for 2 h on ice. Free biotin was removed by buffer exchange, the concentration measured and a 1-μg aliquot analyzed by SDS-PAGE (as above) to check purity. Biotinylation was then confirmed by western blot analysis; 200 ng of biotinylated target mAb was separated by SDS-PAGE (as above) and transferred onto nitrocellulose using an iBlot system (Thermo Fisher Scientific). The membrane was then blocked using 1× TBS (50 mM Tris, 150 mM NaCl; both Sigma, MO, USA) + 3% bovine serum albumin (BSA; Sigma) pH 7.4 for 1 h at room temperature with gentle agitation on a roller mixer. It was then washed for 3 × 5 min using TBS-T (1× TBS + 0.05% Tween 20; Sigma) and detected using a 1:10,000 dilution of streptavidin horseradish peroxidase (HRP; Abcam, UK) in 1× TBS + 3% BSA pH 7.4 for 1 h at room temperature. The membrane was then washed as described previously and protein detected using Amersham ECL detection reagent (GE Healthcare Life Sciences, IL, USA), analyzed by chemiluminescence using a G:Box gel doc system (Syngene, India).

Phage display

Phage display was performed as described previously [48]. Briefly, targets were submitted to three rounds of phage display, with deselection against antibodies of similar isotype used to remove cross-specific binders from the phage output. For trastuzumab, a therapeutic antibody cocktail (rituximuab, Humira, Avastin and human IgG1) was used for deselection. For rituximab, adalimumab and ipilimumab CDR mAbs, deselection was performed with anti-CTLA4 hIgG4, anti-CTLA4 hIgG1 and anti-TNFa hIgG1 antibodies, respectively.

Primary screen

Following phage display, the Affimer coding regions resulting from panning rounds 2 and 3 were subcloned into pEtLECTRA vectors: cHA-His6-Cys for trastuzumab and cHA-His6 for the other mAbs. Colonies were picked (Table 1) and Affimer proteins were expressed in 1-ml cultures and purified using Ni-NTA resin (Qiagen, Germany). A primary screen was performed using the iQue Screener (Intellicyte, NM, USA). Biotinylated targets and deselection targets were immobilized onto QSH DevScreen iQue beads following the manufacturer's instructions (Intellicyte). Affimer protein concentrations were normalized to 2.5 μg/ml and 10 μl added to 10-μl prepared beads in a 384-well plate. Alexa488-conjugated anti-HA antibody (BioLegend, CA, USA) was used to quantify Affimer reagent binding. Clones were sequenced to identify unique sequences (Table 1).

Affimer protein expression

Medium-scale recombinant Affimer protein production (50–100 ml) was performed to generate 1–2 mg of Affimer material, which was purified by Ni-NTA magnetic beads (Qiagen). 5 ml LB (made using LB [Lennox] EZ mix powder; Sigma) containing 50 μg/ml kanamycin sulphate (Sigma) and 1% (w/v) glucose (Sigma) was inoculated with a sequence-checked glycerol stock for the Affimer reagent of interest and grown for 16 h at 37°C, 220 rpm. 1 ml of starter culture was used to inoculate 100 ml Terrific Broth (Melford, UK) containing 50 μg/ml kanamycin sulphate and cultures were grown at 37°C, 220 rpm until an OD_{600} of 0.6–0.8 was reached. The temperature was then reduced to 25°C, IPTG (Sigma) added to a final concentration of 1 mM and cultures incubated at 25°C, 220 rpm overnight. Cells were harvested by centrifugation (10,000×g, 10 min, 4°C) and resuspended in Affimer purification lysis buffer (pH 8.0) comprising 50 mM sodium phosphate (Sigma), 500 mM sodium chloride (VWR, PA, USA), 30 mM imidazole (Sigma), 10% (v/v) SoluLyse (Genlantis, SA, USA), 25 U/ml Benzonase Nuclease HC (Millipore, MA, USA) and for the trastuzumab Affimer reagent 5 mM TCEP (Generon, UK) was also added. The resuspended cells were sonicated for 5 min (10 s on, 10 s off), then the insoluble fraction was removed by centrifugation (10,000×g, 30 min, 4°C) and the supernatant filtered (0.45 μm) to remove any remaining insoluble material. Cleared lysates were purified with Ni-NTA magnetic beads (Qiagen) using an automated process (washed in 50 mM imidazole, eluted in 400 mM imidazole). Purified trastuzumab Affimer reagents were buffer exchanged into pH 6.5 CBS (100 mM sodium citrate tribasic dehydrate + 150 mM sodium chloride; both Sigma) + 5 mM TCEP + 0.02% sodium azide (Severn Biotech, UK). Other Affimer reagents were buffer exchanged into pH 7.4 PBS (100 mM sodium phosphate + 150 mM sodium chloride; both Sigma) + 0.02% sodium azide. The concentration (A280/extinction coefficient) and purity (1 μg aliquot analyzed by SDS-PAGE) of all purified Affimers was measured as described previously.

ELISA validation

Selected Affimer binders (Table 1) were tested by ELISA. Affimer proteins were passively adsorbed onto Maxisorp plates at 200 nM overnight at 4°C. Plates were washed with 1× PBS-T (PBS diluted from 10× PBS; Gibco + 0.05% Tween 20; Sigma), using 3 × 300 μl per well on a BioTek (VT, USA) 405-plate washer. Wells were then blocked with 1× casein-blocking buffer (diluted in PBS from 10× casein-blocking buffer; Sigma) for 2 h at room temperature with gentle agitation. Plates were washed as previously and incubated with biotinylated target (at target dependent dilution) for 1 h at room temperature with gentle agitation. Plates were washed again and bound target was detected using a 1:10,000 dilution of streptavidin poly-HRP (Pierce, WI, USA) for 1 h at room temperature with gentle agitation and visualized using tetramethylbenzidine (TMB; Surmodics, MN, USA). TMB incubation time was target dependent, usually 5–10 min, and ODs were read at 450 nm and 630 nm (reference wavelength).

Affimer binders selected from the validation ELISA were then tested in a sandwich ELISA. Affimer reagents were passively adsorbed onto Maxisorp plates at 1 μg/ml overnight at 4°C. Plates were washed and blocked as described previously before incubation with titrated target (twofold dilution from 2000 ng/ml) for 1 h at room temperature with gentle agitation. Plates were washed again and bound target was detected with a 1:100,000 dilution of HRP-conjugated anti-hIgG antibody (Bethyl, TX, USA) for 1 h at room temperature with gentle agitation and visualized using TMB (Surmodics). TMB incubation time was target dependent, usually 5–10 min, and ODs were read at 450 nm and 630 nm (reference wavelength).

Assay optimization

The sandwich ELISA protocol was used to test selected Affimer proteins for specificity, lot-to-lot variation and full curve metrics.

A modified sandwich ELISA protocol was used for Fabs (anti-Trastuzumab HCA168, anti-Rituximab HCA186 and anti-Adalimumab HCA202; BioRad, CA, USA). They were passively adsorbed onto Maxisorp plates at 5 μg/ml overnight at 4°C, washed as described previously and blocked with 5% BSA in PBS-T (the manufacturer recommended blocking). Plates were washed again then the titrated target series was incubated for 1 h at room temperature with gentle agitation before a final wash. Bound target was detected with a 1:10,000 dilution of mouse anti-human IgG (Fc) CH2 domain antibody (anti-hFc; BioRad) for 1 h at room temperature with gentle agitation and visualized using QuantaBlu (following manufacturer's protocol; Thermo Fisher Scientific).

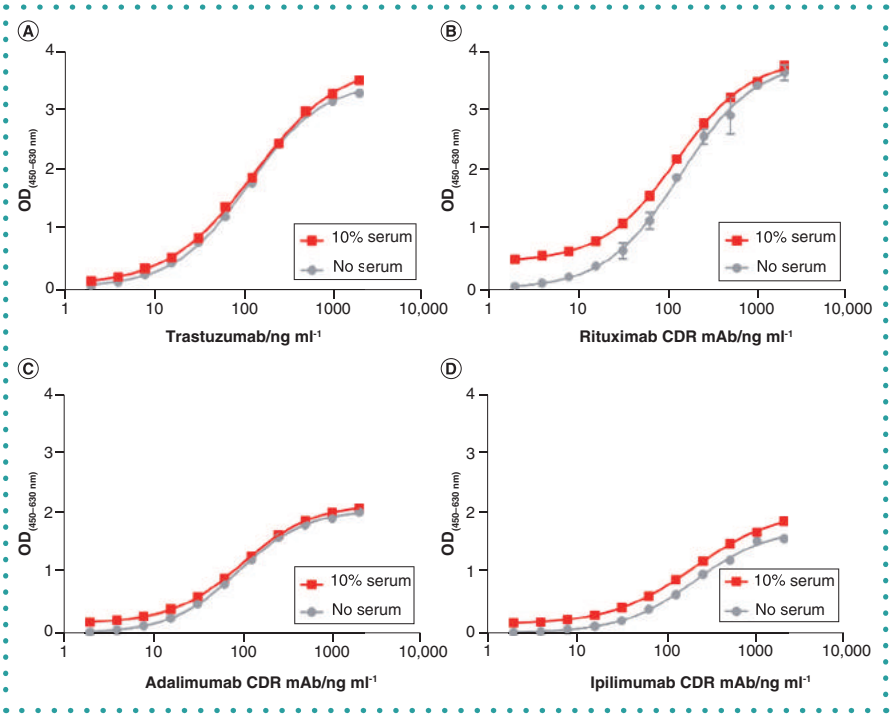

Figure 1. Sandwich ELISA dose response curves for target therapeutic antibodies with (A) anti-trastuzumab (B) anti-rituximab CDR mAb, (C) anti-Adalimumab CDR mAb and (D) anti-ipilimumab CDR mAb Affimer reagent capture surfaces. Detection of each target therapeutic antibody was compared in buffer (gray) and 10% human serum (red). Anti-hIgG-HGF was used as detection reagent, with TMB substrate visualization read at 450 nm (minus 630 nm reference). Data points are the mean of triplicate measurements and error bars indicate standard deviation from the mean. NB: the majority of the error bars are so small as to be occluded by the data point symbol.
CDR: Complementary-determining region; mAb: Monoclonal antibody.

Flexibility of detection methods was tested using the sandwich ELISA protocol with the following minor adaptations: the two generic antibodies (anti-hIgG; Bethyl at 1:100,000 and anti-hFc; BioRad at 1:10,000) used the protocol as described except that visualization was with QuantaBlu. The anti-hIgG Affimer reagent (0.5 μg/ml) was pre-incubated with a 1:15,000 dilution of streptavidin-HRP (Abcam) in blocking buffer before addition to test plate for detection (1 h at room temperature with gentle agitation) and visualization with TMB.

RESULTS & DISCUSSION

Affimer reagent selection

An Affimer phage display library [36] was screened against four therapeutic antibodies: trastuzumab (Herceptin) and mAbs containing the CDR corresponding to the parental therapeutics rituximab (Rituxan), adalimumab (Humira) and ipilimumab (Yervoy). Screening was performed in three successive rounds against biotinylated target mAbs. Each target underwent SDS-PAGE to assess the molecular weight and purity and biotinylation was confirmed by western blot analysis. A negative selection procedure [48] was used to direct Affimer binding towards the antibody idiotype and deselect against the antibody isotype. Small amounts of isotype-specific antibody were premixed with the phage library in the second and third panning rounds, to block cross-reactive Affimer binders and selectively isolate specific anti-idiotypic Affimer reagents. Outputs from the phage panning were subcloned, recombinantly produced and purified in a small-scale automated process. A high-throughput primary screen was performed using the bead-based iQue screener (Intellicyt), with target and deselection targets immobilized onto different beads, such that selective Affimer binders with no cross-reactivity were identified. Clones were sequenced and a subset found to be unique. Of these, the highest affinity binders identified from iQue screening were selected for medium-scale (50–100 ml) protein production and purification, prior to further ELISA validation. The number of clones analyzed from the primary screen is summarized for each target in Table 1.

An ELISA was used to validate the Affimer proteins as capture reagents for the biotinylated antibody targets. The best-performing Affimer reagents were then tested in a sandwich format, using an Affimer capture surface for the nonbiotinylated mAb target and HRP-conjugated anti-human IgG antibody (anti-hIgG-HRP) as a detection reagent. Based upon the results of this screen, a lead candidate Affimer reagent for each target was chosen for further characterization. The lead Affimer candidate was selected to have the greatest target specificity and a binding strength optimal for the required assay range.

Performance characterization of Affimer reagents in PK assay

A sandwich ELISA was developed to assess the performance of the selected anti-idiotypic Affimer reagents in quantifying therapeutic antibody concentrations. The calibration range of the assay is 1.95–2000 ng/ml, corresponding to a serum concentration of 0.0195–20 μg/ml with samples diluted 1:10. This exemplifies the potential of Affimer binders as critical PK assay reagents, with the scope for clinically relevant serum concentrations to be measured if samples are diluted further and curves run in more diluted matrix [49–53]. The anti-idiotypic Affimer reagent was used as capture reagent for the target mAb, detection was with anti-hIgG-HRP and visualization with 3,3′, 5,5″-TMB as the HRP substrate. In this assay format each Affimer reagent detected its target mAb across a broad dynamic range (Figure 1). PK assays aim to measure the target therapeutic in human serum samples, so require minimal sample matrix effects; that is, minimal variation in assay performance due to the serum matrix in which the assay is performed. A sample matrix effect was observed in the detection of the rituximab CDR mAb in 10% human serum (Figure 1B), noted as an increase in background absorbance relative to measurements in buffer. For all other targets, minimal sample matrix effects were observed and each Affimer reagent displayed comparable detection of the target mAb in 10% human serum as

Table 2. Calibration curve accuracy and precision metrics.					
		Trastuzumab	Rituximab CDR mAb	Adalimumab CDR mAb	Ipilimumab CDR mAb
Quantifiable range (ng/ml)	ULOQ	1000	1000	1000	1000
	LLOQ	ca. 8	ca. 2	ca. 4	ca. 15
Inter-assay	% CV	2.3–6.2	2.0–19.4†	1.4–7.1	2.7–11.4
	% recovery	98.1–104.5	95.8–104.6	98.4–106.1	94.4–110.9
Intra-assay	% CV	2.8–24.9†	0.7–19.5	1.2–17.3†	0.3–12.0
	% recovery	96.2–109.6	84.0–122.3†	95.4–112.7	91.7–122.6†

†Values approaching FDA limits obtained at a limit of quantification.
CDR: Complementary-determining region; LLOQ: Lower limit of quantification; mAb: Monoclonal antibody; ULOQ: Upper limit of quantification.

shown in buffer (Figure 1). This confirms the success of the selection protocols in generating anti-idiotypic Affimer reagents that specifically detect clinically relevant mAb concentrations within a human sample matrix. The robustness of Affimer reagent performance in the presence of serum overcomes any need for advance sample preparation.

Target specificity of the anti-idiotypic reagents within patient sample matrices is crucial to ensure the efficacy of the assay, as the predominance of natural antibodies in the matrix may give rise to inaccurate measurements if any cross-reactivity exists. In the sandwich assay format, each Affimer reagent was highly specific in binding its therapeutic antibody target, showing no cross-reactivity in the presence of high concentrations (1 mg/ml) of alternative mAbs, which contain highly homologous constant domain regions to the other therapeutic antibodies and human IgGs (Figure 2). This highlights the value of the deselection protocols in driving binding towards the idiotype and demonstrates the high specificity of the isolated Affimer reagents.

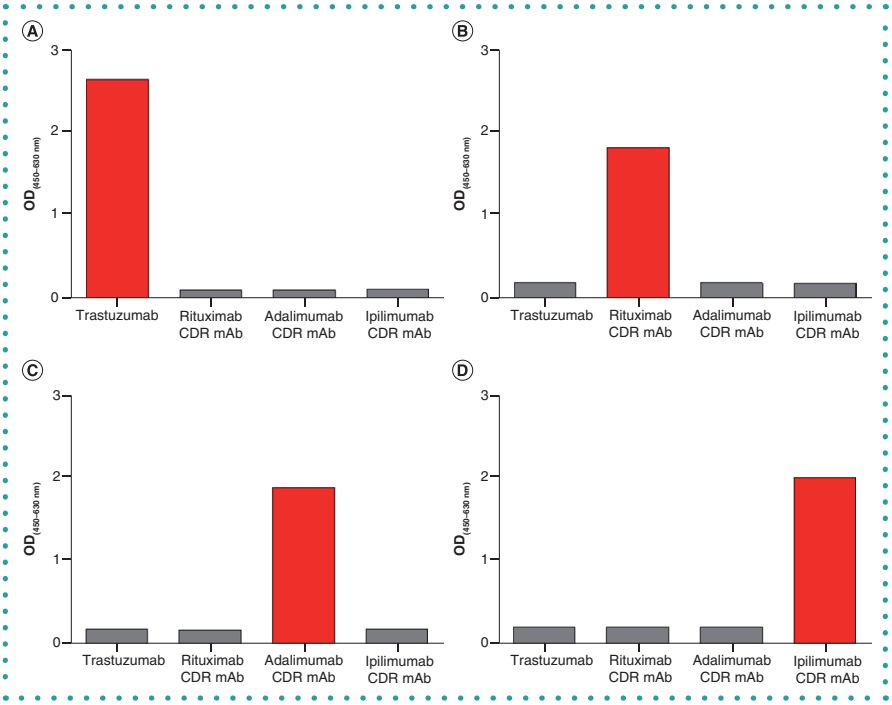

Figure 2. Specificity of therapeutic antibody detection in a sandwich ELISA using (A) anti-trastuzumab, (B) anti-rituximab CDR mAb, (C) anti-adalimumab CDR mAb and (D) anti-ipilimumab CDR mAb Affimer reagent capture surfaces. For each capture surface, detection of 1 mg/ml trastuzumab, rituximab CDR mAb, adalimumab CDR mAb and ipilimumab CDR mAb was compared in a 10% human serum matrix. Anti-hIgG-HRP was used as detection reagent, with TMB substrate visualization read at 450 nm (minus 630 nm reference).
CDR: Complementary-determining region; mAb: Monoclonal antibody.

Affimer PK assay calibration curves assessed against regulatory criteria

The performance of the calibration curves for each anti-idiotypic Affimer sandwich assay was assessed using section III, B, 2 of the US FDA criteria for bioanalytical method validation [54]. Calibration curves were assessed in terms of the accuracy and precision of mAb quantification within a 10% human serum matrix. Triplicate measurements at each nominal concentration (1.95–2000 ng/ml as twofold dilutions) of target were performed and a four-parameter logistic regression was fitted as a calibration curve. For each measurement, an interpolated concentration was then back-calculated from this curve. Intra-assay accuracy was determined by percentage recovery; the mean interpolated concentration as a percentage of the nominal concentration. Intra-assay precision was determined by the coefficient of variation (% CV); the standard deviation of the interpolated concentration as a percentage of the mean. This was repeated in a total of three separate experiments and the local means used to calculate inter-assay accuracy (% recovery) and precision (% CV). Each of the calibration curves for the four anti-idiotypic Affimer reagents meet the following FDA performance requirements; at least 75% and a minimum of six non-zero standards (inside ▶

Table 3. Anti-Trastuzumab Affimer batch accuracy and precision metrics.

Trastuzumab batch comparison					
Calibration range (ng/ml)		Inter-batch		Intra batch	
LLOQ	ULOQ	%CV	%Recovery	%CV	%Recovery
Ca. 8	1000	0.9–13.7	99.0–117.9†	2.2–20.0†	92.8–120.1†

†Values approaching FDA limits obtained at a limit of quantification.
LLOQ: Lower limit of quantification; ULOQ: Upper limit of quantification.

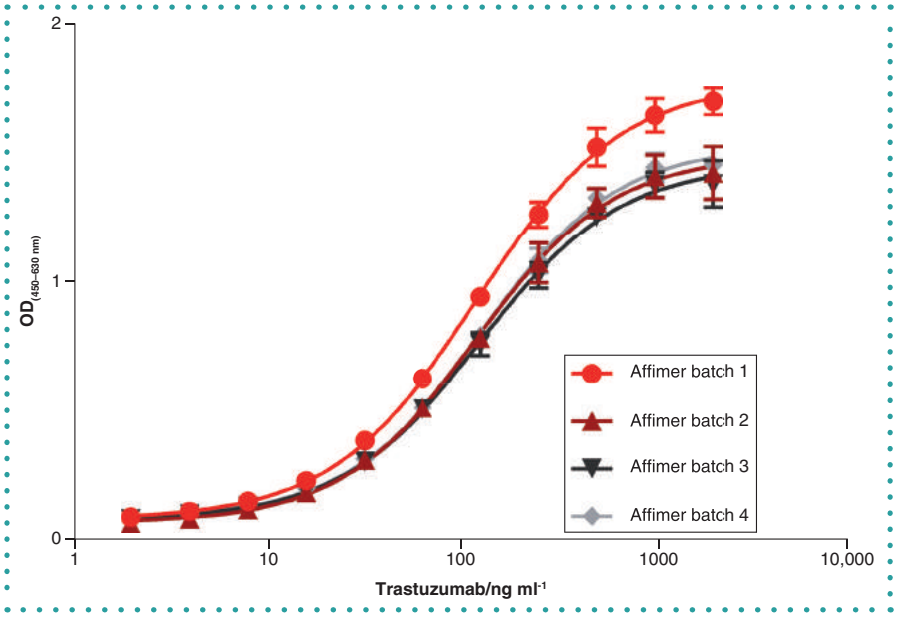

Figure 3. Lot-to-lot reproducibility of the anti-trastuzumab Affimer reagent as a capture surface in a sandwich ELISA. For four separate lots of anti-trastuzumab Affimer capture reagent the dose–response curves of trastuzumab in a 10% human serum matrix are compared. Anti-hIgG-HRP was used as detection reagent, with TMB substrate visualization read at 450 nm (minus 630 nm reference). Data points are the mean of triplicate measurements and error bars indicate standard deviation from the mean.

▶ the anchor points) have intra-assay and inter-assay calibration metrics of ≤20% CV and 80–120% recovery, with ≤25% CV and 75–125% recovery at the lower and upper limits of quantification (LLOQ/ULOQ) (Table 2) [54]. The LLOQ and ULOQ are the lowest and highest amount of analyte that can be quantitatively determined with acceptable precision and accuracy, giving the quantifiable range for each therapeutic mAb.

The quantifiable range of ipilimumab CDR mAb is comparable to that of a commercially available ELISA kit (10–1000 ng/ml) [55]. The other Affimer ELISAs offer a wider quantifiable range than commercially available ELISA kits for trastuzumab (11–300 ng/ml), rituximab (3–300 ng/ml) and adalimumab (30–1000 ng/ml) [56–58]. As the anti-idiotypic Affimer-based assay calibration curves meet accuracy and precision standards over wide detection ranges, this reduces the need for dilutions and repetitions, allowing for a wider range of samples to be analyzed within a single assay. Furthermore, this is achieved with just a single specific capture reagent and universal detection format, rather than requiring two separate specific anti-idiotypic reagents, as in the case of many PK bridging assays [24]. Antibodies are not limited to the bridging format but sufficiently high-quality reagents are required.

Consistent lot-to-lot reproducibility in the performance of Affimer reagents

Once validated for use in PK assays, it is important that a reliable and consistent supply of the anti-idiotypic reagent is available over the course of clinical development and usage. Anti-idiotypic antibodies can suffer from poor lot-to-lot reproducibility; therefore, extensive standardization may be required between lots to ensure assay performance is maintained [12,25]. This can lead to delays in the drug development process. Affimer reagents should offer low lot-to-lot variability due to their simple and robust bacterial manufacturing process. The reproducibility of the anti-trastuzumab Affimer binder was assessed as an example of lot-to-lot consistency in these reagents. Four separate lots were manufactured and compared by analyzing the consistency of the sandwich ELISA calibration curves (Figure 3) in terms of accuracy and precision.

With each Affimer lot, triplicate measurements of 1.95–2000 ng/ml trastuzumab (twofold dilution series) were made in 10% human serum (Figure 3) and concentrations then back-calculated from the calibration curve. Although the curve for lot 1 was slightly higher than the other three assessed, the interpolated values of each curve (intra-curve), as well as the mean of all four curves (inter-curve), met the criteria for accuracy and precision, within the previously validated quantifiable range (7.8–1000 ng/ml) (Table 3). This confirms lot-to-lot consistency in assay performance and demonstrates the high reproducibility of the Affimer reagent. Anti-idiotypic Affimer proteins therefore offer the assurance of supply required for critical reagents in the bioanalysis of potential therapeutics, preventing delays due to extensive lot-to-lot normalization.

Comparison of Affimer- & Fab-based PK assay performance

Anti-idiotypic Fabs are alternative reagents that can be selected *in vitro* and produced recombinantly [11,59]. The selected anti-idiotypic Affimer reagents were compared with equivalent Fab reagents, as capture

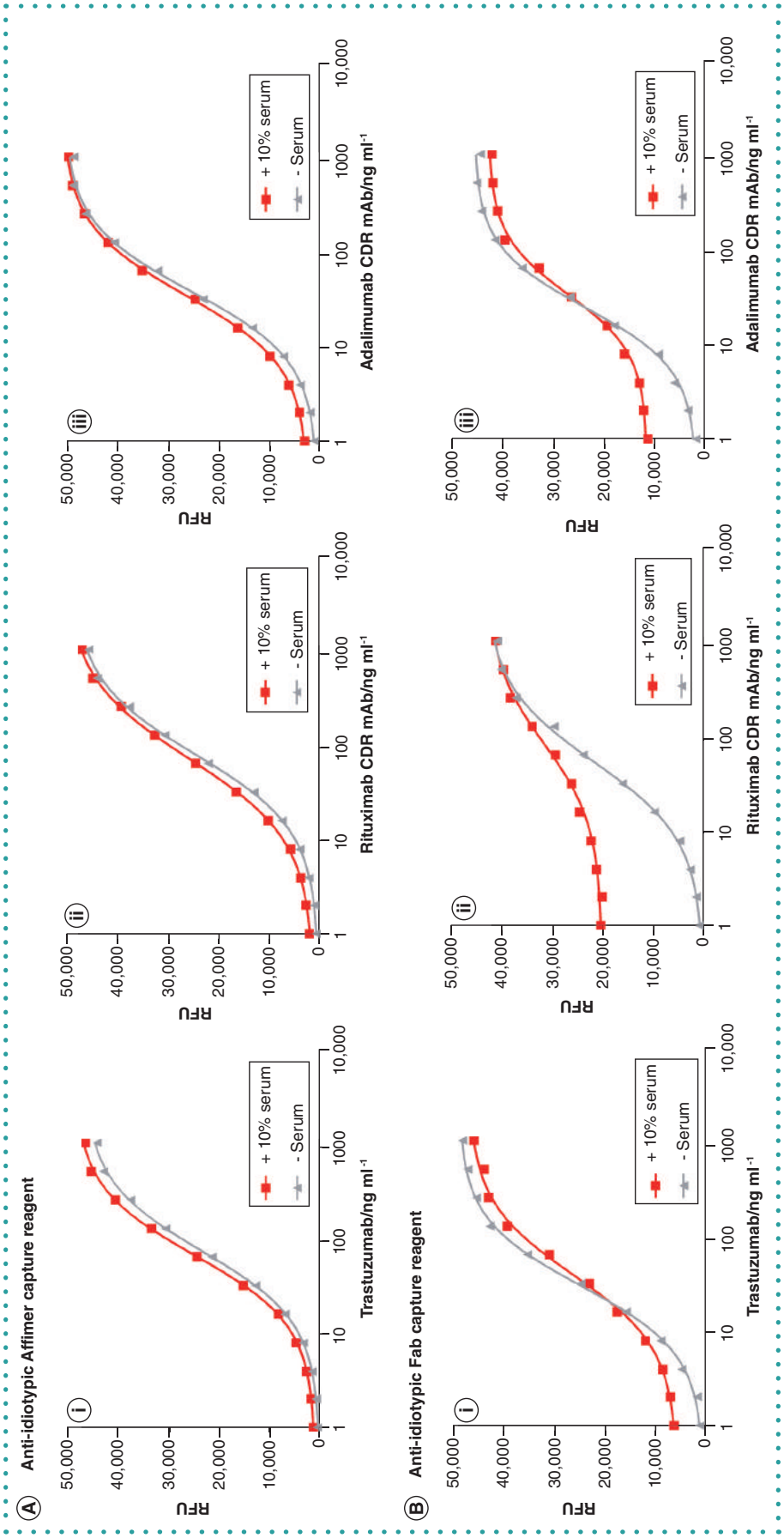

Figure 4. Comparison of (A) anti-idiotypic Affimer reagents and (B) anti-idiotypic Fabs as capture reagents for (i) trastuzumab (ii) rituximab CDR mAbs and (iii) adalimumab CDR mAbs in a sandwich ELISA. Each anti-idiotypic Affimer capture reagent was coated at 1 μg/ml (70 nM) and each anti-idiotypic Fab coated at 5 μg/ml (96 nm). Dose–response curves were obtained for the target therapeutic antibody in buffer (gray) and a 10% human serum matrix (red). Anti-hFc-HRP was used as detection reagent, with fluorogenic QuantaBlu substrate visualization.
CDR: Complementary-determining region; Fab: Antigen-binding fragment; mAb: Monoclonal antibody.

reagents for trastuzumab, rituximab CDR mAbs and adalimumab CDR mAbs, in a sandwich ELISA (Figure 4). Affimer proteins were coated at 1 μg/ml and Fabs at 5 μg/ml, to generate approximately equivalent molar concentrations of capture reagent (~70 nM and 96 nM, respectively). An Fc specific detection reagent, HRP-conjugated anti-human IgG (Fc) CH_2 domain antibody (anti-hFc-HRP), was used to prevent cross-reactivity with the Fab and the fluorogenic substrate QuantaBlu was used for visualization. Using this detection reagent, each Affimer capture reagent achieved a broad dynamic range for target detection with no clear sample matrix effects observed in 10% human serum (Figure 4A). The Fab capture reagents displayed reduced dynamic ranges for the detection of each target (Figure 4B). Greater sample matrix effects were observed in 10% human serum with the anti-adalimumab Fab and particularly the anti-rituximab Fab, compared with the equivalent Affimer binder (Figure 4B, ii & iii). This reduces the dynamic range of the Fab reagents still further in this assay format and may lead to inaccurate analysis in patient samples due to serum cross-reactivity issues.

The anti-idiotypic Affimer reagents therefore exhibit increased target specificity relative to the Fabs. A single capture Affimer reagent offers such specificity that a humanized therapeutic antibody can be detected in a background of human IgGs in serum, using a universal anti-human FC (anti-hFc) detection antibody. The Fab capture surface offers insufficient specificity for the use of a universal detection ▶

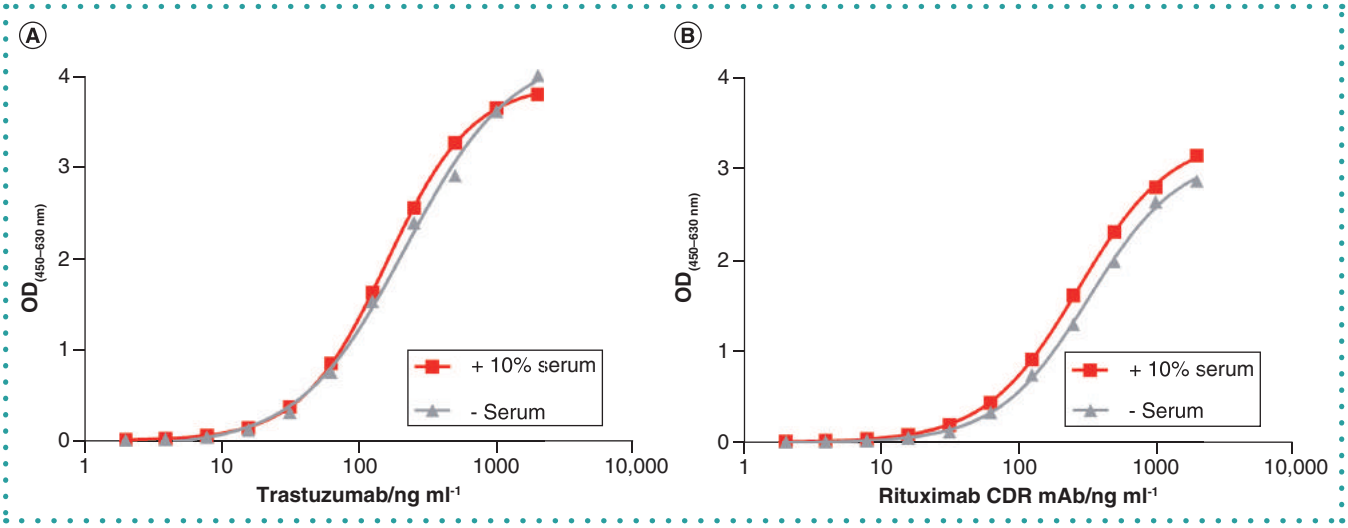

Figure 5. Sandwich ELISA dose response curves using anti-hIgG Affimer as detection reagent with (A) anti-trastuzumab and (B) anti-rituximab CDR mAb Affimer reagent capture surfaces. Therapeutic antibodies were detected in buffer (gray) and a 10% serum matrix (red). Visualization was with TMB substrate read at 450 nm (minus 630 nm reference).

format; cross-reactivity leads to the capture of serum hIgGs and their detection by anti-hFc leads to matrix effects. This issue is not inherent to antibodies, but a sufficiently high-quality reagent would need to be generated. Otherwise, in this case a bridging assay format, using the anti-idiotypic Fab as capture and detection reagent, would be necessary to enhance specificity. However, bridging assays often require optimization of a low-capture reagent coating density, to prevent bivalent binding of the therapeutic antibody that precludes binding of the anti-idiotypic detection reagent [12]. The use of such low-capture reagent concentrations leads to low sensitivities and high susceptibility to inconsistencies [12]. To avoid this, two different anti-idiotypic reagents with non-overlapping binding sites would need to be found, which is very unlikely due to steric issues. Hence, the universal detection format afforded by the anti-idiotypic Affimer capture approach is extremely desirable and less optimization should be required from assay to assay. Furthermore, the enhanced dynamic range offered by the Affimer reagents reduces the need for multiple dilutions and minimizes repetition of measurements.

Universal Affimer detection reagent

Both anti-hIgG-HRP and anti-hFc-HRP antibodies have been successfully used as detection reagents, alongside anti-idiotypic Affimer capture reagents. Further flexibility in detection format was demonstrated by the use of a universal anti-hIgG Affimer detection reagent (Figure 5), giving an Affimer-only assay format. The anti-hIgG Affimer was biotinylated and pre-incubated with streptavidin-HRP prior to detection and visualization with TMB.

For detection of both trastuzumab and rituximab CDR mAbs, minimal matrix effects were observed in 10% serum (Figure 5) and the dynamic ranges were comparable to those obtained with anti-hIgG antibodies. The intra-assay curve metrics for trastuzumab in 10% serum gave a quantifiable range of 2–2000 ng/ml, with ≤18.0% CV and 93.9–115% recovery. In 10% serum rituximab CDR mAb had a quantifiable range of 7.8–2000 ng/ml, with ≤17.7% CV and 95.3–110.7% recovery. This again demonstrates the excellent specificity of the Affimer capture surfaces, allowing a number of different universal detection formats to be successfully employed, which offers assay developers flexibility to suit individual assay requirements. The Affimer sandwich assay format obviates the need for antibodies and each binding reagent is an easily manufactured recombinant protein. Furthermore, the detection reagent is universal, so should be applicable across assays, simplifying assay development and reagent manufacture.

The generation of anti-idiotypic affinity reagents against therapeutic mAbs presents a particular challenge. In order to specifically recognize a humanized therapeutic antibody within the high background of human IgGs present in serum, reagents must be highly specific for the mAb idiotype. Here we demonstrate Affimer reagents to be easily selected and manufactured non-immunoglobulin reagents that can address this challenge. Anti-idiotypic Affimer reagents against trastuzumab and CDR mAbs of rituximab, adalimumab and ipilimumab therapeutic antibodies have been identified and characterized. A simple negative selection protocol successfully drove binding towards the target idiotype, generating highly specific Affimer binders that display minimal matrix effects in 10% human serum and no cross-reactivity with nonspecific mAbs, without any need for affinity maturation. Compared with equivalent Fabs, the anti-idiotypic Affimer capture surfaces offered such exquisite specificity that a flexible universal detection format (anti-hIgG antibody, anti-hFc antibody or anti-hIgG Affimer) can be used, avoiding bridging assays and simplifying assay development. A sandwich ELISA using anti-idiotypic Affimer capture and universal anti-hIgG-HRP antibody detection was developed within a 10% human serum matrix. Calibration curves met the FDA criteria for accuracy and precision over favorable dynamic ranges in comparison to Fabs and commercially available kits, confirming the applicability of anti-idiotypic Affimers to PK assays. The lot-to-lot consis-

tency of the anti-trastuzumab Affimer was also confirmed, giving assurance of supply.

Overall, it is clear that the Affimer platform can be reliably used to develop anti-idiotypic reagents for immunoassays, to measure relevant concentrations of therapeutic mAbs with suitable accuracy and precision metrics for calibration curves. As well as being simple to identify and easy to produce, the anti-idiotypic Affimer reagents offer performance improvements in terms of high specificity, low matrix effects, broad dynamic ranges, flexible universal detection formats and low lot-to-lot variation. The fast reagent development time, ease of assay development and assurance of supply make the highly specific anti-idiotypic Affimers promising reagents to meet the demands of clinical development timelines and prevent delays, particularly in the growing biosimilars arena, where speed to market is essential. The development of antibody therapeutics continues to expand and anti-idiotypic Affimer reagents offer the potential for critical partner PK assays.

FUTURE PERSPECTIVE

Increasing numbers of biologics entering drug development and achieving regulatory approval, combined with the rising rates of patients suffering with chronic diseases, ensures that critical reagents for pharmacokinetic studies will remain an essential building block within the drug development pipeline. Current pharmacokinetic assay reagents can be costly to produce and require long development times, which hinder the drug development process. As the technology driving non-immunoglobulin alternatives to antibodies expands, bioanalysts will continue to explore both antibody and non-antibody-based critical reagents when establishing PK and therapeutic drug monitoring assays. Reagent selection will depend upon superior performance, delivery speed and simple and cost-effective assay design and development. We foresee that these critical reagents may also have application in both drug monitoring and patient selection in the future.

AUTHOR CONTRIBUTIONS

HA, CT and AAT performed phage display and isolation of Affimer reagents. AN, AD, HD, AW, RF and JN performed the ELISAs and validation experiments. HA, MJM, MJ and DCT conceived the idea, supervised the experiments and wrote the paper. All the authors read and edited the manuscript.

FINANCIAL & COMPETING INTERESTS DISCLOSURE

MJM and DCT: Inventors of the Adhiron/Affimer technology and own personal shares in Avacta Life Sciences. The Adhiron patent (patent application number PCT/GB2014/050435) is owned by the University of Leeds and licensed to Avacta Ltd. AM, AD, HC, AW, RF, JN and MJ all work for Avacta Life Sciences. The authors have no other relevant affiliations or financial involvement with any organization or entity with a financial interest in or financial conflict with the subject matter or materials discussed in the manuscript apart from those disclosed.

No writing assistance was utilized in the production of this manuscript.

OPEN ACCESS

REFERENCES

Papers of special note have been highlighted as: • of interest

1. Carter PJ, Lazar GA. Next generation antibody drugs: pursuit of the 'high-hanging fruit'. *Nat. Rev. Drug Discovery.* 17(3), 197–223 (2018).
2. Leavy O. Therapeutic antibodies: past, present and future. *Nat. Rev. Immunol.* 10(5), 297 (2010).
3. Shepard HM, Phillips GL, Thanos CD, Feldmann M. Developments in therapy with monoclonal antibodies and related proteins. *Clin. Med.* 17(3), 220–232 (2017).
4. Elgundi Z, Reslan M, Cruz E, Sifniotis V, Kayser V. The state-of-play and future of antibody therapeutics. *Adv. Drug Delivery Rev.* 122, 2–19 (2016).
5. Grilo AL, Mantalaris A. The increasingly human and profitable monoclonal antibody market. *Trends Biotechnol.* 37(1), 9–16 (2018).
6. Kaplon H, Reichert JM. Antibodies to watch in 2018. *mAbs* 10(2), 183–203 (2018).
7. Chin SE, Ferraro F, Groves M, Liang M, Vaughan TJ, Dobson CL. Isolation of high-affinity, neutralizing anti-idiotype antibodies by phage and ribosome display for application in immunogenicity and pharmacokinetic analyses. *J. Immunol. Methods.* 416, 49–58 (2015).
8. Keizer RJ, Huitema AD, Schellens JH, Beijnen JH. Clinical pharmacokinetics of therapeutic monoclonal antibodies. *Clin. Pharmacokinet.* 49(8), 493–507 (2010).
9. Lim SY, Chan CE, Lisowska MM, Hanson BJ, MacAry PA. The molecular engineering of an anti-idiotypic antibody for pharmacokinetic analysis of a fully human anti-infective. *PloS One* 10(12), e0145381 (2015).
10. Könning D, Rhiel L, Empting M *et al.* Semi-synthetic vNAR libraries screened against therapeutic antibodies primarily deliver anti-idiotypic binders. *Sci. Rep.* 7(1), 9676 (2017).

• **Describes anti-idiotypic vNAR reagents.**

11. Tornetta M, Fisher D, O'Neil K *et al.* Isolation of human anti-idiotypic antibodies by phage display for clinical immune response assays. *J. Immunol. Methods.* 328(1–2), 34–44 (2007).
12. Salimi-Moosavi H, Winters A, Abbott C *et al.* A multifactorial screening strategy to identify anti-idiotypic reagents for bioanalytical support of antibody therapeutics. *Anal. Biochem.* 470, 52–60 (2015).
13. Ameri M, Zhou E-M. Idiotypes and anti-idiotypic antibodies: a review. *Comp. Clin. Pathol.* 14(4), 171–178 (2006).
14. van Schie KA, Wolbink G-J, Rispens T. Cross-reactive and pre-existing antibodies to therapeutic antibodies – effects on treatment and immunogenicity. *mAbs.* 7(4), 662–671 (2015).
15. Warnke C, Hermanrud C, Lundkvist M, Fogdell-Hahn A. Anti-drug antibodies. *Drugs Ther. Stud.* 2(1), e11 (2012).
16. Krishna M, Nadler SG. Immunogenicity to biotherapeutics–the role of anti-drug immune complexes. *Front. Immunol.* 7, 21 (2016).
17. Godar M, Morello V, Sadi A *et al.* Dual anti-idiotypic purification of a novel, native-format biparatopic anti-MET antibody with improved *in vitro* and *in vivo* efficacy. *Sci. Rep.* 6, 31621 (2016).

18. Sullivan MA, Brooks LR, Weidenborner P *et al.* Anti-idiotypic monobodies derived from a fibronectin scaffold. *Biochemistry.* 52(10), 1802–1813 (2013).
- **Describes anti-idiotypic monobody reagents.**
19. Ladjemi MZ. Anti-idiotypic antibodies as cancer vaccines: achievements and future improvements. *Front. Oncol.* 2, 158 (2012).
20. Mader A, Kunert R. Humanization strategies for an anti-idiotypic antibody mimicking HIV-1 gp41. *Protein Eng. Des. Sel.* 23(12), 947–954 (2010).
21. Vázquez AM, Hernández AM, Macías A *et al.* Racotumomab: an anti-idiotype vaccine related to N-glycolyl-containing gangliosides–preclinical and clinical data. *Front. Oncol.* 2, 150 (2012).
22. Vogel M, Keller-Gautschi E, Baumann MJ *et al.* Designed ankyrin repeat proteins as anti-idiotypic-binding molecules. *Ann. NY Acad. Sci.* 1109(1), 9–18 (2007).
23. Yu X, Yang YP, Dikici E, Deo SK, Daunert S. Beyond antibodies as binding partners: the role of antibody mimetics in bioanalysis. *Annu. Rev. Anal. Chem.* 10, 293–320 (2017).
24. Lee JW, Kelley M, King LE *et al.* Bioanalytical approaches to quantify "total" and "free" therapeutic antibodies and their targets: technical challenges and PK/PD applications over the course of drug development. *AAPS J.* 13(1), 99–110 (2011).
25. Wang X, Quarmby V, Ng C *et al.* Generation and characterization of a unique reagent that recognizes a panel of recombinant human monoclonal antibody therapeutics in the presence of endogenous human IgG. *mAbs.* 5(4), 540–554 (2013).
26. Vazquez-Lombardi R, Phan TG, Zimmermann C, Lowe D, Jermutus L, Christ D. Challenges and opportunities for non-antibody scaffold drugs. *Drug Discov. Today.* 20(10), 1271–1283 (2015).
27. Chames P, Van Regenmortel M, Weiss E, Baty D. Therapeutic antibodies: successes, limitations and hopes for the future. *Br. J. Pharmacol.* 157(2), 220–233 (2009).
28. Bradbury A, Pluckthun A. Standardize antibodies used in research: to save millions of dollars and dramatically improve reproducibility, protein-binding reagents must be defined by their sequences and produced as recombinant proteins, say Andrew Bradbury, Andreas Pluckthun and 110 co-signatories. *Nature* 518(7537), 27–30 (2015).
29. Bordeaux J, Welsh AW, Agarwal S *et al.* Antibody validation. *BioTechniques* 48(3), 197–209 (2010).
30. Coelho M, Gauthier P, Pugniere M, Roquet F, Pelegrin A, Navarro-Teulon I. Isolation and characterisation of a human anti-idiotypic scFv used as a surrogate tumour antigen to elicit an anti-HER-2/neu humoral response in mice. *Br. J. Cancer* 90(10), 2032–2041 (2004).
31. Wang Y, Li P, Majkova Z *et al.* Isolation of alpaca anti-idiotypic heavy-chain single-domain antibody for the aflatoxin immunoassay. *Anal. Chem.* 85(17), 8298–8303 (2013).
32. Alvarez-Rueda N, Ladjemi MZ, Béhar G *et al.* A llama single domain anti-idiotypic antibody mimicking HER2 as a vaccine: Immunogenicity and efficacy. *Vaccine* 27(35), 4826–4833 (2009).
33. Škrlec K, Štrukelj B, Berlec A. Non-immunoglobulin scaffolds: a focus on their targets. *Trends Biotechnol.* 33(7), 408–418 (2015).
34. Jost C, Plückthun A. Engineered proteins with desired specificity: DARPins, other alternative scaffolds and bispecific IgGs. *Curr. Opin. Struct. Biol.* 27, 102–112 (2014).
35. Gilbreth RN, Koide S. Structural insights for engineering binding proteins based on non-antibody scaffolds. *Curr. Opin. Struct. Biol.* 22(4), 413–420 (2012).
36. Tiede C, Tang AA, Deacon SE *et al.* Adhiron: a stable and versatile peptide display scaffold for molecular recognition applications. *Protein Eng. Des. Sel.* 27(5), 145–155 (2014).
37. Tiede C, Bedford R, Heseltine SJ *et al.* Affimer proteins are versatile and renewable affinity reagents. *eLife* 6, e24903 (2017).
38. Schlichthaerle T, Eklund A, Schueder F *et al.* Site-specific labeling of Affimers for DNA-PAINT microscopy. *Angew. Chem. Int. Ed.* 57(34), 11060–11063 (2018).
39. Lopata A, Hughes R, Tiede C *et al.* Affimer proteins for F-actin: novel affinity reagents that label F-actin in live and fixed cells. *Sci. Rep.* 8(1), 6572 (2018).
40. Zhurauski P, Arya SK, Jolly P *et al.* Sensitive and selective Affimer-functionalised interdigitated electrode-based capacitive biosensor for Her4 protein tumour biomarker detection. *Biosens. Bioelectron.* 108, 1–8 (2018).
41. Robinson JI, Baxter EW, Owen RL *et al.* Affimer proteins inhibit immune complex binding to FcγRIIIa with high specificity through competitive and allosteric modes of action. *Proc. Natl Acad. Sci. USA* 115(1), E72–E81 (2018).
42. Hughes DJ, Tiede C, Penswick N *et al.* Generation of specific inhibitors of SUMO-1–and SUMO-2/3–mediated protein-protein interactions using Affimer (Adhiron) technology. *Sci. Signal.* 10(505), eaaj2005 (2017).
43. Xie C, Tiede C, Zhang X *et al.* Development of an Affimer-antibody combined immunological diagnosis kit for glypican-3. *Sci. Rep.* 7(1), 9608 (2017).
44. Arrata I, Barnard A, Tomlinson DC, Wilson AJ. Interfacing native and non-native peptides: using Affimers to recognise α-helix mimicking foldamers. *Chem. Commun.* 53(19), 2834–2837 (2017).
45. Sharma R, Deacon SE, Nowak D *et al.* Label-free electrochemical impedance biosensor to detect human interleukin-8 in serum with sub-pg/ml sensitivity. *Biosens. Bioelectron.* 80, 607–613 (2016).
46. Rawlings AE, Bramble JP, Tang AA *et al.* Phage display selected magnetite interacting Adhirons for shape controlled nanoparticle synthesis. *Chem. Sci.* 6(10), 5586–5594 (2015).
47. Kyle HF, Wickson KF, Stott J *et al.* Exploration of the HIF-1α/p300 interface using peptide and Adhiron phage display technologies. *Mol. BioSyst.* 11(10), 2738–2749 (2015).
48. Ah-San Tang A, Tiede C, Hughes DJ, McPherson MJ, Tomlinson DC. Isolation of isoform-specific binding proteins (Affimers) by phage display using negative selection. *Sci. Signal.* 10(505), eaan0868 (2017).
49. Hampson G, Ward TH, Cummings J *et al.* Validation of an ELISA for the determination of rituximab pharmacokinetics in clinical trials subjects. *J. Immunol. Methods* 360(1–2), 30–38 (2010).
50. Desvignes C, Edupuganti SR, Darrouzain F *et al.* Development and validation of an enzyme-linked immunosorbent assay to measure adalimumab concentration. *Bioanalysis* 7(10), 1253–1260 (2015).
51. Weber JS, O'Day S, Urba W *et al.* Phase I/II study of ipilimumab for patients with metastatic melanoma. *J. Clin. Oncol.* 26(36), 5950–5956 (2008).
52. Cardinali B, Lunardi G, Millo E *et al.* Trastuzumab quantification in serum: a new, rapid, robust ELISA assay based on a mimetic peptide that specifically recognizes trastuzumab. *Anal. Bioanal. Chem.* 406(18), 4557–4561 (2014).
53. Damen CW, de Groot ER, Heij M *et al.* Development and validation of an enzyme-linked immunosorbent assay for the quantification of trastuzumab in human serum and plasma. *Anal. Biochem.* 391(2), 114–120 (2009).
54. Guidance for industry: Bioanalytical method validation. US Department of Heath and Human Services Food and Drug Administration (2018).
55. abcam. Ipilimumab ELISA Kit (Yervoy®). https://www.abcam.com/ipilimumab-elisa-kit-yervoyreg-ab237653.html
56. abcam. Trastuzumab ELISA Kit (Herceptin®) https://www.abcam.com/trastuzumab-elisa-kit-herceptin-reg-ab237645.html
57. abcam. Rituximab ELISA Kit (Mabthera®). https://www.abcam.com/rituximab-elisa-kit-mabthereareg-ab237640.html
58. abcam. Adalimumab ELISA Kit (Humira®). https://www.abcam.com/adalimumab-elisa-kit-humirareg-ab237641.html
59. Ylera F, Harth S, Waldherr D, Frisch C, Knappik A. Off-rate screening for selection of high-affinity anti-drug antibodies. *Anal. Biochem.* 441(2), 208–213 (2013).

BioTechniques

Highly efficient library preparation for Ion Torrent sequencing using Y-adapters

Leonie F Forth[1] & Dirk Höper*[,1]

ABSTRACT

Library preparation is a crucial step in next-generation sequencing workflows. Key determinants of successful library preparation are the available amount of input DNA and the efficiency of the conversion of this DNA into functional library molecules. While the standard blunt-end ligation protocol for Ion Torrent libraries has a theoretical maximum efficiency of 25%, Y-adapters enable highly efficient library preparation by (i) sticky-end ligation and (ii) rendering both DNA strands functional for sequencing, hence resulting in a theoretical efficiency of up to 100%. Moreover, the generation of adapter dimers is reduced. Therefore, we designed, optimized and validated Y-adapters compatible with Ion Torrent sequencing. These facilitate higher library yields combined with overall high sequencing performance regarding the key characteristics read-length, base quality, and library complexity.

METHOD SUMMARY

We developed, optimized, and validated Y-adapters for Ion Torrent sequencing, which are neither commercially available nor have been described elsewhere before. These Y-adapters enable highly efficient library preparation by (i) sticky-end ligation and (ii) rendering both DNA strands, hence theoretically up to 100% of the input DNA strands are functional for sequencing. Moreover, with low DNA input, the portion of adapter dimers is substantially reduced when using the described Y-adapters.

KEYWORDS

design • high-throughput sequencing • improved library preparation • Ion Torrent • library yield • next-generation sequencing • sticky-end ligation • Y-adapter

[1]*Friedrich-Loeffler-Institut, Institute of Diagnostic Virology, 17493 Greifswald-Insel Riems, Germany;*
**Author for correspondence: dirk.hoeper@fli.de*

BioTechniques 67: 229-237 (November 2019)
10.2144/btn-2019-0035

GRAPHICAL ABSTRACT

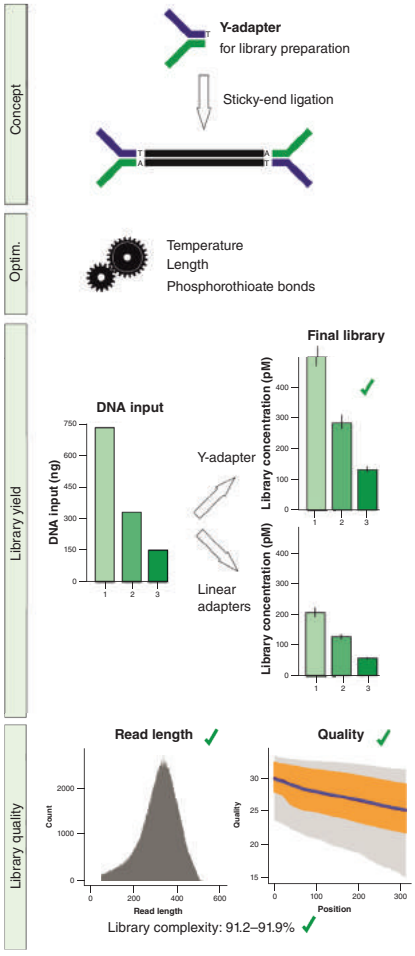

High-throughput sequencing is widely used for a variety of sequence-based analyses in different fields [1–3]. Library preparation represents a decisive step in a sequencing workflow, and problems or limitations at this point can jeopardize the whole sequencing project as the available input material may be limited. Therefore, efficient conversion of genetic material into a sequenceable library is urgently necessary. Today, Illumina and Ion Torrent instrument families are dominating the market of second-generation sequencing platforms. Both platforms differ in the two key features of clonal library amplification and sequence detection [4,5]. Nevertheless, they share some characteristics of the shotgun DNA library preparation process: the necessity of DNA fragmentation to a defined fragment size range followed by fragment end polishing and the addition of platform-specific adapters by ligation [6]. In both cases, each library fragment needs to have specific sequence features at the 5′- and the 3′-ends, respectively, in order to be functional (Figure 1). In a generic Ion Torrent library preparation workflow, two different linear adapters (A and P1) are ligated onto the DNA fragments in order to incorporate the necessary functionalities for sequencing. In these A-P1 libraries, where A and P1 represent the two different linear adapters, statistically only 50% of the ligated sequence fragments carry the combination of A and P1 adapter that is obligatory for sequencing (A-P1). As a result, the sequence information stored in the other half of ligated fragments carrying identical adapters on both ends (A-A or P1-P1) is lost. In addition, only 25% of the total input DNA strands are sequenceable overall, since only one strand of the functional fragments (A-P1) will be clonally amplified. By contrast, generic sequencing on Illumina platforms is based on so-called Y-adapters. The advantage of these Y-shaped adapters is that one adapter comprises the necessary functionalities for both the 5′- and the 3′-ends. After ligation of this adapter to both fragment ends, both DNA strands are available for sequencing, yielding a higher proportion of functional molecules (up to 100% of the DNA strands). In addition, the Y-adapters are ligated in a sticky-end fashion, with a nontemplated A-overhang at the 3′-ends of the DNA fragments in combination with a T-overhang of the adapters. The higher efficiency of A-T cloning compared with blunt-end ligation has been shown before [7]. Hence, the conversion of DNA fragments into library molecules is ▶

enhanced due to the advantages of ligating only one adapter together with the benefit of sticky-end ligation. Additionally, adapter dimer formation is significantly reduced compared with blunt-end ligation. Adapter dimers are undesirable, since they are quantified as part of the functional library and equally sequenced, although no information of the sample is included, thereby wasting sequencing capacity [8].

While for the Illumina platforms Y-adapters are the standard (as was the case for the discontinued 454 platform), there are no such adapters commercially available for the Ion Torrent platforms. Therefore, in order to take advantage of the enhanced library preparation enabled by the application of Y-adapters, here we set out to design and validate custom Y-adapters compatible with Ion Torrent platforms. Overall, the available information regarding the design of such adapters is scarce. To our knowledge, only one approach on the development and implementation of Y-adapters has been published, thereby focusing on adapters for the Roche 454 Titanium platform [9]. While a step-by-step library preparation workflow was provided, no detailed comparative analyses regarding adapter design, ligation efficiency and sequencing parameters were included. Therefore, we investigated the influence of different parameters such as length and melting temperature of the double-stranded part as well as the number and distribution of phosphorothioate (PT) bonds in order to yield an optimal design. The functionality and performance of the adapters was assessed based on qPCR quantification of the libraries, sequence output, read length, and quality of the generated reads, as well as complexity of the obtained datasets, and compared with commercially available linear adapters.

MATERIALS & METHODS

Preparation of Y-adapters

HPLC-purified or NGS-grade oligonucleotides (Supplementary Table S1) were ordered at metabion (Planegg/Steinkirchen, Germany) and dissolved in oligo buffer (1× TE, pH 8.0, 50 mM NaCl) at a concentration of 100 µM. For the assessment of different determinants of the Y-adapter performance, experiments were conducted with differing lengths of double-stranded regions, inosine nucleotides for shift in melting temperature and PT bonds at varying positions. For hybridization of the Y-adapter, 25 µl of the 100-µM stock solutions of the top and the matching bottom oligonucleotide were combined and filled with oligo buffer to a final volume of 100 µl to yield 25-µM adapters. The temperature profile for hybridization of the two oligonucleotides was as follows [10]: 95°C for 1 min, followed by decreasing the temperature by 0.1°C per second to the 15°C final temperature, followed by an unlimited hold at 14°C. Finally, adapters were aliquoted and stored at –20°C for further use.

Library preparation & sequencing

The workflow from sample to sequencing was performed according to the previously published detailed protocol [11], except for library preparation. In summary, DNA was extracted from overnight *Escherichia coli* DH10B cultures and mongoose tissue using a QIAamp DNA Mini Kit (Qiagen, Hilden, Germany) and from a tick cell line using the High Pure PCR Template Preparation Kit (Roche, Mannheim, Germany). Where not specified otherwise, 200–500 ng DNA was used as input material and fragmented with a Covaris M220 Focused-ultrasonicator™ (Covaris, Brighton, UK), aiming for a fragment size of 500–600 bp. For library preparation with Y-adapters, the GeneRead DNA Library I Core Kit (Qiagen) was deployed, in contrast to the established protocol. Following end repair and A-addition as per the manufacturer's instructions, 1 µl of 25 µM custom Y-adapter was used for adapter ligation. For comparison with commercial standard Ion Torrent adapters, library preparation was conducted in parallel, employing the GeneRead DNA Library L Core Kit (Qiagen) on the same batch of fragmented DNA according to the manufacturer's instructions, using each 1 µl barcoded adapter and

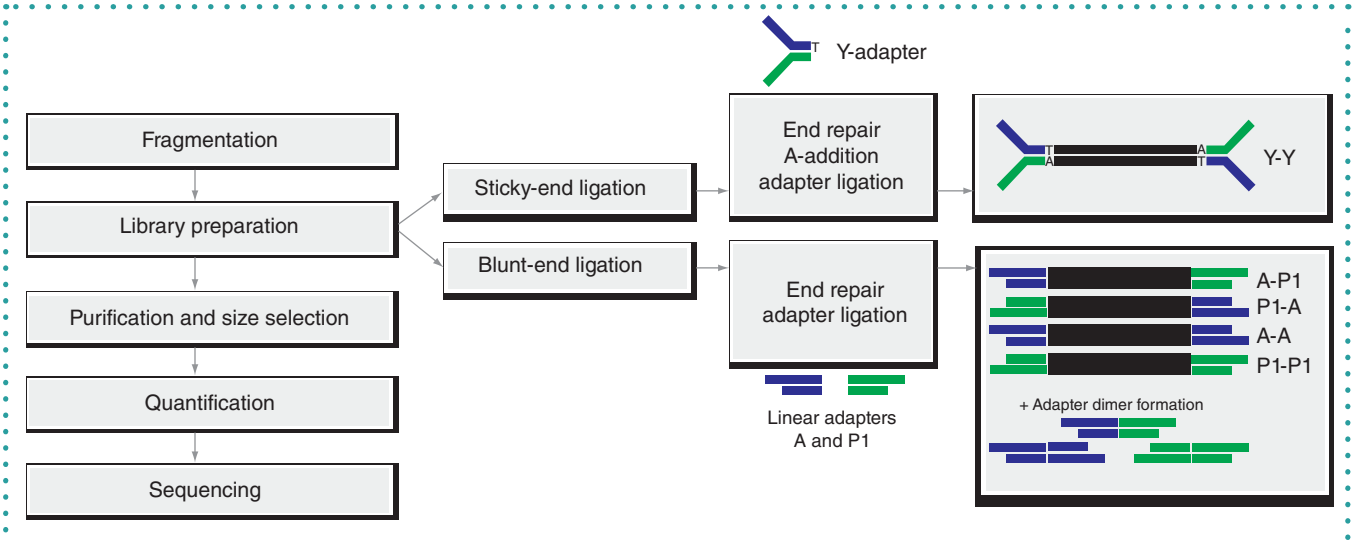

Figure 1. General overview of a generic library preparation workflow with the different concepts of sticky- and blunt-end ligation employing Y-adapters and linear adapters, respectively. Y-adapters are ligated in a sticky-end fashion to the fragment, thereby yielding library molecules, of which both strands fulfill the prerequisites for sequencing. By contrast, two different linear adapters that are ligated in a blunt-end mechanism beside the functional library molecule (A-P1) also create nonsequenceable molecules as byproducts (A-A, P1-P1), resulting in lower conversion of sample DNA to functional library. Additionally, blunt-end ligation increases the chances for the formation of unwanted adapter dimers and input fragment concatemers.

P1 adapter (Ion Xpress™ Barcode Adapters, Thermo Fisher Scientific, Darmstadt, Germany). Subsequently, the libraries were purified using 1.8 volumes AMPure XP magnetic beads (Beckman Coulter, Krefeld, Germany) according to the manufacturer's instructions. Finally, the library was eluted twice with 50 µl DNase-free water for a total of 100 µl purified library. In the experiments with low DNA input, one fifth of the purified library was retained for subsequent library analysis. Size exclusion was performed with AMPure XP magnetic beads in two steps for a final fragment size distribution of 500–600 bp according to Wylezich and colleagues [11]. After quality control (QC) with an Agilent High Sensitivity DNA Chip on a Bioanalyzer 2100 (both Agilent Technologies, Waldbronn, Germany), the libraries were quantified using KAPA Library Quantification Kit for Ion Torrent platforms (Roche) according to the manufacturer's instructions. After the PCR had finished, a melting curve analysis was performed to distinguish between library and adapter dimer molecules. Sequencing performance of Y-adapter libraries was tested and validated on an Ion Torrent PGM or an Ion S5 XL sequencer (Thermo Fisher Scientific). All steps for template preparation and sequencing were done as per the manufacturer's instructions, except for an additional denaturation of the library pool at 96°C for 2 min, followed by immediate cooling on ice right before the addition of the library pool to the emulsion PCR reaction. This denaturation of the library pool is necessary because both strands can serve as template molecules and will otherwise lead to polyclonal reads.

Data analysis

For a rough estimation of the melting point of the Y-adapters' double-stranded region, the software MELTING v5.2.0 [12] was used. This software was chosen as it considers the influence of suboptimal base pairing through inosine nucleotides. Specified parameters comprised the salt and oligonucleotide concentrations (50 mM Na^+, 10 mM $Tris^+$, 25 µM each oligonucleotide) as present in the buffer used for hybridization of the two oligonucleotides. For reliable comparison of sequencing data, an additional trimming was conducted after the trimming already performed by the Ion Torrent Software Suite, since the 3′ adapter extensions of the sequences occurring with custom sequences were not trimmed by the Ion Torrent Software Suite. To this end, Trim Galore v. 0.4.3 at Galaxy Europe [13] was used for 3′ Y-adapter and quality trimming (additional command line parameters: -e 0.1 -q 20 -O 3, with sequences shorter than 50 nt removed). For the quality assessment of the generated sequence data, FastQC [14] and qrqc [15] with R-Studio (Version 1.1.456; RStudio, Inc. [16]) and R (Version 3.5.1; R Core Team [17]) were used. Consistent analysis of the sequence quality was ensured by bringing the datasets to a uniform sequencing read length and amount. To this end, the 15 nt always exhibiting a deviating per base sequence content at the 5′-end in both the standard and Y-adapter libraries were removed. Moreover, to ensure comparability, long reads were shortened to a length of 310 nt, and reads shorter than 310 nt were removed, resulting in 342,715 reads corresponding to 1,370,860 bases in the analyzed datasets.

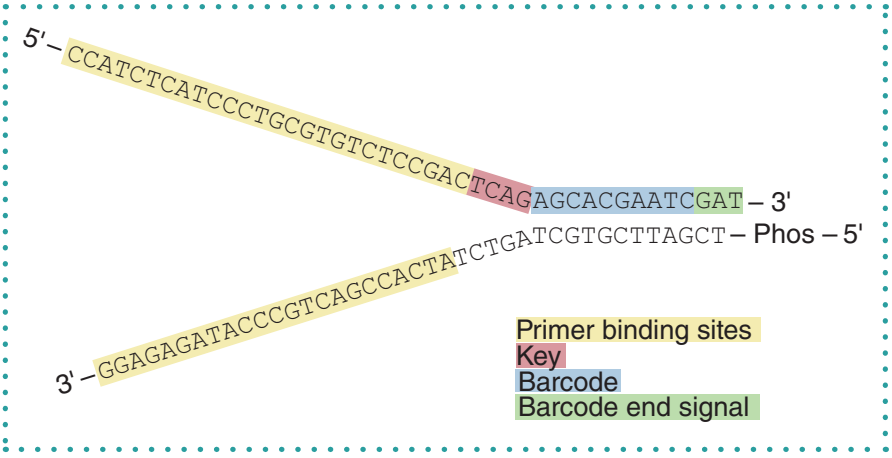

Figure 2. Schematic architecture of a custom Y-adapter comprising the necessary structural elements for Ion Torrent sequencing.

RESULTS & DISCUSSION

In general, Y-adapters are composed of two oligonucleotides (hereinafter named top ▶

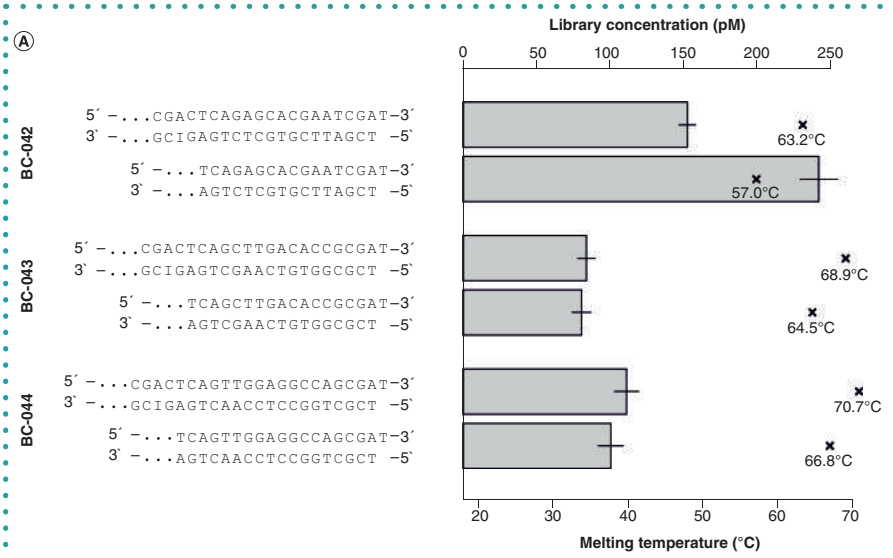

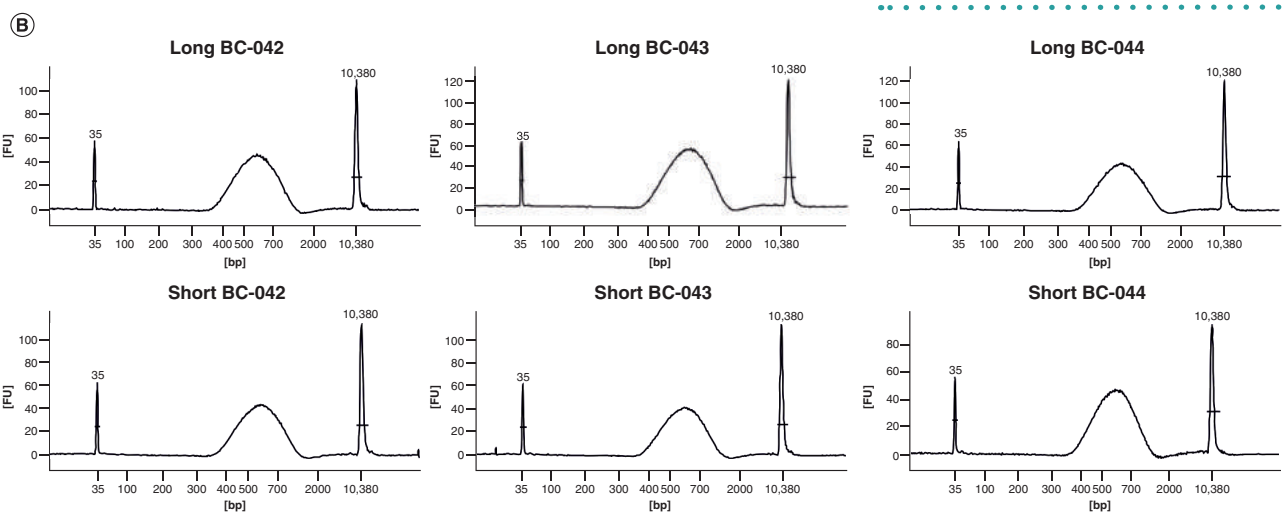

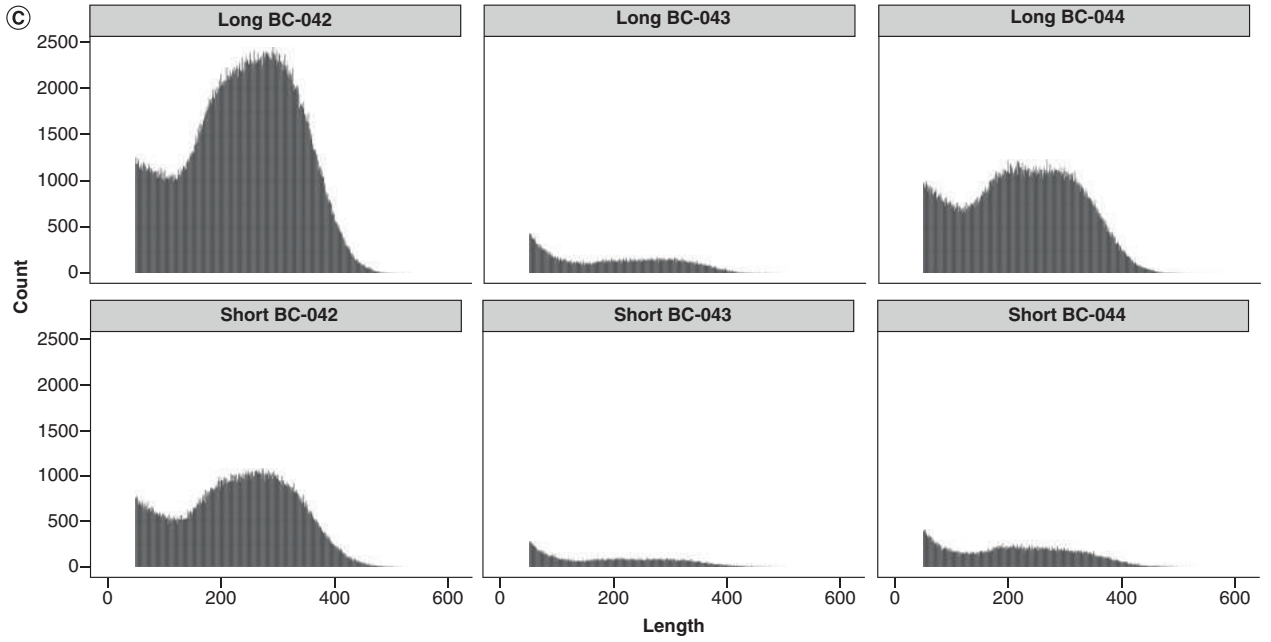

Figure 3. Summary of construction and results obtained with the initial Y-adapters. (A) Initial design of the stem regions with three different barcodes (BC-042, 043, 044) and two variants each of the stem length. The bar plot shows the library yield (upper x-axis), with 500 ng *Escherichia coli* DNA input for each of the designs; mean and standard deviation were calculated from three dilutions used in qPCR quantification. ×: Melting temperature (lower x-axis) of the respective stem. (B) Size distribution of the generated libraries as determined by Bioanalyzer high-sensitivity DNA analysis. (C) Read length histogram of sequencing results of equimolar pools of the long and short adapters in one run each, respectively. For comparison, please see Figure 7B showing the expected size distributions.

▶ and bottom oligo) that include a mutual complementary region forming a double-stranded region in the final adapters. Additionally, each oligonucleotide comprises a noncomplementary part representing unique 3′ and 5′ features. This design results in the Y-shaped structure of a ready-to-use adapter (Figure 2).

We used the information available for established Y-adapters for Roche/454 sequencing [10] as a starting point for the initial design of our Y-adapters for Ion Torrent platforms. Importantly, the sequence of the barcoded oligonucleotide of the commercial Ion Xpress™ Barcode is identical with the top oligo in order to conserve all necessary functionalities and to avoid sequencing interference (Figure 2).

The functionalities encompass the priming sites for clonal amplification and sequencing, as well as the sequence key used for the recognition of library molecules and signal normalization, and the barcode with the barcode end signal (the bases GAT). The T nucleotide forms the overhang required for sticky-end ligation. The bottom oligo comprises information of the P1 adapter, which is the primer binding site for the clonal amplification, and is 5′-phosphorylated to promote ligation to the library fragment. The original P1 adapter also contains an extension for probe binding for optional library quantification by probe-based qPCR that is not included in our design. Since the described regions must be unaltered to ensure full functionality of the adapter for amplification and sequencing, the necessary double-stranded region, also called 'stem', can only be formed by the barcode and the immediately adjacent regions.

In the initial experiments, two adapter variants analogous to the 454 Y-adapter design were tested, mainly differing in the stem length (20–22 bp and 16–18 bp) and used barcode (Figure 3A). In the long variant, barcode (including end signal), key and additional four base pairs upstream of the barcode formed the stem, while in the short variant only the barcode (including end signal) and key were complementary. The simple fusion of the 454 structural elements and Ion Torrent sequences to meet requirements for sequencing delivered varying results in library yield as quantified by KAPA-PCR (Figure 3A). By contrast, the traces of the high-sensitivity DNA electrophoresis showed a uniform size distribution for all six libraries with a peak at 600 bp (Figure 3B). After equimolar pooling of the libraries containing the short/long adapter versions in one run each, the sequencing results of single libraries did not fit the expectation of the read-length distribution (compare Figure 7B) and comparable read ▶

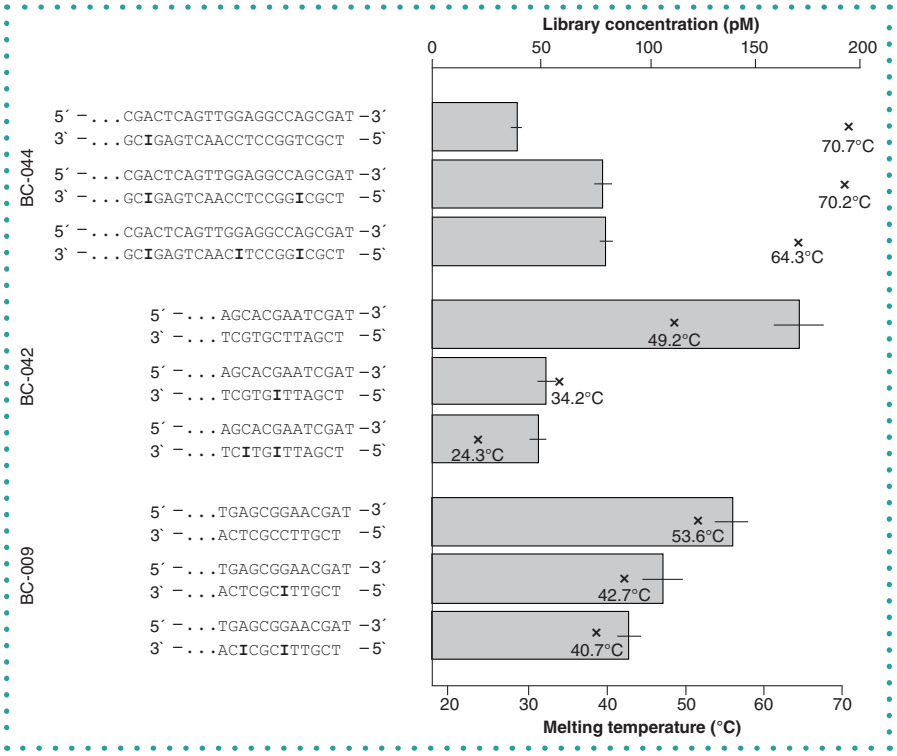

Figure 4. Influence of the stem melting temperature on library yield. Design of the stem regions with three different barcodes and varying numbers of inosine nucleotides (bold). Input: 250 ng of cell culture DNA. The barplot shows the library yield (upper x-axis) for each of the designs, mean and standard deviation were calculated from three dilutions used in qPCR quantification.
×: Melting temperature (lower x-axis) of the respective stem.

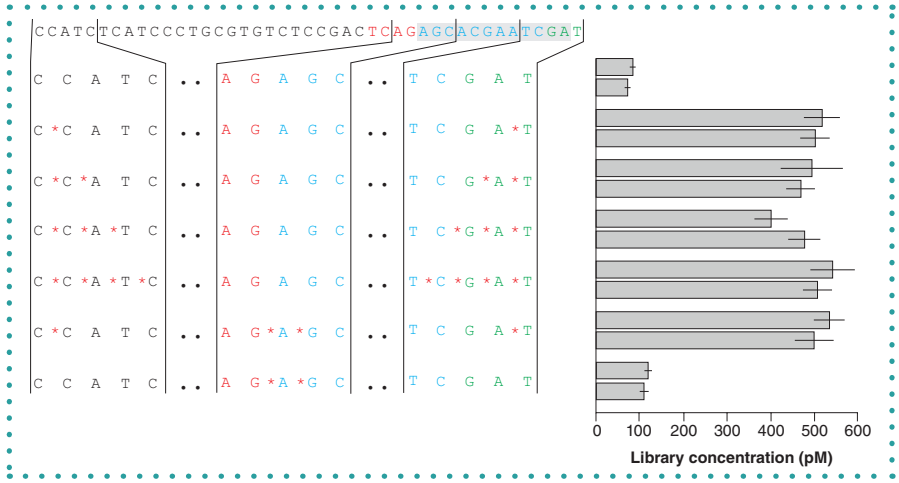

Figure 5. Influence of phosphorothioate bonds on library yield. Design of the top oligonucleotides with barcode BC-042 and varying numbers of phosphorothioate bonds and different positions. Libraries were prepared from 500 ng fragmented *Escherichia coli* DNA in two independent experiments. The bar plot shows the library yield for each of the designs; mean and standard deviation were calculated from three dilutions used in qPCR quantification. Colored adapter sequence: Black: primer binding sites; red: key; blue: barcode; green: barcode end signal. The adapter part forming the double-stranded stem is shown with grey background.
*Phosphorothioate bonds.

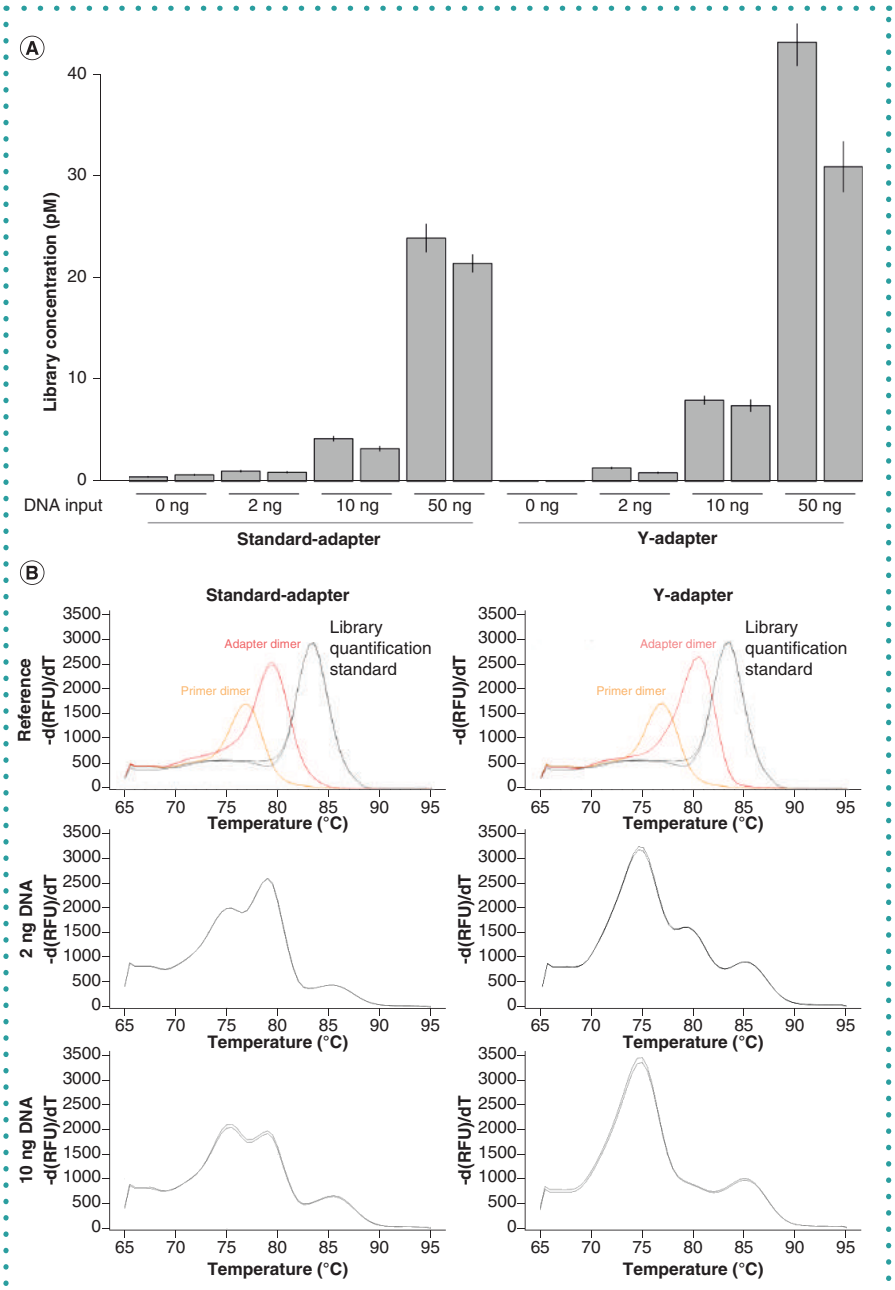

Figure 6. Influence of Y-adapters on library yield and quality at low DNA input. (A) Library concentration after library preparation without and with 2, 10 and 50 ng fragmented *Escherichia coli* DNA input. For optimal comparability, experiments were performed in duplicates with standard adapter BC-042 and Y-adapter BC-042, respectively. Mean and standard deviation were calculated from three dilutions used in qPCR quantification. (B) Melting curves generated after qPCR quantification for 2- and 10-ng DNA input, visualizing the presence of adapter dimers. Reference was assembled of single peaks for nontemplate control (primer dimer; yellow), library without input (adapter dimer; red) and library quantification standard (153 bp; black).

▶ amounts, indicating suboptimal adapter design (Figure 3C). This knowledge gained from the initial experiments served as a starting point for testing of varied adapters for identification of critical characteristics. For a comparable performance regarding the read length and quality, the melting temperature and the inclusion of PT bonds protecting the adapters from degradation were necessary.

Narrow optimum range of T_m

The initial experiments showed that the library yield was highest using the adapter with the shortest barcode of 10 bp in combination with an overall short complementary region (see Figure 3). This implied that the T_m of the stem region was an important determinant of the functionality of the adapter. The melting point can be adjusted by (i) the length of the complementary double-stranded region and (ii) the inclusion of inosine nucleotides. Hypoxanthin, the nucleobase of inosine, can pair with any natural DNA base; however, the pairing is favored with cytosine, corresponding to the highest stability [18]. To test for the impact of the T_m, we analyzed the consequences of the substitution of one or more bases by inosines. As shown in Figure 4, the reduction of the T_m of the Y-adapter with barcode 44 (BC-044) approximately doubled the performance when reducing T_m to 64°C but still did not reach the performance of adapters with lower T_m. On the other hand, the inclusion of one or two inosine bases into BC-042 reduced both the T_m (from 49°C to 34°C) and the performance by approximately 70%. Likewise, in case of BC-009, the reduction of T_m by inclusion of inosines reduced the performance of library preparation. The available data suggest the existence of a temperature optimum between approximately 45°C and 55°C (Figure 4).

Phoshorothioate bonds are necessary at specific sites

Phoshorothioate (PT) bonds prevent degradation by endo- and exonucleases through the substitution of a nonbridging oxygen atom for a sulphur atom in the internucleotide linkage [19,20]. PT bonds are usually present in sequencing library adapters to prevent adapter and library decomposition. Interestingly, the position of the PT bonds varies: while in Roche 454 adapter oligonucleotides both ends each contained four PT bonds, Ion Torrent adapters have two PT bonds in the middle of the adapter at the end position of the shorter strand. Therefore, we determined if, how many, and at which sites PT bonds are necessary for optimal library yield and sequencing performance. To this end, we used optimized adapters with a short double-stranded region from previous experiments and included PTs at the end and parting positions of the two adapter strands (Figure 5). The results of library quantification (Figure 5 & Supplementary Figure S1) clearly underline the necessity of at least one PT ▶

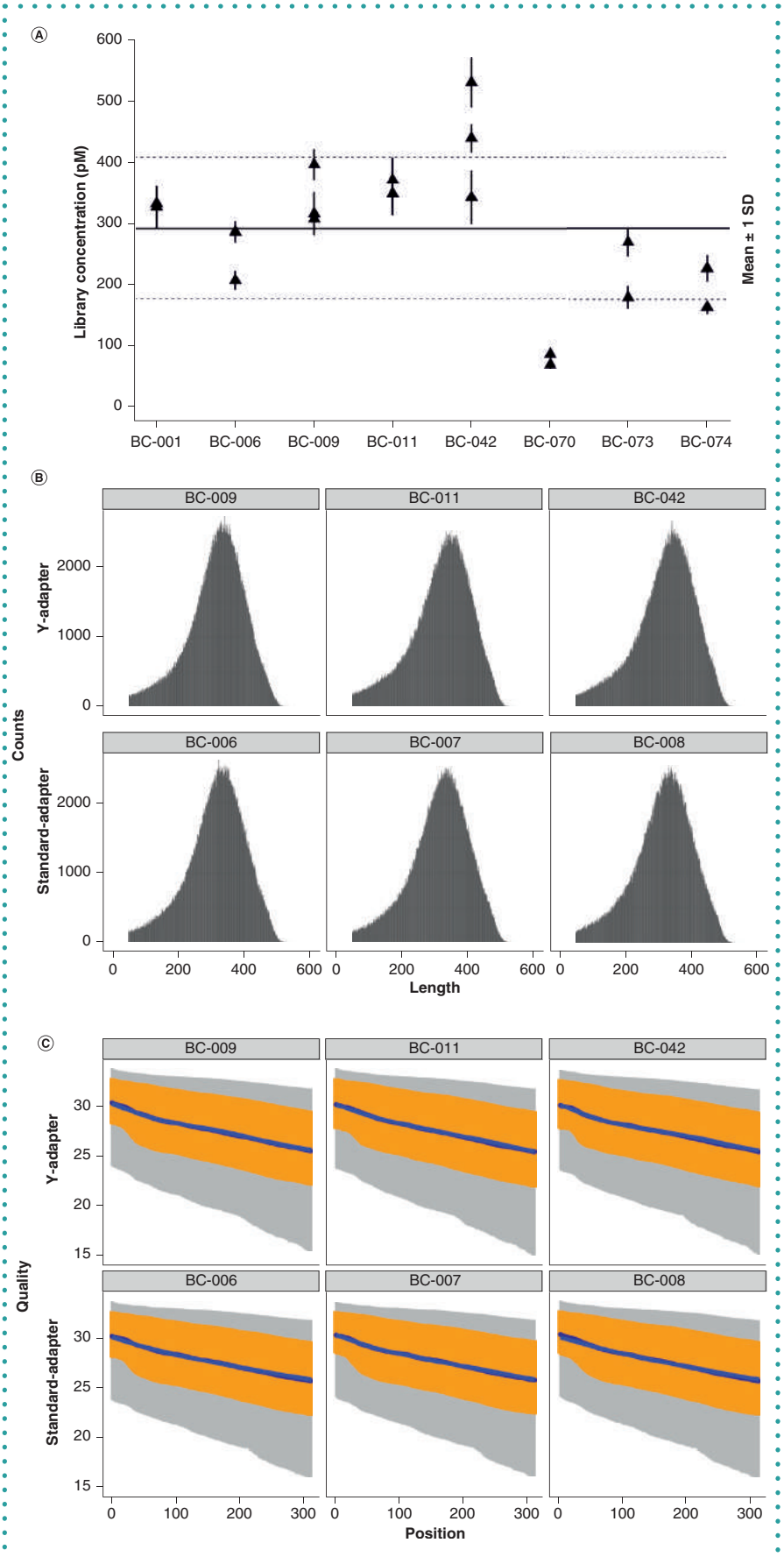

Figure 7. Performance of optimized custom Y-adapters. (A) Eight optimized Y-adapters for Ion Torrent sequencing were compared on their ligation efficiency when ligated to the same fragmented *Escherichia coli* DNA, 500 ng, in two or three (BC-009, BC-042) independent experiments. The plot shows the library yield for each of the adapters; mean and standard deviation were calculated from three dilutions used in qPCR quantification. The horizontal line indicates the mean concentration of all libraries shown in the plot, the dashed lines indicate the mean ± 1 standard deviation. (B) Key metrics of sequence data generated on an Ion S5 XL using standard Ion Torrent adapters or custom Y-adapters. Read length histograms for *E. coli* libraries prepared using Y-adapters (top) or standard adapters (bottom). (C) Quality plot of the same libraries after trimming to a uniform sequence length and number of bases.

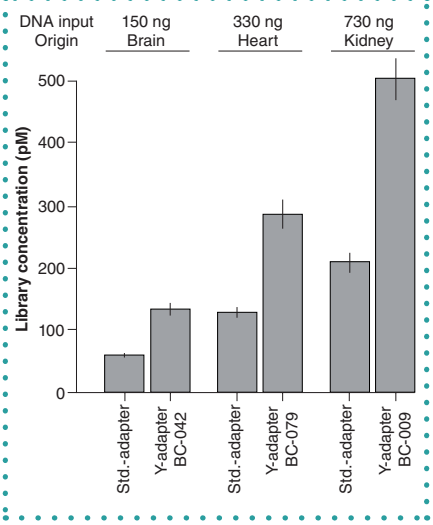

Figure 8. Yield for libraries prepared from three distinct field samples using custom Y-adapters or standard adapters with different DNA input as indicated at the top. Shown are the mean yield, including standard deviation calculated from three dilutions used in qPCR quantification.

bond at the ends of the adapter oligonucleotides. However, the library yield regarding the presence of one, two, three and four PT bonds was comparable. The PT bonds are likely preventing primer site degradation and enzymatic cleavage of the adapter's T overhang, which in consequence would obstruct sticky end ligation to the A-tailed library fragments. While the PT bonds in the termini of the adapter oligonucleotides had a significant impact, the internal PT bonds resulted in no beneficial effect. An additional protective effect could not be observed in combination with the terminal PT bonds, nor could any protection at all be seen in the case of internal PT bonds alone (Figure 5).

Y-adapters result in reduced adapter-dimer formation

In cases of limited sample material, efficient conversion of sample to library is crucial. Therefore, we compared the library yield at low input amounts of 2, 10 and 50 ng (Figure 6A). Additionally, we quantified the formation of adapter dimers without any input DNA in the library preparation. The Y-adapter dimer formation is substantially reduced in comparison to standard adapters. At 2 ng input into library preparation, the quantification implies comparable library yield with Y- and standard adapters. However, the library yield in the standard adapter library is overestimated due to adapter-dimer formation, which is noticeable in the melting curve of the quantification PCR (Figure 6B). The adapter dimers, perceived as library molecules in the quantification, occupy sequencing capacities during a run without providing template information and are therefore undesirable. At 10 ng input DNA, Y-adapter libraries already have higher concentrations, although the presence of adapter dimers can still be identified in the melting curve of standard adapter libraries (Figure 6B). At 50 ng input DNA, the enhanced library yield caused by sticky-end ligation of Y-adapters is clearly visible (Figure 6A) and potential adapter dimers are no longer observable in the melting curves (Supplementary Figure S2).

Y-adapters enable uniform ligation efficiency

Since the library preparation represents a decisive step in a sequencing workflow, adapters are required to function reliably and comparably in independent preparations. Pooling (multiplexing) of different samples in one sequencing run calls for a batch of adapters performing comparably well. For verification of uniform performance of the developed Y-adapters, eight adapters with different barcodes were manufactured based on obtained knowledge of melting temperature and PT bond requirements obtained from the previous experiments. The performances were compared regarding efficiency in library preparation and functionality in sequencing. The same fragmented *E. coli* DNA served as input material for all library preparations. Overall, we observed high library yields for seven out of eight adapters used (Figure 7A). However, sticky-end ligation to adapter carrying barcode 70 (BC-070) resulted in significantly less library, demonstrating the need for evaluation of Y-adapter performance before their routine use in a production environment. Despite the lower efficiency of the BC-070 adapter in library preparation, all libraries performed equally well when sequenced multiplexed in one full Ion S5 sequencing run. Sequencing of this equimolar library pool produced equal read amounts for all libraries, including BC-070. The key signal was strong and the read length distribution as expected on basis of the library size.

Y-adapters equal sequencing performance of commercial linear adapters

The highest library yields are meaningless if the ligated adapters do not perform well in sequencing. For comparison, the same fragmented *E. coli* DNA was ligated to three commercial adapters and three custom Y-adapters. The achieved library yields ranged between 211 and 288 pM for ligation with linear adapters and 399 and 442 pM for ligation with Y-adapters, respectively. Sequencing was performed in one Ion S5 run and resulted in overall tantamount read lengths for all libraries (Figure 7B). For direct comparison of sequencing quality, the reads were trimmed to the same length to subtract template-independent decay of the read quality towards the ends. This trimming provided an equal amount of bases, which showed a comparable quality distribution for standard and Y-adapters (Figure 7C). The percentage of sequences remaining after deduplication varied between 90.5 and 93.0% for standard adapters, and between 91.2 and 91.9% for Y-adapters, as determined by FastQC. In consequence, Y-adapters truly enable higher library yields at constant complexity levels, an advantage in comparison with library amplification that generates higher quantity at the cost of reduced library complexity and increased bias [21,22].

Evaluation on field samples

The Y-adapter ligation efficiency was compared on samples for diagnostic metagenomic analyses, with different samples combined with varying amounts of DNA input (Figure 8). Thereof, libraries for sequencing on Ion Torrent platforms were prepared using the blunt end ligation with linear adapters in comparison to sticky end ligation with custom Y-adapters. The results clearly show that the Y-adapters resulted in a more than twofold higher library concentration at the same input. This observation is independent of the amount of starting material. Additionally, the custom Y-adapters were successfully applied in the discovery of a novel picornavirus in an open diagnostic metagenomics approach on a case series of diseased lambs [23]. In this example of one possible application, extracted RNA was reverse transcribed into cDNA, which after fragmentation served as input for library preparation.

In summary, we developed and validated Y-adapters for Ion Torrent sequencing, which are neither commercially available nor have been described elsewhere before. Y-adapters enable more efficient library preparation by (i) sticky-end ligation and (ii) rendering both DNA strands functional for sequencing. The described Y-adapters enable higher library yields in comparison to standard Ion Torrent adapters. Moreover, the generation of adapter dimers that reduce sequencing output is minimized. With regard to the key performance characteristics (read-length, base quality, library complexity), libraries generated using our presented Y-adapters equal those of Ion Torrent standard libraries. Due to the higher possible library yield, the Y-adapters truly enable an efficient conversion of sample to functional library molecules and therefore enable omitting library amplification. Moreover, the herein described information builds a basis for

other researchers in the broad applications of high-throughput sequencing to enhance their library yield by designing their own custom Y-adapters compatible with Ion Torrent platforms. Manufacturing custom adapters drastically reduces the adapter cost per library. In addition, the presented Y-adapters may be of interest to research groups performing sequencing on both Ion Torrent and Illumina platforms, since it facilitates a unified, amplification-free, automatable protocol for Illumina and Ion Torrent library preparation only differing in the sequences of the added adapters.

FUTURE PERSPECTIVE

With the costs for sequencing and analysis further decreasing, NGS use will further increase for various types of scientific analyses and will become a standard technique in routine diagnostics. From the viewpoint of diagnostics, the restrictions imposed by the manufacturers – that is, the use of only certified library preparation and sequencing reagents from the original supplier – can be beneficial because they ensure reproducibility and standardization. From the scientific viewpoint, however, this is an unwanted restriction because it removes an element of choice and innovation. The presented Ion Torrent custom Y-adapters provide a more efficient and cheaper conversion of DNA into library and additionally provide a starting point for innovation and hence introduction of new flexibility, ultimately leading to further increase in the application of NGS in all fields.

SUPPLEMENTARY DATA

To view the supplementary data that accompany this paper please visit the journal website at: www.future-science.com/doi/suppl/10.2144/btn-2019-0035

DATA AVAILABILITY

Escherichia coli sequencing data of the comparison of custom Y-adapters with standard adapters have been deposited within the European Nucleotide Archive under the project accession number PRJEB30332.

AUTHOR CONTRIBUTIONS

Study design and conceptualization, LF and DH; experimental studies, LF; data interpretation and discussion, LF and DH; manuscript preparation and review, LF and DH.

No writing assistance was utilized in the production of this manuscript.

FINANCIAL & COMPETING INTERESTS DISCLOSURE

This research was funded by the German Federal Ministry of Education and Research within project "DetektiVir" (grant number 13N13783). The authors have no other relevant affiliations or financial involvement with any organization or entity with a financial interest in or financial conflict with the subject matter or materials discussed in the manuscript apart from those disclosed.

ACKNOWLEDGMENTS

The authors gratefully acknowledge Jenny Lorke and Patrick Zitzow for excellent technical assistance and support.

REFERENCES

1. Levy SE, Myers RM. Advancements in next-generation sequencing. *Annu. Rev. Genomics Hum. Genet.* 17, 95–115 (2016).
2. Buermans HP, den Dunnen JT. Next generation sequencing technology: advances and applications. *Biochim. Biophys. Acta.* 1842(10), 1932–1941 (2014).
3. Reuter JA, Spacek DV, Snyder MP. High-throughput sequencing technologies. *Mol. Cell* 58(4), 586–597 (2015).
4. Bentley DR, Balasubramanian S, Swerdlow HP *et al.* Accurate whole human genome sequencing using reversible terminator chemistry. *Nature* 456(7218), 53–59 (2008).
5. Rothberg JM, Hinz W, Rearick TM *et al.* An integrated semiconductor device enabling non-optical genome sequencing. *Nature* 475(7356), 348–352 (2011).
6. Head SR, Komori HK, LaMere SA *et al.* Library construction for next-generation sequencing: overviews and challenges. *BioTechniques* 56(2), 61–77 (2014).
7. Zhao G, Li J, Hu T, Wei H, Guan Y. Realizing directional cloning using sticky ends produced by 3′-5′ exonuclease of Klenow fragment. *J. Biosci.* 38(5), 857–866 (2013).
8. Quail MA, Kozarewa I, Smith F *et al.* A large genome center's improvements to the Illumina sequencing system. *Nat. Methods* 5(12), 1005–1010 (2008).
9. Zheng Z, Advani A, Melefors Ö *et al.* Titration-free 454 sequencing using Y adapters. *Nat. Protoc.* 6(9), 1367–1376 (2011).
10. Roche. Multiplex Identifier (MID) Adaptors for Rapid Library Preparations. In: *Technical Bulletin GS FLX System & GS Junior System.* 8–9 (2010).
11. Wylezich C, Papa A, Beer M, Höper D. A versatile sample processing workflow for metagenomic pathogen detection. *Sci. Rep.* 8(1), 13108 (2018).
12. Dumousseau M, Rodriguez N, Juty N, Le Novère N. MELTING, a flexible platform to predict the melting temperatures of nucleic acids. *BMC Bioinformatics* 13(1), 101 (2012).
13. Afgan E, Baker D, Batut B *et al.* The Galaxy platform for accessible, reproducible and collaborative biomedical analyses: 2018 update. *Nucleic Acids Res.* 46(W1), W537–W544 (2018).
14. Babraham Bioinformatics. FastQC. http://www.bioinformatics.babraham.ac.uk/projects/fastqc
15. GitHub. vsbuffalo/qrqc. http://github.com/vsbuffalo/qrqc
16. RStudio. www.rstudio.com
17. The R Project for Statistical Computing. www.R-project.org
18. Alseth I, Dalhus B, Bjørås M. Inosine in DNA and RNA. *Curr. Opin. Genet. Dev.* 26, 116–123 (2014).
19. Spitzer S, Eckstein F. Inhibition of deoxyribonucleases by phosphorothioate groups in oligodeoxyribonucleotides. *Nucleic Acids Res.* 16(24), 11691–11704 (1988).
20. Vosberg HP, Eckstein F. Effect of deoxynucleoside phosphorothioates incorporated in DNA on cleavage by restriction enzymes. *J. Biol. Chem.* 257(11), 6595–6599 (1982).
21. Dabney J, Meyer M. Length and GC-biases during sequencing library amplification: a comparison of various polymerase-buffer systems with ancient and modern DNA sequencing libraries. *BioTechniques* 52(2), 87–94 (2012).
22. Kozarewa I, Ning Z, Quail MA, Sanders MJ, Berriman M, Turner DJ. Amplification-free Illumina sequencing-library preparation facilitates improved mapping and assembly of (G+C)-biased genomes. *Nat. Methods* 6(4), 291–295 (2009).
23. Forth LF, Scholes SFE, Pesavento PA *et al.* Novel picornavirus in lambs with severe encephalomyelitis. *Emerg. Infect. Dis.* 25(5), 963–967 (2019).

Benchmarks

BioTechniques

Optimized transformation, overexpression and purification of S100A10

Xiaolin Yan[1,2], Marie-France Lebel-Beaucage[3], Samuel Tremblay[1,2], Line Cantin[1,2], Gary S Shaw[4] & Elodie Boisselier*[,1,2]

ABSTRACT

As a member of the S100 protein family, S100A10, has already been purified. However, its purity, or even yield, have often not beenreported in the literature. To facilitate future biophysical experiments with S100A10, we aimed to obtain it at a purity of at least 95% in a reasonably large amount. Here, we report optimized conditions for the transformation, overexpression and purification of the protein. We obtained a purity of 97% and performed stability studies by circular dichroism. Our data confirmed that the S100A10 obtained is suitable for experiments to be performed at room temperature up to several days.

METHOD SUMMARY

The *GST-S100A10* gene carried by the pGEX-6P-1 vector was overexpressed in transformed *Escherichia coli* and purified by glutathione *S*-transferase (GST) affinity chromatography. The GST tag was cleaved by PreScission protease, excess glutathione was removed by centrifugal filtration and buffer exchange and the GST tag removed by a second GST affinity chromatography. S100A10 was identified by LC/MS-MS and the stability of the secondary structure was analyzed by circular dichroism at different temperatures.

KEYWORDS

GST • overexpression • purification • S100A10 • transformation

[1]*Department of Ophthalmology, Faculty of Medicine, Université Laval, Quebec, QC, Canada;* [2]*CUO–Recherche, Centre de Recherche du CHU de Québec, Hôpital du Saint-Sacrement, CHU de Québec, Quebec, QC, Canada;* [3]*Departement of Chemistry, Biochemistry & Physics, Faculty of Sciences, Université du Québec à Trois-Rivières, Quebec, QC, Canada;* [4]*Departement of Biochemistry, Schulich School of Medicine & Dentistry, University of Western Ontario, London, ON, Canada;* **Author for correspondence: Tel.: +1 418 682 7511 ext. 84429; Elodie.Boisselier@fmed.ulaval.ca*

BioTechniques 67: 246-248 (November 2019)
10.2144/btn-2019-0081

S100A10 is of great interest because it has different functions using different mechanisms of action [1–3]. For example, S100A10 forms a ternary complex with annexin A2 and AHNAK to act as a platform enabling membrane repair [4]. In addition, the protein forms a heterotetramer with annexin A2 to regulate exocytosis and endocytosis [5]. In addition to its crucial role in breast, stomach and kidney cancer research, S100A10 represents a potential biomolecular marker for early gallbladder cancer diagnostic and therapeutic applications [6].

The purification of a given protein is an essential prerequisite for any biophysical or biochemical study. In the case of S100A10, the retrieved purification publications reported neither yield data nor solubilized protein amounts [4,7–15]. Among these publications, one mentioned a purity degree of S100A10 greater than 90% [15] and the other reported 95% [14], but without any specific supporting data. In this work, we address purity and yield in a clear and comprehensive way, aiming for a purity higher than 95% and a sufficient amount of S100A10 to carry out biophysical studies. Based on previous experimental conditions with the same expression host, we implemented modifications at each step to optimize the published protocol.

The plasmid used for transformation is a pGEX-6P-1 vector containing the *GST-S100A10* coding sequence. Five additional amino acids, GPLGS, were added at the beginning of the native S100A10 sequence, initially composed of 97 amino acids. We used 50 ng of the plasmid for transformation into 100 µl of commercial *Escherichia coli* BL21-Codon Plus (DE3)-RIL competent cells (Agilent Technologies, Inc., CA, USA) in a 900-µl transformation cell culture medium. After a heat pulse at 42°C, the bacteria cell culture was incubated at 37°C, 250 rpm for 1 h.

Initially, the heat pulse was set for 20 s, and we tested two different transformation cell culture media, Luria-Bertan (LB) and super optimal broth with catabolite repression (SOC). The culture with LB medium produced no colonies. The richer medium, SOC, appeared to be appropriate and should be used for transformation of *E. coli* BL21-Codon Plus (DE3)-RIL competent cells. We also tested different heat pulse durations using the SOC medium and found that 15 s, 20 s and 30 s produced 608, 700 and 395 colonies, respectively (Figure 1A). While the 20-s heat pulse leads to the most colonies, 30 s would be suitable if a single individualized colony is needed from the agar plate.

After 1 h of incubation, 100 µl of bacteria cell culture was spread on a LB ampicillin agar plate. Triplicate samples were incubated at 37°C overnight. Three colonies were chosen from each bacteria preculture, each were incubated in a 4 ml of 2 Yeast Extract Tryptone (2YT) ampicillin medium at 37°C and 250 rpm overnight. The colonies were then subjected to two conditions, with and without induction, leading to six different cell cultures. For each, 200 µl of preculture was pooled into 50 ml of LB ampicillin medium, incubated at 37°C and 250 rpm until an optical density of 600 nm ($OD_{600\ nm}$) of 0.6 to 0.8. Overexpression was initiated by the addition of 0.5 ml of 100 mM isopropyl β-D-1-thiogalactopyranoside. After 4 h of incubation at 37°C and 250 rpm, each cell culture was centrifuged at 3270×g and 4°C for 30 min. The cell pellet was subjected to lysozyme in phosphate-buffered saline (PBS; 1×), followed by three cycles of freeze–thaw and sonication. Lysed cells were centrifuged at 15,000×g and 4°C for 30 min, supernatants and cell pellets were suspended into PBS (1×) and compared on 12% SDS-PAGE.

The induction of overexpression at 37°C for 4 h was initiated once the $OD_{600\ nm}$ reached 0.6, 0.7 or 0.8. The highest proportion of *GST-S100A10* overexpressed in the supernatant (48%) was obtained at $OD_{600\ nm}$ = 0.8 (Figure 1B). Also, the total amount of *GST-S100A10* overexpressed in this condition is higher than in the two other cases ▶

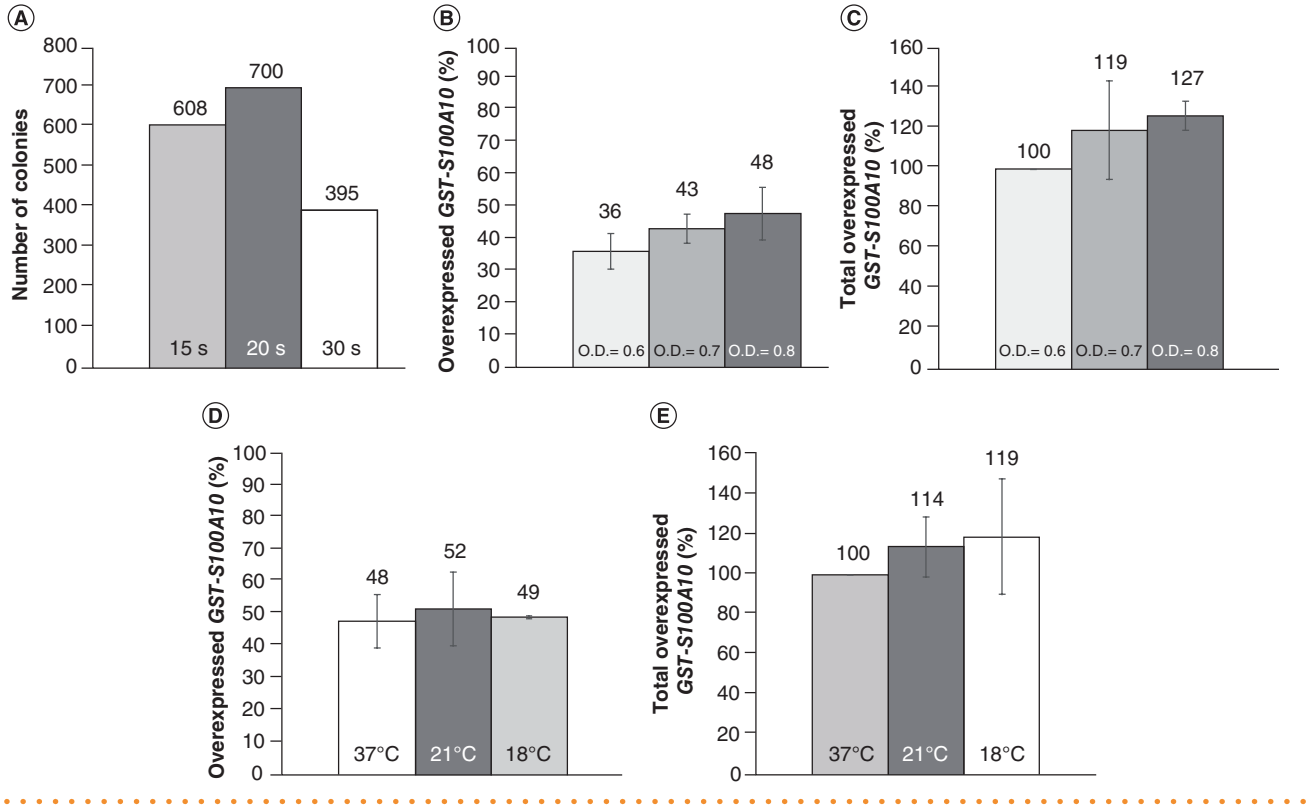

Figure 1. Transformation and overexpression results. (A) Transformation results in a super optimal broth with catabolite repression medium at different heat pulse durations. (B) Percentage of *GST-S100A10* overexpressed at 37°C in the supernatant with $OD_{600\,nm}$ = 0.6, 0.7 and 0.8; 100% = total overexpressed *GST-S100A10* at different conditions. (C) Percentage of total *GST-S100A10* overexpressed at 37°C and $OD_{600\,nm}$ = 0.6, 0.7 and 0.8; 100% = total overexpressed *GST-S100A10* at 37°C and $OD_{600\,nm}$ = 0.6. (D) Percentage of GST-S100A10 in the supernatant overexpressed at $OD_{600\,nm}$ = 0.8 and 37°C, 21°C and 18°C; 100% = total overexpressed *GST-S100A10* at different conditions. (E) Percentage of total *GST-S100A10* overexpressed at $OD_{600\,nm}$ = 0.8 and 37°C, 21°C and 18°C, 100% = total overexpressed *GST-S100A10* at 37°C and $OD_{600\,nm}$ = 0.8.

▶ (Figure 1C). Indeed, starting the induction with IPTG at $OD_{600\,nm}$ = 0.8 allows the largest amount of soluble *GST-S100A10* to be obtained.

In parallel, at $OD_{600\,nm}$ = 0.8, the induction of overexpression was started at either 21 or 18°C for 16 h. Similar results were obtained at 21°C (52%), 18°C (49%) and 37°C (48%) (Figure 1D). However, the total amount of *GST-S100A10* overexpressed at 21 and 18°C was higher than at 37°C (Figure 1E). These results show that a lower temperature favors solubility, probably due to a better recombinant protein structure formation [16].

All precultures showing overexpression of *GST-S100A10* were aliquoted in a glycerol solution and frozen at −80°C.

GST-S100A10 from bacterial supernatant was first purified using GST affinity chromatography at 4°C. Eluted fractions were collected and deposited on 12% SDS-PAGE. Fractions containing *GST-S100A10* were mixed together, and the buffer was exchanged with centrifugal filtration before cleaving the GST. One buffer exchange was tested directly with PreScission protease (PSP) cleavage buffer, and another with a pH 9.5 Tris and NaCl buffer followed by PSP cleavage buffer. After the 2-h cleavage at 4°C, S100A10 was purified using different chromatographic conditions: either i) a second and a third GST affinity chromatography; ii) a second GST affinity chromatography and a third ion-exchange chromatography; or iii) only a second GST affinity chromatography. Eluted fractions were collected and verified on 17% SDS-PAGE (Figure 2A), and the protein purity was analyzed with ImageJ. The highest purity (97%) was obtained using the buffer-exchange centrifugal filtration with a pH 9.5 Tris and NaCl buffer and PSP cleavage buffer, followed by a second affinity chromatography. Indeed, a pH higher than 8 inhibits the binding of reduced glutathione to GST, while NaCl increases the ionic strength of the solution to weaken the ionic binding between the proteins (instructions 71-5016-96 AM – GSTrap™ FF, 1 ml and 5 ml). These conditions help to remove most of the reduced glutathione during centrifugal filtration, and GST is captured successfully by the second-affinity chromatography. This method also exhibits a relatively high yield of 12.8-mg S100A10 per liter of bacteria culture, which was determined by UV-visible spectroscopy.

The SDS-PAGE gel containing S100A10 was analyzed by LC/MS-MS (Proteomics Platform, Centre de Recherche du CHU de Québec, QC, Canada). It was identified as S100A10 with a 100% probability. Purified protein samples were kept at four different temperatures: 4, 20, -20 or -80°C. Protein stability was analyzed by circular dichroism at 4°C in triplicate at day 0, 1, 2, 7, 15, 30 and 60. The different temperatures on different days were all compared with day 0, until day 60 (Figure 2B). No significant difference in the samples' spectra

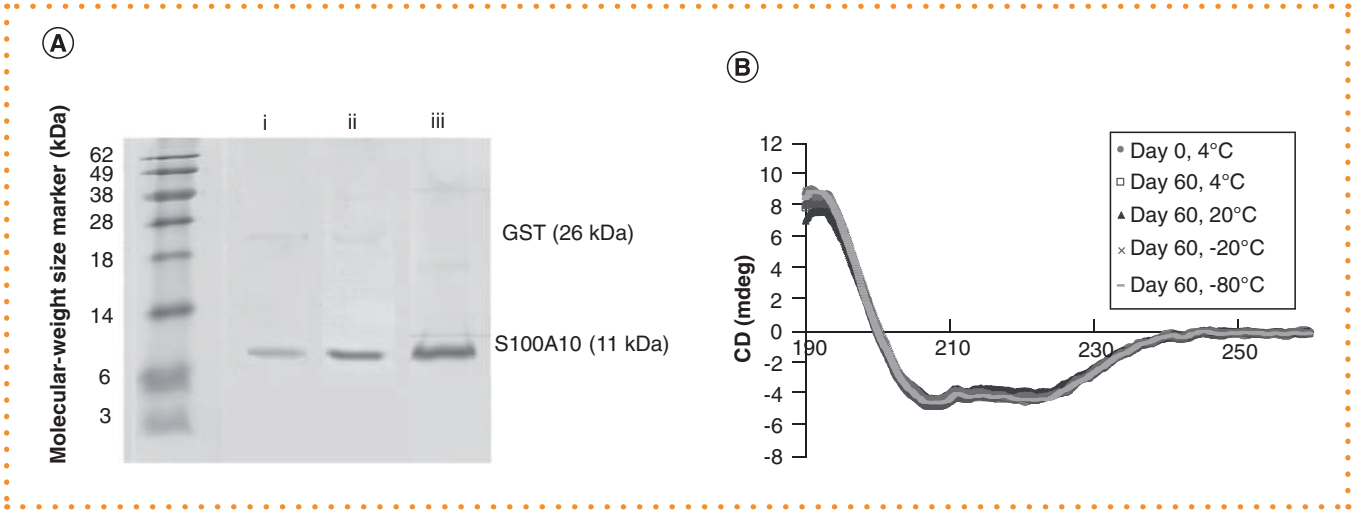

Figure 2. (A) S100A10 purification on 17% SDS-PAGE: i) after a buffer exchange with PreScission protease (PSP) cleavage buffer, then with a second GST affinity chromatography, and a third GST affinity chromatography, ii) after a buffer exchange with PSP cleavage buffer, then with a second GST affinity chromatography, and a third ion-exchange chromatography, or iii) after a buffer exchange and a second GST affinity chromatography. (B) Analysis of stability: circular dichroism spectra of S100A10 stored at different temperatures for 60 days compared with spectra at 4°C on day 0.

was noted, demonstrating the stability of S100A10 at all temperatures tested. Therefore, the protein can be stored for at least 60 days, allowing researchers to perform biophysical experiments at room temperature.

FUTURE PERSPECTIVE

The obtention of purified S100A10 protein will allow for future biophysical studies, in particular those aiming to describe its membrane binding. Conditions to modify its binding or leading to its loss of function can be investigated. These studies will contribute to determining the role of S100A10 in membrane repair and possibly additional functions.

AUTHOR CONTRIBUTIONS

XY and EB prepared the manuscript. EB designed the study. XY, LC and GSS contributed to the design of the study. XY performed plasmid transformation, protein overexpression, protein purification and protein stability analysis. MFLB and ST contributed to protein purification. XY analyzed the data. All the authors read and approved the final version of the manuscript.

FINANCIAL & COMPLETING INTERESTS DISCLOSURE

The authors are indebted to the Natural Sciences and Engineering Research Council of Canada (NSERC, Ottawa, Canada), the Eye Disease Foundation, the CHU de Québec Foundation for their financial support. EB is a research scholar from the Fonds de recherche du Québec – Santé (FRQS) in partnership with the Antoine Turmel Foundation. XY is a PhD student that received a scholarship from The Quebec Network for Research on Protein Function, Engineering, and Applications (PROTEO). GSS acknowledges funding from the Canadian Institutes of Health Research (MOP-93520). The authors have no other relevant affiliations or financial involvement with any organization or entity with a financial interest in or financial conflict with the subject matter or materials discussed in the manuscript apart from those disclosed.

The authors would like to thank Enago (www.enago.com) for English language review.

OPEN ACCESS

REFERENCES

1. Miwa N, Uebi T, Kawamura S. S100-annexin complexes – biology of conditional association. *FEBS J.* 275(20), 4945–4955 (2008).
2. Donato R. Intracellular and extracellular roles of S100 proteins. *Microsc. Res. Tech.* 60(6), 540–551 (2003).
3. Donato R, Cannon BR, Sorci G *et al.* Functions of S100 proteins. *Curr. Mol. Med.* 13(1), 24–57 (2013).
4. Rezvanpour A, Santamaria-Kisiel L, Shaw GS. The S100A10-annexin A2 complex provides a novel asymmetric platform for membrane repair. *J. Biol. Chem.* 286(46), 40174–40183 (2011).
5. Nakata T, Sobue K, Hirokawa N. Conformational change and localization of calpactin I complex involved in exocytosis as revealed by quick-freeze, deep-etch electron microscopy and immunocytochemistry. *J. Cell Biol.* 110(1), 13–25 (1990).
6. Chen H, Xu C, Jin Q, Liu Z. S100 protein family in human cancer. *Am. J. Cancer Res.* 4(2), 89–115 (2014).
7. Santamaria-Kisiel L, Shaw GS. Identification of regions responsible for the open conformation of S100A10 using chimaeric S100A11-S100A10 proteins. *Biochem. J.* 434(1), 37–48 (2011).
8. De Seranno S, Benaud C, Assard N *et al.* Identification of an AHNAK binding motif specific for the Annexin2/S100A10 tetramer. *J. Biol. Chem.* 281(46), 35030–35038 (2006).
9. Rezvanpour A, Phillips JM, Shaw GS. Design of high-affinity S100-target hybrid proteins. *Protein Sci.* 18(12), 2528–2536 (2009).
10. Chehab T, Santos NC, Holthenrich A *et al.* A novel Munc13–4/S100A10/annexin A2 complex promotes Weibel-Palade body exocytosis in endothelial cells. *Mol. Biol. Cell.* 28(12), 1688–1700 (2017).
11. Jost M, Gerke V. Mapping of a regulatory important site for protein kinase C phosphorylation in the N-terminal domain of annexin II. *Biochim. Biophys. Acta* 1313(3), 283–289 (1996).
12. Xin D, Zou X, Zuo M, Liu C. The expression and antibody preparation of S100A10 protein. *Chin. J. Cell Mol. Immunol.* 30(11), 1166–1169 (2014).
13. Rety S, Sopkova J, Renouard M *et al.* The crystal structure of a complex of p11 with the annexin II N-terminal peptide. *Nat. Struct. Biol.* 6(1), 89–95 (1999).
14. Streicher WW, Lopez MM, Makhatadze GI. Annexin I and annexin II N-terminal peptides binding to S100 protein family members: specificity and thermodynamic characterization. *Biochemistry* 48(12), 2788–2798 (2009).
15. Nazmi AR, Ozorowski G, Pejic M, Whitelegge JP, Gerke V, Luecke H. N-terminal acetylation of annexin A2 is required for S100A10 binding. *Biol. Chem.* 393(10), 1141–1150 (2012).
16. San-Miguel T, Pérez-Bermúdez P, Gavidia I. Production of soluble eukaryotic recombinant proteins in *E. coli* is favoured in early log-phase cultures induced at low temperature. *Springerplus* 2(1), 89 (2013).

Benchmarks

Improvement of multiplex semi-nested PCR system for screening of rare mutations by high-throughput sequencing

Yingchun Zhang[1,2], Xu Chi[4], Laibao Feng[1,3], Xingwen Wu[1,2] & Xiaoquan Qi*[,1,2]

ABSTRACT

The CRISPR/Cas9 system is an efficient gene-editing method, but it is difficult to obtain mutants for some specific species and special genome structures. A previously reported multiplexed, semi-nested PCR target-enrichment approach, which does not rely on transgenic technology, has been shown to be an effective and affordable strategy for the discovery of rare mutations in a large sodium azide-induced rice population. However, this strategy has the potential for further optimization. Here, we describe an improved multiplex semi-nested PCR target-enrichment strategy with simplified processing procedures, reduced false-positive rates and increased mutation detection frequency (1 mutation/73 Kb).

METHOD SUMMARY

Here we demonstrate that the purification of PCR products using a dilution strategy provides a cost-effective and simple processing procedure for the multiplex semi-nested PCR target-enrichment strategy. The improved platform has halved the processing time and saves up to 66% on sample preparation costs compared with previously reported protocols.

KEYWORDS

dilution • improvement • multiplexed target enrichment • mutants • next generation sequencing

*[1]Key Laboratory of Plant Molecular Physiology, Institute of Botany, Chinese Academy of Sciences, Beijing, 100093, PR China; [2]The Innovative Academy of Seed Design, Chinese Academy of Sciences, Beijing, 100101, PR China; [3]University of Chinese Academy of Sciences, No.19 (A) Yuquan Road, Shijingshan District, Beijing, 100049, PR China; [4]Beijing Institute of Genomics, Chinese Academy of Sciences, Beijing, 100101, PR China; *Author for correspondence: xqi@ibcas.ac.cn*

BioTechniques 67: 294-298 (December 2019)
10.2144/btn-2019-0001

Creating mutant materials is an essential step for studying gene function, and making a large number of useful mutants is beneficial for scientists. This is particularly true in the case of routinely established loss-of-function mutations, which enable the selection of beneficial traits and phenotypes that can assist breeding and the characterization of gene functions in plants and animals. Several technologies, such as map-based cloning [1,2], map-based sequencing [3], T-DNA insertion, RNA interference, TALENs [4] and CRISPR/cas9 [5–8], have been applied in plant functional genomics research. In 2000, targeting induced local lesions in genomes (TILLING) was first proposed as a reverse genetic approach to identify mutations in a mutated population of *Arabidopsis thaliana* [9]. It does not rely on transgenic technology and has been widely applied for target gene functional analysis in major crops [10–15]. Although the CRISPR/cas9 system has rapidly developed to achieve site/gene-specific mutation, it has been a challenge to obtain mutants for some species and special genome structures. This is further hampered by off-target effects when applied to engineered nuclease research, biotechnology and medical research [16]. Therefore, TILLING is still a competitive approach for the generation of mutants.

In 2014, the strategy of discovering rare mutations was improved, which combined multiplexed semi-nested PCR enrichment with NGS library construction for sequencing target amplicons in extensively pooled DNA samples. The approach not only decreases the number of PCR cycles, which reduces point mutations during amplification, but also enables enriching multiple targets efficiently and specifically. The detailed characteristics of this strategy have been described by Chi *et al.* [17]:

1. The 12-plex PCR reduces the complexity of experimental processes, saving much of the cost of labor and time;
2. Multiplex semi-nested PCR improves specificity of amplification;
3. Application of a tridimensional pooling (8 × 8 × 8), which sequenced 24 bulked samples including 512 screened individuals within each 3D pool;
4. It was particularly well suited to enrich target exon sequences of genes with many introns;
5. It was suitable for high accuracy of the approach of NGS library.

This strategy has been applied to screen rare mutations in a large chemical-induced mutant rice population (M_2) and detect rare disease mutations in a large human population. It can confirm the results of genome-wide association studies (GWAS) and exome sequencing. However, some problems remain to be solved in the multiplex semi-nested PCR approach:

1. The enriched DNA fragment length was determined by the shortest amplification fragments of the tridimensional (X, Y and Z) pools. Although the expected average length of target enrichment was about 500 bp, the detected average length was only 146 bp in the previous study;
2. Experimental processes were relatively complicated and required three rounds of PCR, including column purification of the first two rounds of PCR products and gel purification of the third-round PCR products;
3. A large mass (around a total of 2.5 µg of rice genomic DNA) of genomic DNA of 3D pooling and DNA fragments of

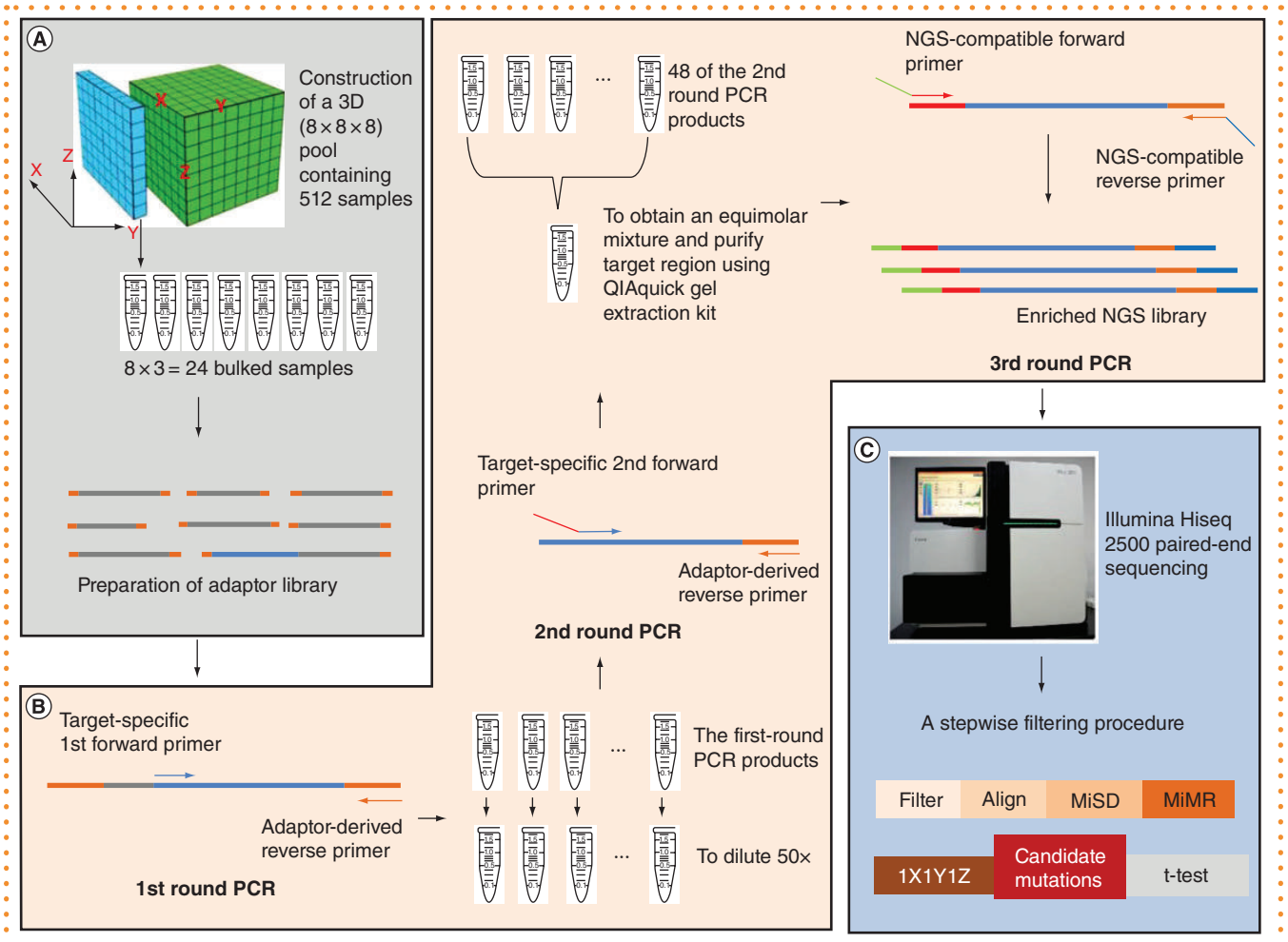

Figure 1. Strategy to improve the semi-nested PCR-based multiple target enrichment method. (A) Preparation of adapter libraries; each library includes 24 bulked DNA samples from a 3D (8 × 8 × 8) pool containing 512 DNA samples. (B) Target preparation. The first-round PCR was amplified by a target-specific forward primer and an adapter-derived reverse primer. The first-round PCR products were diluted 50-fold in ddH_2O, to be used as the template for the second-round PCR. The second-round PCR was amplified by a target-specific nested primer and a nested adapter-derived reverse primer. A total of 48 of the second-round PCR products were equimolarly mixed into one sample followed by agarose gel purification. Subsequently, NGS-compatible forward and reverse primers were used for the third-round PCR. (C) Sequencing and data analysis. All amplicons from the entire library were mixed and sequenced (by the Illumina Hiseq 2500 platform), and overlapping 250 bp paired-end sequences were generated. Data were analyzed by a stepwise filtering procedure in a single pool of 512 DNA samples. Finally, the candidate mutants were confirmed by Sanger sequencing.

adaptor ligation (about 1 µg) was required for the entire experiment;

4. To achieve high-quality NGS sample preparation, a substantial amount of amplification products (each PCR requires 90 µl reaction solutions) was required in the first two rounds of PCR;
5. Massive amounts of purified products of the second PCR (144 of the second PCR samples) were equimolarly mixed into one sample followed by agarose gel purification.

To solve these problems, we first simplified the experimental processes and reduced the amount of adaptor-ligated templates (Figure 1). The spin column was replaced by dilution during purification of the first PCR products and the 50-µl PCR reaction system was replaced by 10 µl in target preparation. Then, we set different gradients of three factors: PCR reaction volume, dilution gradient of the primer concentration, and the concentration of adaptor-ligated template in the first round of PCR reaction. There was little difference between the amplification pattern when using spin columns or dilution, which indicated that it was feasible to replace spin column purification with dilution. The dilution gradients of the first PCR products were set as 25, 50 and 100 times. The gradients of the primer concentrations of ITSP1s (target-specific primer) were set as 0.66 µl (control) and 0.44 µl, AP1 (5 µM) (adaptor-derived primer), including 0.26 µl (control) and 0.17 µl in the first PCR reaction (10 µl reaction system). The result (Supplementary Figure S1A) suggested that the substitution of spin column with dilution was successful, in that the sequencing depth and enriched fragment length was substantially improved by using dilution. Furthermore, no apparent differences were observed for the bands of different dilutions of the first-round PCR products and no apparent differences were ▶

Table 1. Comparison between improvement and non-improvement of multiplex semi-based PCRs.

Experimental procedure	Multiplex semi-based PCR			Improvement of multiplex semi-based PCR		
	Bulked samples (n)	Processing time (days)	Cost ($)	Bulked samples (n)	Processing time (days)	Cost ($)
Adaptor ligation library	48	6	30	48	6	30
Number of enriched targeted DNA fragments	36	7	219	36	7	219
First-round PCR	432	2	400	144	1	50
Second-round PCR	432	2	400	144	1	50
Spin column	288	3	44	NA	NA	NA
Gel purification	2	1	10	6	2	20
Total number of experimental procedures	1238	21	1103	342	17	369
Mutation density	1 mutation/336 Kb			1 mutation/73 Kb		
Efficiency of detecting positive mutations	57%			95%		

observed for the bands of different dilution gradients of the first-round PCR products, as well as the second-round PCR products (Figure 1B & Supplementary Figure S1A). Based on these results, a 10-µl reaction system of the first-round PCR was established empirically.

To improve the second-round PCR system, we set three gradients for the first-round PCR products. First, we diluted the PCR products by 10, 30, 60 and 100 times, then for each dilution we used three different template volumes (0.5, 1 and 3 µl) for the second-round PCR. As shown in Figure 1B & Supplementary Figure S1B, with four dilution gradients and three gradients of concentration of the second PCR template, the bands showed similar amplification efficiency. There were no significant differences observed among the PCR products of the second-round PCR template. Based on these results, we decided that 1 µl of the first-round PCR products (50-times dilution) was an appropriate template quantity in the second-round PCR reaction system.

Taken together, we have developed a simpler, more effective approach for library construction for screening rare mutations (Figure 1). Compared with the previous report [17], our method involves three innovations:

1. We replaced the spin column purification step by simple dilution of the PCR products. This not only decreased the cost of the experiment, but also simplified the experimental process;
2. The volume of PCR reaction system was reduced by four-fifths in the first and second-round of PCR, and the amount of input genomic DNA was reduced by 90%;
3. The numbers of mixed samples of the second PCR products were reduced by 40–50% to improve the equality of the molars of the PCR products.

To verify the reliability of our improved protocol for screening mutants, we used a known point mutation 31B8 (X_8, Y_2, Z_7: *Os07g11440* G929D) as a positive control. In the spin column experiment, 1.49 Gb high-quality reads were obtained from the tri-dimensional samples, with on-target ratios of 38.00% for Z_7, 53.24% for Y_2 and 45.68% for X_8, respectively. Compared with the spin column results, there were 1.69 Gb high-quality reads mapped to the targeted sequences by dilution treatment, and the ratio of mapped reads were much higher (96.41, 95.94 and 50.86%, respectively) (Supplementary Table S1). After diluting the first-round PCR product, we found that there were significant improvements of the fragment length and sequencing depth compared with spin column (Figure 2A & B, & Supplementary S2). The results suggested that the newly optimized PCR reaction system was better than the multiplex semi-nested-based target-enrichment strategy, in that the average fragment length and the average sequencing depth were both increased.

We further applied our approach for screening mutants of target genes in a mutagenized rice population. A total of 69,820,404 high-quality reads (6.98 Gb) were obtained from approximately 10 Kb target gene regions and 48 bulked templates (pool 1 and 2), derived from 1024 M_2 individuals of a rice sodium azide-induced mutated population. The mean proportion of on-target reads across all 48 bulks was 60.6%, rising to 80.73% in one case (Supplementary Table S2). The average length of the 36 target fragments was 371 bp in pool 1 and 381 bp in pool 2, ranging from 0–1189 bp in pool 1 and from 0–755 bp in pool 2; thus, the average length achieved was similar to the pilot experiment (Figure 2C, Supplementary Figure 3SA & 3SB). The enriched fragment length of pool 1 was significantly correlated with that of pool 2 (R^2 = 0.9741; Figure 2C). The total enriched fragment length of the 512 M_2 progeny was 3.03 Mb in pool 1 and 3.6 Mb in pool 2 (Supplementary Table S7). The average sequencing depth was 8553 in pool 1 and 10,496 in pool 2 (Figure 2D, Supplementary 3SC & 3SD). The sequencing depth of pool 1 was correlated with that of pool 2 (R^2 = 0.7664; Figure 2D). The results above suggest that the enriched fragments and sequencing depth were reproducible and consistent between pools 1 and 2. The ratio of on-target region (ranging from 60.6 to 80.73%) has higher specificity than in previous reports (ranging from 13.44 to 73.87%). Overall, these results suggest ▶

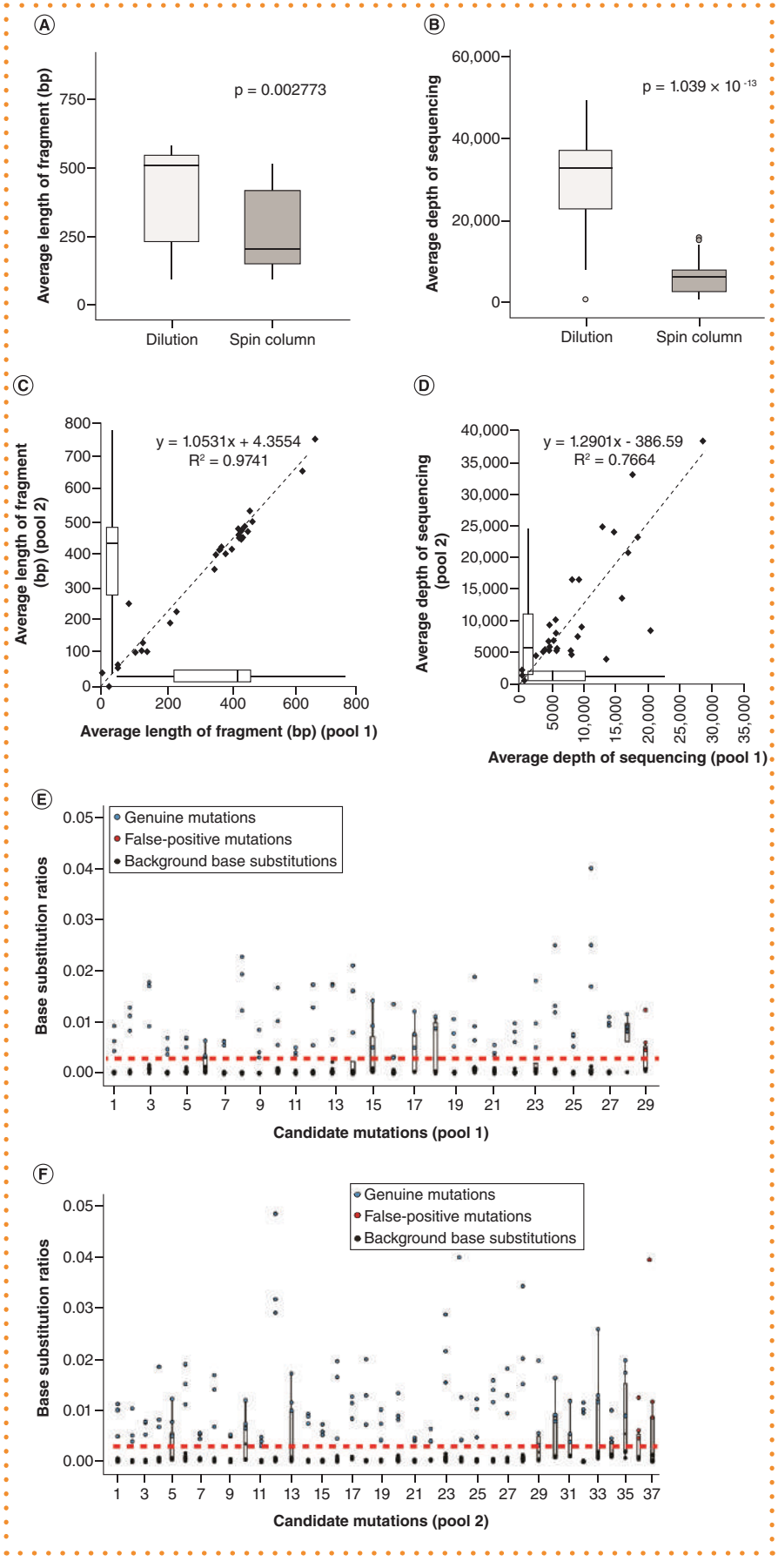

Figure 2. Screening the mutants in rice. (A & B) The average length of fragments and the average depth of sequencing in the pilot experiment. (C) The relationship between the average length of fragments of pool 1 (x-axis) and pool 2 (y-axis). The two populations of the 3D pool were significantly correlated (correlation coefficient = 0.9741). The average length of fragments (A) was consistent with the pilot experiment (larger than 400 bp) in two populations. (D) The relationship between the average depth of sequencing of pool 1 (x-axis) and pool 2 (y-axis). The two populations of the 3D pool were significantly correlated (correlation coefficient = 0.7664). The average depth of sequencing (B) was consistent with the theoretical value (higher than 512×). (E & F) Identification of the candidate mutations. Red dashed lines indicate the one-tailed left-hand border, equivalent to 95% of the 'true mutations' base-substitution rate (3.02×10^{-3}). Confirmed genuine mutations are marked by blue dots. Sequencing errors are marked by red dots.

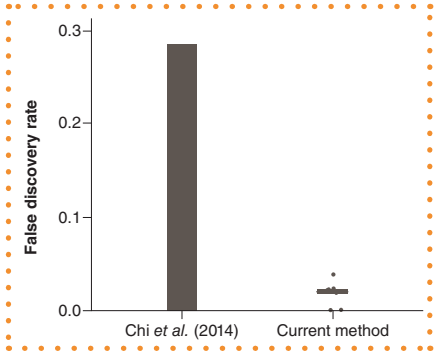

Figure 3. Comparison of the false discovery rate of the previous and current methods. The bar plot represents the false discovery rate of the method in Chi *et al.* [17], which was eight false positives out of 28 candidate mutations. The box plot to the right shows the false discovery rate of the current method of random selection of raw sequencing reads 20 times in order to generate a similar sequencing depth compared with the previous method. The average number of candidate mutations of these 20 permutations is roughly 52 (Supplementary Table S8), which includes one constantly detected false-positive position (18 out of 20 permutations) and one which only presented in one occurrence.

▸ that optimization of the multiplex semi-nested-based PCR target-enrichment approach provides a more effective method of enriching multiple DNA target fragments.

After stepwise filtering [17], we obtained 63 candidate mutations. Sanger sequencing confirmed that the 63 identified candidates were all genuine mutations (Figure 2E & F, Supplementary Table S3), among which 28 genuine mutations were detected from the 512 M_2 progeny in pool 1 (3.03 Mb enriched target sequences) and 35 from pool 2 (3.6 Mb enriched target sequences), equivalent to a mutation rate of one per 164 and 195 Kb, respectively (Supplementary Table S3). These results indicate that our improved approach increases both the efficiency of screening genuine mutants (from 1 mutation/336 Kb to 1 mutation/147 Kb), and accuracy (eight false-positive mutations out of 28 candidates in the previous study vs 0 false positives from the current approach). Furthermore, the number of experimental procedures, processing time and the cost is reduced by nearly twofold, 0.5-fold and twofold, respectively (Table 1). Due to the script availability issue, we welcome any researchers who are interested in this method to send their alignment file to us and we will send back the analyzed results.

To better compare our current results with the previous method, 35,234,100 high-quality reads, which equals the previous method, were randomly selected from the raw reads for analysis. A total of 20 permutations were performed and an average of 52 mutations were identified (Supplementary Table S8). Some of the mutations were not detected during the 20 repetitive analyses, probably because of the decrease in sequencing depth. Compared with the previous method, the false discovery rate of the current method was significantly lower than the previous one (Figure 3). Although the current method uses Illumina's (CA, USA) HiSeq 2500 Sequencing platform and the previous method used HiSeq 2000, the HiSeq 2500 was reported to have a lower Q30 (≥80%) than HiSeq 2000 (≥85%) according to Illumina's data sheets [18,19]. Taken together, these results suggest that the increased rate of precision (the true positives divided by the predicted positives) is due to the improvement of method rather than the change in sequencing platform.

Through comparison among several methods of target enrichment, we propose that the improved multiplex semi-nested target-enrichment method has a simpler experimental procedure and lower cost of implementation (Supplementary Table S4). Our new strategy reduces false-positive mutations and experimental costs, enhances mutations sensitivity and allows for screening mutants in other crop species.

SUPPLEMENTARY DATA

To view the supplementary data that accompany this paper please visit the journal website at: www.future-science.com/doi/suppl/10.2144/btn-2019-0001

AUTHOR CONTRIBUTIONS

XQ and YZ conceived and designed the experiments. YZ performed the experiments. YZ analyzed the data with contribution from LF. XC wrote the Perl script of data analysis. YZ wrote the paper with contribution from XQ and XW. All authors read and approved the final manuscript.

ACKNOWLEDGMENTS

We thank Zhanquan Zhang and Juncong Sun for discussion of the manuscript.

FINANCIAL & COMPETING INTEREST DISCLOSURE

This work was supported by the fund of National Transgenic Megaproject of China (2016ZX08009001-006). Funding for open access was received from grant no. 2016ZX08009001-006. The authors have no other relevant affiliations or financial involvement with any organization or entity with a financial interest in or financial conflict with the subject matter or materials discussed in the manuscript apart from those disclosed.

No writing assistance was utilized in the production of this manuscript.

DATA AVAILABILITY

The short-read sequence data from this study have been deposited under NCBI BioProjects PRJNA555498. All relevant data contained within the paper are available from the corresponding author on request.

REFERENCES

4. Komatsuda T, Pourkheirandish M, He C *et al.* Six-rowed barley originated from a mutation in a homeodomain-leucine zipper I-class homeobox gene. *Proc. Natl Acad. Sci. USA* 104, 1424–1429 (2007).
5. Krattinger S, Wicker T, Keller B. Map-based cloning of genes in triticeae (wheat and barley). In: *Genotics and Genomics of the Triticeae, Plant Genetics and Genomics: Crop and Models.* Muehlbauer G, Feuillet C (Eds). Springer, NY, USA, 337–357 (2009).
6. Su CF, Wang W, Gong SL, Zuo J, Li S, Xu S. High density linkage map construction and mapping of yield trait QTLs in maize (*Zea mays*) using the genotyping-by-sequencing (GBS) technology. *Front. Plant Sci.* 8, 706 (2017).
7. Alonso IM, Ecker JR. Moving forward in reverse: genetic technologies to enable genome-wide phenomic screens in Arabidopsis. *Nat. Rev. Genet.* 7, 524–536 (2006).
8. Shan Q, Wang Y, Li J *et al.* Targeted genome modification of crop plants using a CRISPR-Cas system. *Nat. Biotechnol.* 6, 1365–1368 (2013).
9. Feng Z, Zhang B, Ding W *et al.* Efficient genome editing in plants using a CRISPR/Cas system. *Cell Res.* 23, 1229–1232 (2013).
10. Li JF, Norville JE, Aach J *et al.* Multiplex and homologous recombination-mediated genome editing in *Arabidopsis* and *Nicotinana benthamiana* using guide RNA and Cas9. *Nat. Biotechnol.* 31, 688–691 (2013).
11. Nekrasov V, Staskawicz B, Weigel D, Jones JDG, Kamoun S. Targeted mutagenesis in the model plant *Nicotiana benthamiana* using Cas9 RNA-guided endonuclease. *Nat. Biotechnol.* 31, 691–693 (2013).
12. McCallum CM, Comai L, Greene EA, Henikoff S. Targeted screening for induced mutations. *Nat. Biotechnol.* 18, 455–457 (2000).
13. Leung H, Wu C, Baraoidan M *et al.* Deletion mutants for functional genomics: progress in phenotyping, sequence assignment, and database development. *Rice Genetics IV.* 4, 239–251 (2001).
14. Caldwell DG, McCallum N, Shaw P, Muehlbauer GJ, Marshall DF, Waugh R. A structured mutant population for forward and reverse genetics in barley (*Hordeum vulgare* L.). *Plant J.* 40, 143–150 (2004).
15. Slade AJ, Fuerstenberg SI, Loeffler D. Steine MN, Facciotti D. A reverse genetic nontransgenic approach to wheat crop improvement by TILLING. *Nat. Biotechnol.* 23, 75–81 (2005).
16. Till BJ, Reynolds SH, Weil C *et al.* Discovery of induced point mutations in maize genes by TILLING. *BMC Plant Biol.* 4, 12 (2004).
17. Triques K, Sturbois B, Gallais S *et al.* Characterization of Arabidopsis thaliana mismatch specific endonucleases: application to mutation discovery by TILLING in pea. *Plant J.* 51, 1116–1125 (2007).
18. Cooper JL, Till BJ, Laport RG *et al.* TILLING to detect induced mutations in soybean. *BMC Plant Biol.* 24(8), 9 (2008).
19. Cho SW, Kim S, Kim Y *et al.* Analysis of off-target effects of CRISPR/Cas-derived RNA-guided endonucleases and nickases. *Genome Res.* 24, 132–141 (2014).
20. Chi X, Zhang YC, Xue ZY *et al.* Discovery of rare mutationsin extensively pooled DNA samples using multiple target enrichment. *Plant Biotechnol. J.* 12, 709–717 (2014).
21. Illumina. HiSeq™ 2000 sequencing system (2010). https://www.illumina.c om/documents/products/datasheets/datasheet_hiseq2000.pdf
22. Illumina. HiSeq™ 2500 sequencing system (2015). https://www.illumina.com/documents/products/datasheets/datasheet_hiseq2500.pdf

Online Contents

Did you know *BioTechniques* also publishes exclusive, online-only interviews, educational webinars & method videos?

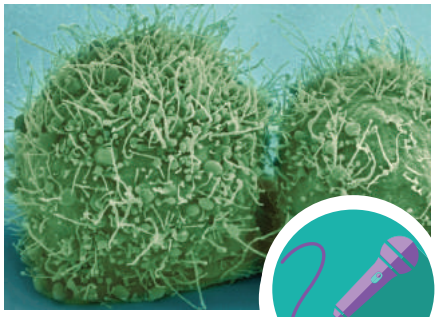

NATIONAL CENTER FOR MICROSCOPY AND IMAGING RESEARCH

PODCAST

PRECISION THERAPEUTICS FOR CANCER AND SCIENCE IN POLITICS

We spoke to Hans Keirstead, CEO and Founder of Avita Biomedical.

http://bit.ly/HansKeir

SHUTTERSTOCK.COM

Visit the *BioTechniques* website today to see the latest updates in laboratory methods

EVENTS

ISFG 2019 CONFERENCE REPORT

Read the highlights of the International Society for Forensic Genetics 2019 meeting, including latest advances in forensic genetics.

http://bit.ly/ISFG19BTN

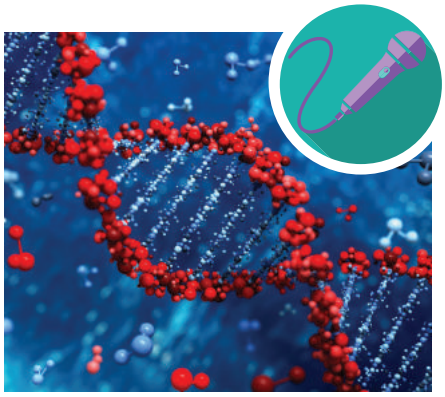

BIOTECHNIQUES.COM

PODCAST

DNA SEQUENCING WITH JOANNE HACKETT

Joanne discusses Genomics England's goals, completion of major milestones in genomics research and their approach to precision medicine.

http://bit.ly/JoanneDNA

FEATURE

A PRIME TIME FOR GENOME EDITING

Tristan Free takes a look at the latest improvement on CRISPR-Cas9, prime editing.

http://bit.ly/PrimeEdFree

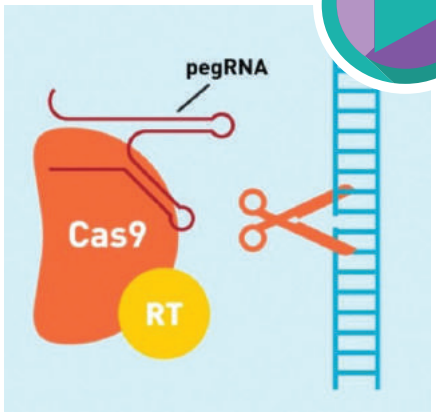

SUSANNA M. HAMILTON, BROAD INSTITUTE COMMUNICATIONS

New Products

Olympus SLIDEVIEW™ VS200 solution with reliable, flexible, and high-throughput slide scanning

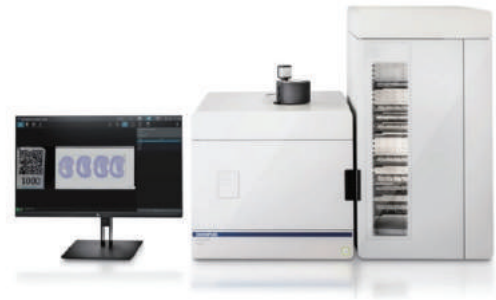

The new Olympus SLIDEVIEW™ VS200 slide scanner captures high-quality virtual slide images and offers flexibility to empower advanced quantitative image analysis for brain, cancer and stem cell research, as well as drug discovery.
By employing Olympus X Line™ objectives at the core of the system, users obtain flatter images with a wider field of view and no intensity fall-off near the periphery. Scientists can see more of their slides in less time with the system's lineup of flexible features, including:

- Five imaging modes: brightfield, fluorescence, darkfield, phase contrast and simple polarization.
- Mix and match observation methods: combine observation methods to view structures that are only visible under certain conditions.
- Optimized for X Line objectives: specially designed light path provides more homogeneous illumination. X Line objectives also improve numerical aperture, chromatic aberration correction and flatness.
- Scan multiple slide sizes at once: supports 26 × 76 mm (1 × 3 in.), 52 × 76 mm (2 × 3 in.), 76 × 102 mm (3 × 4 in.) and 102 × 127 mm (4 × 5 in.) slides.

In addition to increased image quality, researchers will benefit from increased slide capacity and hot-swap capabilities. Scientists can run scans to finish overnight and have more time to focus on meaningful work. Reliable sensor technology enables the loader to automatically detect trays, the number of slides and the size of the slides while the integrated barcode reader automatically captures and records slide information.
The intuitive user interface and robust data management system streamline the workflow further so users can easily scan, save, access and share slides.

For more information, visit www.olympus-lifescience.com

Zymo launches RNA-Seq library prep kit

Zymo Research is excited to announce the fastest and easiest total RNA-Seq library prep kit that allows users to go from sample to sequencer in a single day! This probe-free technology makes RiboFree total RNA libraries from any organism in as little as 3.5 h. A simple-to-follow workflow has 100 fewer steps in the protocol and 60% less pipetting than the TruSeq® total RNA kit.

For more information, visit https://www.zymoresearch.com/pages/total-rna-seq-library-prep

Cytek biosciences hits flow cytometry milestone: 40 color analysis from a single sample

The Cytek Aurora advanced flow cytometry system features a unique combination of patent-pending innovative technologies and is available with up to five lasers to enable analyzing up to 40 markers simultaneously in one sample. With the Aurora, users can combine all of their markers in one sample and achieve high resolution for each individual marker. The Aurora provides scientists flexibility in dye choices, the power to extract sample autofluorescence, the ability to get up and running quickly with its intuitive workflows, and the means to extract highly multiplexed high-quality data – from a single test – all at a fraction of the price of other technologies and flow cytometry systems.

For more information, visit www.cytekbio.com

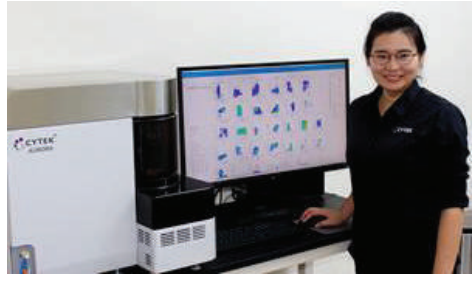

Eppendorf launches innovative, first-of-its-kind 25 ml conical tubes

Eppendorf, a leader in conical tube production and design and inventor of the Eppi™ tube, has launched a brand new 25 ml conical tube that is easier to use, minimizes storage space and is more sustainable.

Since many researchers work with sample volumes between 15 ml and 25 ml, but only 15 ml and 50 ml tubes were available, Eppendorf saw the need in the industry for a 25 ml conical tube.

The 25 ml conical tube is the same diameter as the conventional 50 ml conical tube and comes with either the new patented SnapTec™ snap cap or screw cap, both of which have high centrifugation stability. The wide opening, combined with the lower height, offers easy sample access, and allows for up to 30% more storage in fridges or freezers. When working with low-volume pipettes and tips, the risk of cross-contamination between pipette and tube by touching the inner tube wall is also minimized.

One of the most innovative features is the patented SnapTec cap, which is unique within the conical tube market. This cap is firmly connected to the tube and allows single-handed opening and closing for quick liquid extraction or addition of sample.

"In addition to the convincing handling and application benefits, we designed the Eppendorf 25 ml conical tube to work with the lab equipment you already have so there's straightforward integration into the existing lab environment," said Nils Gerke, Business Manager of Consumables.

For more information, visit www.eppendorf.com/25ml

Shimadzu's Nexera preparative supercritical fluid chromatography system meets SFC purification needs for pharmaceutical industry

The Nexera semi-prep SFC system is part of SSI's Nexera UC platform, which accommodates a wide variety of analyses and purifications. The platform is based around the Nexera ultra-high-performance liquid chromatograph. Each Nexera UC semi-prep system is configurable to user specifications in order to optimally perform the desired purification function, including chiral or achiral purifications, single injections, stacked injections and fraction collections from several microliters to liters.

This complete SFC solution reduces the need for costly and hazardous solvents used in normal phase prep LC, while shortening purification run time and dry down time. Innovative technologies include a flexible format combination injector/fraction collector, CO_2 pump with integrated chiller that requires less lab space and allows for benchtop use, a novel gas–liquid separator (GLS) design to ensure high recovery and low carryover, and easy-to-use preparative software to streamline operations.

Importantly, the newly designed gas-liquid separator realizes a higher recovery ratio and lower carryover than earlier SFC systems. Moreover, the elegant design of the new GLS reduces the total size of the recovery system and allows for easy rinsing compared to earlier cyclone-style or centrifugal-type GLS systems.

For more information, visit www.ssi.shimadzu.com/products/liquid-chromatography/nexera/nexera-prep-sfc.html

Index to Advertisers

FastPrep® Instruments and Kits

A complete solution for environmental samples

Lyse, homogenize or grind any environmental sample to extract and purify high yields of DNA, RNA and proteins

- Soil
- Water
- Feces
- Bioaerosol
- Rhizosphere
- Sediment
- Sludge
- Compost
- Wood

See why our FastDNA™ SPIN Kit for Soil is the gold standard in DNA isolation – cited in over 7,000 publications

SelectScience®
The Fastest Way to Expert Opinion

"I can get results that are quick, easy, and contaminant-free"

Brandi Kiel Reese
Texas A&M University

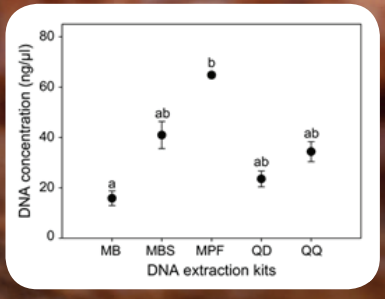

The FastDNA SPIN Kit for Soil (MPF) outperforms 4 other commercial kits with DNA extraction of plankton communities from a freshwater reservoir.

Liu, M.; Xue, Y.; Yang, J. Rare Plankton Subcommunities Are Far More Affected by DNA Extraction Kits Than Abundant Plankton. *Front. Microbiol.* **2019**, *10*, 454.

LEARN MORE
www.mpbio.com/environment

MP™

MP Bio North America: **custserv@mpbio.com** | **1-800-854-0530**
MP Bio Europe: **custserv.eur@mpbio.com** | **00800-7777-9999**